AFML-TR-73-56

COMPUTER ANALYSIS OF ALLOY SYSTEMS

LARRY KAUFMAN
HARVEY NESOR
ManLabs, Inc.

TECHNICAL REPORT AFML-TR-73-56

MARCH 1973

Air Force Materials Laboratory
Air Force Systems Command
Wright-Patterson Air Force Base, Ohio

NOTICE

When Government drawings, specifications, or other data are used for any purpose other than in connection with a definitely related Government procurement operation, the United States Government thereby incurs no responsibility nor any obligation whatsoever; and the fact that the government may have formulated, furnished, or in any way supplied the said drawings, specifications, or other data, is not to be regarded by implication or otherwise as in any manner licensing the holder or any other person or corporation, or conveying any rights or permission to manufacture, use, or sell any patented invention that may in any way be related thereto.

Copies of this report should not be returned unless return is required by security considerations, contractual obligations, or notice on a specific document.

AFML-TR-73-56

COMPUTER ANALYSIS OF ALLOY SYSTEMS

LARRY KAUFMAN

HARVEY NESOR

ManLabs, Inc.

FOREWORD

This report was prepared by ManLabs, Inc., 21 Erie Street, Cambridge, Massachusetts 02139, under USAF Contract No. F33615-71-C-1471. This contract was initiated under Project No. 7353, "Research on Metals and Ceramics Leading to Superior Materials for Advanced Air Force System Application," Task No. 735302, "Correlation of Structures and Properties." Funds for this project are supplied to the Air Force Materials Laboratory by the Office of Aerospace Research. The work was administered by the Metals and Ceramics Division of the Air Force Materials Laboratory, Air Force Systems Command, Wright-Patterson Air Force Base, Ohio, with Dr. L. R. Bidwell, AFML/LLM, as Project Scientist.

This report covers the period from May 1971 to January 1973.

This technical report has been reviewed and is approved.

I. PERLMUTTER
Chief, Metals and Processing Branch
Metals and Ceramics Division
Air Force Materials Laboratory

ABSTRACT

Computer analysis of twenty-three binary and thirteen ternary titanium and columbium base systems has been performed in order to provide phase stability and thermochemical characterization data which can be used to define fabrication procedures for achieving high temperature stability and improved mechanical properties. M_S temperatures have been calculated for titanium base alloys with simultaneous additions of Mo, V, Al, Mn and Sn. The effect of zirconium on the solubility of Si and Be in hcp titanium was calculated along with the occurrence of miscibility gap formation in bcc titanium base systems. Titanium and columbium base ternary systems were analyzed to predict the temperature-composition trajectories of eutectoid and eutectic troughs and the location of melting point minima. A method was developed for calculation of the eutectic temperature and composition of metal alloy-metal carbide systems and applied to the (Fe,Ni,Cr)-TiC case.

TABLE OF CONTENTS

LIST OF TABLES

LIST OF TABLES (Continued)

LIST OF TABLES (Continued)

LIST OF ILLUSTRATIONS

LIST OF ILLUSTRATIONS (Continued)

LIST OF ILLUSTRATIONS (Continued)

I. INTRODUCTION AND SUMMARY

The objective of this investigation is to employ computerized calculation of phase stability (1)* in several titanium- and columbium-base alloy systems to identify ranges of compositional and thermal stability where variations of chemistry and processing procedures can yield oxidation resistance in concert with high strength, formability, and creep resistance. Moreover, the calculations must provide sufficient detail to facilitate utilization of special techniques such as controlled unidirectional cooling to obtain unique structures. Such methods, which can lead to the preparation of in-situ composites, offer a means for substantial improvement in properties. Needless to say, applications of such methods are limited to systems where phase relationships are favorable. Such systems can be identified by extensive Edisonian research or, as in the case of the present study, by application of computer based thermochemical calculations. Since the latter approach has only attained the status of a useful predictive tool in recent years, this investigation has concentrated on specific problems where the computational method can provide explicit results.

Twenty-three binary systems and thirteen ternary systems were analyzed in the course of the present study. The analytical description developed for these systems in terms of lattice stability, compound and solution phase parameters permits explicit calculation of the phase diagrams, thermochemical properties and solution phase metastability. The M_s temperature of titanium-base alloys containing Mo, V, Al, Mn and Sn were calculated over a wide range of composition. This method can be readily applied to a variety of alloying ingredients.

The stability of the titanium-base hcp solution in ternary systems containing silicon, zirconium, and beryllium additions

---

*Underscored numbers in parentheses denote references.

was investigated in order to determine the effect of zirconium additions on the silicon and beryllium solubilities. These elements confer good creep resistance when dissolved in hcp titanium.

Body centered cubic titanium alloys, which offer attractive thermal stability and formability characteristics, may exhibit low temperature miscibility gap formation. Such reactions can have deleterious effects on mechanical stability. At the same time, they can offer a means for enhancing mechanical properties. Several titanium-base ternary systems were analyzed in order to predict miscibility gap formation.

The temperature-composition trajectory of the bcc/hcp/compound eutectoid in the Ti-Cr-Mo and Ti-Mo-Mn systems was calculated. These reactions offer potential for enhancing the mechanical properties of titanium-base alloys.

The Cb-Cr-Zr, Cb-Cr-Hf, Cb-Cr-Mo, Cb-Ti-Zr and Cb-Cr-Al phase diagrams were calculated in order to provide information on high temperature stability, eutectic troughs and melting point minima in these refractory systems. The Cb-Cr-Al analysis suggests that interesting combinations of high temperature and oxidation resistance might be obtained at the composition with the minimum melting temperature.

An approximate method for calculating the eutectic temperature and composition of metal alloy-metal carbide systems has been developed and applied to computing these conditions for the (Fe-Ni-Cr)-TiC case from a knowledge of the component binary systems analyzed in the present study and in earlier investigations (2,3).

During the course of this work, one technical paper has been published (4). In addition, material drawn from this report will be included in the following papers.

1. "Theoretical Approaches to the Determination of Phase Diagrams, Annual Review of Material Science, R. A. Huggins, Ed., Annual Reviews, Inc., Palo Alto, California.

2. "Relation of the Thermochemistry and Phase Diagrams of Condensed Systems," Treatise on Solid State Chemistry, N. B. Hannay, Ed., Plenum Press, New York.

The following binary and ternary systems have been investigated in this study.

Binary Systems:

1. Ti-Be	6. Ti-Ga	11. Mo-Cb	16. Cb-Al	21. Cr-C
2. Zr-Be	7. Ti-Sn	12. Ti-Cr	17. Cr-Al	22. Ti-C
3. Ti-Si	8. Ti-Zr	13. Ti-Mn	18. Fe-Ti	23. Fe-C
4. Zr-Si	9. Ti-V	14. Mo-Cr	19. Ti-Ni	
5. Ti-Al	10. Ti-Mo	15. Cb-Cr	20. Ni-C	

Ternary Systems:

1. Ti-Cb-Mo	8. Cb-Cr-Zr
2. Ti-Mo-V	9. Cb-Cr-Hf
3. Ti-Cb-V	10. Cb-Cr-Mo
4. Ti-Si-Zr	11. Cb-Ti-Zr
5. Ti-Be-Zr	12. Cb-Cr-Al
6. Ti-Mo-Cr	13. Fe-C-Ti
7. Ti-Mo-Mn	14. Fe-C-Ti-Ni-Cr

II. EFFECTS OF PHYSICAL AND ELECTRONIC CHARACTERISTICS ON PHASE STABILITY AND EQUILIBRIA

Measurements of the physical properties of alloys such as electronic specific heat coefficients, magnetic susceptibility, optical absorptivity, soft X-ray spectra, lattice parameters, elastic constants, Hall coefficient, conductivity, etc. are valuable in characterizing the physical and electronic properties of metals and alloys. These techniques can also be employed along with conventional thermal analysis and metallographic techniques to reveal the phase constitution. However, in spite of many well-meaning efforts, utilization of these characteristics to define the electronic structure for the purpose of predicting phase stability has been unsuccessful. The main reason for failure is that the electronic structure is generally characterized by $n(E_F)$, the electronic density of states at the Fermi level, which is supposed to undergo a singular variation with electron/atom ratio as the phase boundary is approached yielding an energy-composition curve with similar characteristics (5). The fallacy in this argument is that it completely ignores phase competition which lies at the basis of all phase diagrams (6). Indeed, the postulated inflection in the energy vs. e/a curve as the phase boundary is approached leads to serious inconsistencies (7), which are not as widely recognized (8) as they should be (9).

The main shortcoming of the $n(E_F)$ vs. e/a description is that it attempts to treat stability as a property of a given phase rather than the outcome of competition between different structures and/or compositions (1,6). Recent attempts to perform meaningful first principle calculations of the energy differences between competing structures of pure metals (10-13) have yielded encouraging results (14) and should be pursued. However, these calculations, which are based on examination of competing phases, have not yet been applied to alloys.

In spite of the basic difficulties in using the $n(E_F)$ vs.

e/a relations to characterize phase stability as noted above (5-9), this basis has been presented as a method for discerning the behavior of titanium alloys (15-20). Although identification of critical e/a or group numbers may be useful as empirical guides for correlating data (17,20,21), assigning fundamental significance to such critical e/a values has little basis. This is demonstrated conclusively by a recent application of PHACOMP techniques to sigma phase formation in Ni-Cr-Mo alloys where the group number of Mo was changed from 4.66 to 9.66 (retaining a value of 4.66 for Cr) in order to conform with the phase boundary between the sigma and fcc phases (22).

By contrast, the author has developed a method based on phase competition as a means for defining the relative stability of metallic structures. One of the first series of alloys considered by means of this technique was titanium alloys (23). More recently this technique, which is characterized by definition of the lattice stability of pure metals, has been applied to a wide variety of alloy systems (24,6,1,14) in order to describe the energetics of stable, metastable, and unstable phases. Considerable success has been encountered in predicting the temperature-composition range for bcc→hcp martensitic reactions in titanium alloys (25-29) as well as the formation of miscibility gaps in bcc alloys. Moreover, the scope of this description permits consideration of metastable transformation products exemplified by the fcc structure, which has been reported (30-33) to occur in a variety of alloys. This approach, recently expanded to take advantage of computer techniques (1), incorporated physical and electronic structure within the framework of phase competition and permits integration of thermochemical and structural data (34). It is encouraging to see that similar activities are now being pursued all over the world (35-40). It should be noted that these phase competition analyses are completely different from the "solute enthalpy of transformation" approaches which have been applied to iron, titanium (19), and rare-earth systems (41). The basis for the latter analysis is questionable to say the least (1, p. 209, 6, p. 89)!

Definition of phase stability by including the physical and electronic factors within the thermochemical framework prior to examination of competitive stability offers the opportunity of independent evaluation of diverse data and identification of the role played by individual factors (23,34,6,1,24). To illustrate this interplay it is instructive to compare recent evaluation of the Debye temperatures of bcc and hcp titanium deduced from physical measurements without considering thermochemical factors (15) with earlier estimates which considered such factors (23,29). The results shown in Table 1 indicate that there is relatively good agreement on the values for the electronic γ for hcp titanium and the Debye temperature for bcc titanium. However, substantial differences exist for the Debye temperature of hcp titanium and the electronic γ of bcc titanium. If the recent values (15) are employed to compute the entropy difference between the b.c.c. at 1155°K (where the transition takes place at one atmosphere) and at 300°K, values near 3 and 2 entropy units respectively result. This compares with an observed value slightly less than one entropy unit. Although the values deduced recently (15) were determined near 4°K, the entropy difference inferred departs so substantially from the thermochemical value that they should be questioned. Paradoxically, Collings and Ho make no mention of the entropy difference between bcc and hcp titanium even though their measurements of physical properties are employed to "deduce" characteristic $n(E_F)$ vs. e/a behavior which is presented as the basis for titanium alloy phase stability (15).

Although detailed description of each of the physical components for all of the competing phases of interest is severely limited at present by the paucity of thermochemical and physical data, application of the above-mentioned computational methods (1-4,6,14,26) provides a means for attacking a variety of practical problems. These include calculation of stable and metastable equilibria in binary and ternary systems, solubility limits and martensitic transformation. Incorporation of the characteristics of the

important omega phase (1, p. 13, 42) has been considered. Moreover, expansion of the bcc/omega/hcp relations in titanium alloys can be viewed as a direct analogue of the current description of fcc/hcp/bcc relation in iron alloys (43). Examples which illustrate the application of these methods to calculation of bcc→hcp martensitic transformation temperatures is illustrated in Section III.

III. CALCULATION OF BCC→HCP TRANSFORMATION TEMPERATURES IN MULTICOMPONENT TITANIUM BASE ALLOYS

Utilization of heat treating techniques which produce martensitic transformations is widely employed in developing high strength titanium base alloys. Suitable application of computational methods can provide information concerning the effects of alloying elements on martensitic transformation temperatures. In this way, the computational method yields information directly applicable to the heat treatment of alloys. Calculation of the temperature range for martensitic transformations (i.e. the T_o-composition curve defining equal free energies of parent and daughter phases) offers the most apparent application of the above-mentioned techniques (1-4, 6, 14, 26). The simplest approach was first applied more than ten years ago (23) and has been successfully employed (25, 27, 29) to a variety of titanium alloy systems. It is interesting to note that application of this method (which requires data on the beta transus) by Jepson et.al. (27) yielded good results for Ti-Al but poor results for Ti-Cb. As a consequence, it is worthwhile re-examining the beta transus data employed in the T_o-x calculations performed by Jepson et.al. (27). Figure 1 compares these results (27) with the calculations reported simultaneously and independently (26) which indicate a more extensive two phase field. The latter results (26) predict a T_o-x curve lying midway between the experimental findings of Jepson et.al. (27) and Huang (28). The inference which can be drawn from this result is that beta transus curves (particularly those determined at low temperatures) must be viewed with caution unless equilibrium has been approached from different directions.

The martensitic transformation of bcc titanium alloys into hcp structures of the same composition can be characterized by defining the free energy difference at M_s (23, 28). This dif-

ference was found to be approximately 50 cal./g.at. for Ti-Zr alloys having M_s temperatures between 800°K and 1100°K. If this criterion is examined by considering alloys which transform at still lower temperatures (i.e. such as Ti-Cb alloys) where extensive data exist, it is found that the driving force is temperature dependent and is approximately equal to 100 - 0.05T cal./g.at. Thus a more general criterion can be described by Equation 1 as

$$100 - 0.05T = (1-x)\Delta F_{Ti}^{\varepsilon\rightarrow\beta}[T] + x\Delta F_{j}^{\varepsilon\rightarrow\beta}[T] + (F_{E}^{\beta}[x,T] - F_{E}^{\varepsilon}[x,T]) \quad (1)$$

Equation 1 is satisfied at $T = M_s$ for any given x where x is the atomic fraction of element j. The titanium-columbium system as well as current systems of interest noted in Table 2 were re-examined to determine if Equation 1 provides an adequate description of the M_s temperatures. Experimental results were taken from Huang et.al. (28). This examination disclosed that Ti-Cb, Ti-Al and Ti-Sn provided good results. However, revisions of the former description of Ti-Mo and Ti-V were required. The revised description is given in Table 2. Only the E parameter has been altered. The previous values (1, 4, 26) being 3671 and 2659 for Ti-Mo and Ti-V respectively. Figure 2 shows the calculated Ti-Mo and Ti-V diagrams reflecting these changes. Comparison with the earlier results (1, 4, 26) shows little change except for the position of the hcp/hcp + bcc phase boundary. Equation 1 was employed to calculate the M_s-composition curves shown for Ti-Mo and Ti-V in Figure 2. In addition calculations for Ti-Cr and Ti-Mo were performed based on the description given in Section VI. The Ti-Mo, Ti-V, Ti-Cr and Ti-Mn results agree with observations (28).

Equation 1 has been generalized to compute the M_s temperature in multicomponent titanium-base alloys as follows. If an alloy contains w atom fractions of j, x atom fractions of k, y atom fractions of ℓ, and z atom fractions of m, then the M_s temperature is given by Equation 2,

$$M_s = NUM/DENOM \tag{2}$$

when

$$NUM = 100 + (1-w-x-y-z)[-1040 + w\epsilon_{ij} + x\epsilon_{ik} + y\epsilon_{i\ell} + z\epsilon_{im}] + w\Delta H_j + x\Delta H_k + y\Delta H_\ell + z\Delta H_m \tag{3}$$

and

$$DENOM = 0.05 + (1-w-x-y-z)[-0.90] + w\Delta S_j + x\Delta S_k + y\Delta S_\ell + z\Delta S_m \tag{4}$$

where

$$\Delta F_j^{\beta\rightarrow\epsilon} = \Delta H_j - T\Delta S_j \tag{5}$$
$$\Delta F_k^{\beta\rightarrow\epsilon} = \Delta H_k - T\Delta S_k$$
$$\Delta F_\ell^{\beta\rightarrow\epsilon} = \Delta H_\ell - T\Delta S_\ell$$
$$\Delta F_m^{\beta\rightarrow\epsilon} = \Delta H_m - T\Delta S_m$$

and

$$\epsilon_{ij} = [(1-w)w]^{-1}[F_E^\epsilon - F_E^\beta]_{ij} \tag{6}$$
$$\epsilon_{ik} = [(1-x)x]^{-1}[F_E^\epsilon - F_E^\beta]_{ik}$$
$$\epsilon_{i\ell} = [(1-y)y]^{-1}[F_E^\epsilon - F_E^\beta]_{i\ell}$$
$$\epsilon_{im} = [(1-z)z]^{-1}[F_E^\epsilon - F_E^\beta]_{im}$$

In Equation 6, $[F_E^\epsilon - F_E^\beta]_{ij}$ is equal to the excess free energy of the hcp phase minus the excess free energy of the bcc phase in the i-j system.

The lattice stability values presented earlier (1), supplemented by the results presented in Sections IV and VI, provide sufficient information to apply Equations 5 and 6 to Ti-Al-Mo, Ti-Al-V, Ti-Al-V-Mn, Ti-Al, Mo-Cr and Ti-Mo-Al-Sn. The results are displayed in Tables 3-16. To illustrate the computational procedure for the Ti-Al-V-Mn case, j = Al, k = V and ℓ = Mn with z = 0. Equation 5 becomes

$$\Delta F_{Al}^{\beta\rightarrow\epsilon} = -1100 + 0.72T \tag{7}$$
$$\Delta F_V^{\beta\rightarrow\epsilon} = +1500 + 0.80T$$
$$\Delta F_{Mn}^{\beta\rightarrow\epsilon} = +800 - 0.52T$$

while Equation 6 becomes

$$\varepsilon_{ij} = -1000 \qquad (8)$$
$$\varepsilon_{ik} = 1425$$
$$\varepsilon_{i\ell} = 8540$$

It should be noted that the M_s temperatures given in Tables 3-16 refer to bcc→hcp reactions where all of the solutes *are in solution*. If the tabulated alloys contain compound phases which co-exist with the bcc phase at the solution temperature, then the alloy composition of the bcc phase will be altered resulting in an M_s temperature corresponding to the new composition of the bcc phase.

Due to the lack of precise M_s data for multi-component titanium base alloys, it is not possible to make a general assessment of the predictions shown in Tables 3-16. However, results for the widely used titanium-6w/o aluminum-4w/o vanadium alloy indicate an M_s near 1525°F $\pm$ 20°F (44) corresponding to 1102°K $\pm$ 10°K. The calculations displayed in Table 4 suggest an M_s temperature of 1077°K for this alloy. The small difference between calculated and observed results could be due to oxygen or nitrogen in the alloy.

IV. EFFECT OF ALLOYING ELEMENTS ON THE STABILITY OF THE HCP PHASE IN TITANIUM ALLOYS

A second problem of greater complexity is the calculation of equilibrium phase stability and solubility limits in ternary titanium alloy systems. This problem is more difficult than that considered in Section III where the composition of the parent and daughter phases are fixed. Here isothermal equilibrium conditions operate. In the present case, the practical problem of interest is definition of the field of stability of the hcp structure in order to determine the temperature-composition range where improvement of mechanical properties due to alloying will not be impaired by transformation or precipitation. The ternary systems of interest are Ti-Si-Zr, Ti-Be-Zr, Ti-Ga-Al and Ti-Sn-Al. This presents a challenge since some of the constituent binary systems have not been detailed experimentally (45-47) and limited thermochemical data have been reported (48, 49). Nevertheless, application of the present techniques provides an adequate description as detailed below and displayed in Figures 3-6 and Tables 17-25 and 27.

Before considering these results, it is instructive to discuss the salient features of the calculations so that the scope of considerations becomes apparent. Only then will the range of other problems to which the current finding can be applied become evident. The basis for the calculation has been detailed earlier (26, 1) so that only phase designation need be discussed.* In line with earlier discussions of phase notation the designation of solution phases bcc = β, hcp = ε, fcc = α and liquid = L will be maintained. Lattice stability parameters for the elements employed

*Two typographical errors in Reference (26) should be noted which have been corrected in Reference (1). First, the melting point of hcp titanium in Table 2 of Reference (26) should be 1697 not 1967°K. Second, Equation 5 of Reference (26) is composed of three separate terms. The last term is $x_*(1-x_*)(L-C)$ as in Equation 91 of Reference (1).

in the previous computations are also maintained (26, 1). In addition to the latter, similar descriptions are required for gallium, tin and silicon which are stable in the orthorhombic (ρ), body centered tetragonal (τ), and diamond cubic (δ) forms respectively as indicated in Tables 17, 21 and 24. Heats of fusion for the stable forms of these elements are taken from Hultgren's compilation (48, 49) while lattice stability parameters have been estimated using Miodownik's discussion of entropy changes as a guide (35). The only additional departure from earlier calculations (26, 1) is that the interaction and compound parameters are treated as temperature dependent in some cases in order to obtain a more accurate description of the system under consideration.

The description of Ti-Be and Zr-Be shown in Figure 3 and Tables 18, 19, and 22 is based on a consideration of the fcc(C15) or Cu_2Mg type $TiBe_2$ phase (ϕ), the ρ (rhombohedral, Be_3Nb type $Ti_{1/4}Be_{3/4}$), δ(rhombohedral, $Be_{17}Nb_2$ type $Ti_{2/19}Be_{17/19}$) and ξ(body centered tetragonal, $Mn_{12}Th$ type $Ti_{1/13}Be_{12/13}$) compound phases in the Ti-Be system. Only one of the compound phases in the Zr-Be system has a counterpart in Ti-Be. This is the $Zr_2Be_{17}\delta$ phase which like its Ti_2Be_{17} counterpart δ phase exhibits the rhombohedral Nb_2Be_{17} structure. The remaining compounds including the hexagonal AlB_2 type $ZrBe_2$, the hexagonal $CuZn_5$ type $ZrBe_5$, and the fcc, $NaZn_{13}$ type $ZrBe_{13}$ do not have stable counterparts in the Ti-Be system. Parameters for these compounds designated η, μ, and ω respectively are given in Table 18. These parameters in combination with the regular solution interaction parameters for the liquid, bcc and hcp phases in Table 18 and the lattice stability parameters for Ti, Zr and Be (1) permit direct calculation of the Ti-Be and Zr-Be phase diagrams shown in Figure 3 and calculation of the free energy of formation of the above mentioned compound phases. Limited phase diagram and thermochemical data for these systems are available for comparison. Recent studies of Ti-Be (50) suggest a

bcc/L/compound eutectic at 1302°K with 5.1 a/o Be in the bcc phase and a hcp/bcc/compound eutectoid at 1087°K with 2.5% Be in the bcc phase. These features are reproduced by the calculations as shown in Figure 3. This study suggested that the eutectoid composition of the hcp phase is less than 0.28 a/o Be in equilibrium with β (2.5 a/o Be) and $TiBe_2$. The solubility of a solute in solution phase which is in equilibrium with a compound phase can be calculated directly from Equations 91-94 of Reference (1) when the solubility is very small as

$$RT\ell nx = (1-x_*)x_*^{-1}\Delta F_i^{\phi\rightarrow\theta} + \Delta F_j^{\phi\rightarrow\theta} + (1-x_*)(L-C) - \Phi \qquad (9)$$

where x is the atom fraction of solute j in the solution phase φ (which consists mainly of i atoms) which is in equilibrium with the compound $i_{(1-x_*)}j_{x_*}$. The latter is characterized by a base phase θ and a compound parameter C. The interaction parameters for the liquid and φ solution phases in the i-j system and L and Φ, respectively. Table 22 summarizes the results obtained from Equation (9) based on the description of Table 18 for the solubility of Be in hcp Ti and Zr. Two solubility equations are shown for Be in hcp Ti. The first corresponds to E = 6000, the second to E = 10,000 in Table 18. The former equation yields a solubility of 0.002 atom fraction of Be in hcp Ti at the eutectoid in keeping with Hunter's finding (50) that the solubility is less than 0.28 a/o (0.0028 at. fr.) Be. Recent observations (44) indicated that the actual solubility may be as low as 0.03 a/o Be. This possibility is reflected by the second alternative which may be due to the formation of Ti-Be compound phases containing more titanium than $TiBe_2$. Present calculations for the Zr-Be system yield a maximum solubility of 0.024 atom fraction Be in bcc Zr at 1200°K. Elliot's compilation suggests a solubility less than 0.030 (46). Experimental evaluation of the solubility of Be in hcp Zr at 1100°K yields a value which is less than 0.001 at. fr. The equation in Table 22 yields 0.0005 at 1100°K. Limited thermochemical data are available at 1300°K to compare with the calculated free energy of formation shown in Table 19 for Zr-Be (49). This comparison yields reasonable results although a similar com-

parison of the associated heats of formation leads to substantial discrepancies. However, it should be noted that the experimental heats of formation (49) are inconsistent with the observation of a stable $ZrBe_2$ phase so that the fault may lie with the experimental data and not the current calculations.

Reference to Table 20 shows that the interaction parameters employed to characterize the liquid, bcc, and hcp forms of titanium and zirconium are similar as might be expected.

The description of Ti-Si and Zr-Si summarized in Tables 20-22 and Figure 4 is in good agreement with the limited thermochemical (48, 49) and phase diagram data (45--47) currently available. Ten compound phases are considered including two sets (orthorhombic FeB type TiSi and ZrSi designated by ω and the hexagonal Mn_5Si_3 type Ti_5Si_3 and Zr_5Si_3 phases designated by ξ) which have the same structure. In addition, the face centered orthorhombic $TiSi_2$ phase is designated by ϕ and the five remaining Zr-Si phases include the tetragonal Ni_3P type Zr_3Si phase, τ; the bc tetragonal Al_2Cu type Zr_2Si phase, π; the Zr_3Si_2 σ phase which exhibits the tetragonal Si_2U_3 or CrFe σ structure; the orthorhombic CrB type Zr_6Si_5 phase, μ; and the orthorhombic $ZrSi_2$ phase, ρ. The solubility of silicon in hcp titanium derived from Table 22 (0.0064 vs. 0.0065 observed at 1123°K; 0.0054 vs. 0.0052 observed at 873°K (45-47)) exhibits an unusually small temperature dependence leading to a temperature dependent interaction parameter for the hcp solid solution in Table 20. The Zr-Si system is characterized by very small solubilities of silicon in both bcc and hcp solutions. The maximum solubility at the bcc/Liquid/Zr_3Si eutectic is calculated to be 0.02 dropping to 0.00045 at 1155°K. At the latter temperature, Hansen (45) suggests a solubility which is less than 0.0065. At this temperature the observed solubility of silicon in hcp zirconium (45) is less than 0.0030, while Table 22 yields 0.00019.

Analyses of the Ti-Zr, Ti-Al, Ti-Ga, and Ti-Sn systems are summarized in Figures 5 and 6 and Tables 17, 23-25. The Ti-Zr system was considered earlier (26, 1), and has been reconsidered here with slight alteration of the B and L parameters to provide a better description of the phase diagram. Similarly, the Ti-Al system has been re-analyzed and temperature dependent components have been included in the L, B, E, and A solution phase parameters as well as the compound phase parameters for the AuCu type TiAl phase, γ, and the tetragonal $TiAl_3$ phase, δ. These changes improve the comparison between calculated and observed (48, 49) thermochemical properties as shown in Table 24. In addition, a compound phase is included at 25 a/o Al representing the hexagonal DO_{19} Ti_3Al structure, designated by ξ, which has counterparts in the ξTi_3Ga and ξTi_3Sn structures. Considerable controversy exists concerning the constitution of the Ti-Al system in the vicinity of Ti_3Al (45-47, 52-55). The limitations of the present "line-compound" description preclude critical analysis of the controversy which centers on ordering vs. miscibility gap decompositions. The present description of Ti_3Al leads to a peritectoid bcc/hcp/Ti_3Al at 1400°K in keeping with the findings of Clark et. al. (52). However, a small alteration of the Ti_3Al compound parameter to 7800 + 3.77T would reduce the stability of this phase sufficiently to eliminate the peritectoid leading to the phase diagram configuration suggested by Blackburn. Such an alteration would decrease the entropy of formation of $Ti_3Al\xi$ shown in Table 24 by 0.043 cal/g.at.°K. Thus, the two alternatives are separated by a 4% entropy difference corresponding to 60 cal./g.at. or 0.0026 e.v./atom at 1400°K!

Partial Ti-Ga and Ti-Sn diagrams are shown in Figure 6 and described in Tables 23 and 24, and include the Ti_2Ga and Ti_2Sn η phases which exhibit the hexagonal Ni_2In structure. Recent phase equilibria and vapor pressure measurements (56) suggest that B = -13,000 for Ti-Ga and B = -21,000 for Ti-Sn, and that the composition of the $\beta/\beta+L$ boundaries in Ti-Ga at 1770°K and 1700°K occur

at 0.16 and 0.26 atom fractions of gallium respectively. The present solution model is too simple to reflect the minimum in the bcc/hcp phase boundaries reported for Ti-Sn (45-47).

Isothermal sections of the Ti-Ga-Al, Ti-Sn-Al, Zr-Si-Ti, and Ti-Be-Zr systems have been computed as shown in Figures 7-10 based on the forgoing description of the component binary systems employing the techniques described earlier (1). In these calculations, the TiGa(γ) and TiSn(γ) counterphases of TiAl(γ) were based on the α structure with C = 0 while the $Ti_2Al(\eta)$ counterphase of $Ti_2Sn(\eta)$ and $Ti_2Ga(\eta)$ was based on the ε structure with C = 0. Similarly, the $Ti_3Si(\tau)$ counterphase of $Zr_3Si(\tau)$ was based on the β structure with C = 0, the $ZrBe_2(\phi)$ counterphase of $TiBe_2(\phi)$ was based on α with C = 0 and the $TiBe_2(\eta)$ counterphase of $ZrBe_2(\eta)$ was based on the β structure with C = 0. The Al-Sn and Al-Ga interaction parameters in Table 25 were estimated from thermochemical data for these binary systems (48, 49).

Figure 10 shows that the liquid phase is present in the Ti-Be-Zr ternary at 1180°K. The inserted portions of Figures 9 and 10 show the computed effects of ternary additions on the solubility of silicon and beryllium in the hcp phase at 800°K. Addition of zirconium to Ti-Si reduces the solubility. In all the other cases, the reverse behavior is predicted. The reason for this behavior can be identified by deriving the ternary analogue of Equation 9. This can be done by equilibrating the partial molor free energies of all three components, i, j, and k, in the solution phase which contains 1-x-y atom fractions of i, and y atom fractions of k with those in the compound phase. The stoichiometry of the compound phase is $(i,k)_{1-x_*}j_{x_*}$. If consideration is restricted to cases where the solubility of j in the solution phase is small and solubility of k in the compound phase is small, then Equations 301 and 304 or Reference (1) combine to yield the following simple result:

$$RT\ln \frac{x(1-y)^{\frac{1-x_*}{x_*}}}{x_o} = y[E_{ij} + E_{ik} - E_{jk} - yE_{ik}x_*^{-1}] \qquad (10)$$

Equation 10 describes the ratio of the solubility of element j (i.e., x/x_o) in the ternary to the corresponding ratio in the binary i-j system. Thus x_o is the solubility of j in i given by Table 22. Equation 10 is only valid for small values of x and x_o. This ratio depends upon the concentration of element j in the i-k solution which is given by y and the stoichiometry $(i,k)_{1-x_*}{}^{j}{}_{x_*}$ of the coexisting compound phase.

Ignoring the right side of Equation 10 for the moment we see that x/x_o will normally tend to increase with increasing y if the right side is zero. This is due to entropic effects and may be considered to reflect base line behavior. The ratio x/x_o can decrease or increase more rapidly than the ideal behavior as a function of the interaction parameters E_{ij}, E_{ik} and E_{jk} as illustrated in Equation 10. The ratio x/x_o will only decrease with increasing y if $E_{ij} + E_{ik} - E_{jk}$ is negative. In the event that the solubility of k in the compound is not small (i.e., $(Zr,Ti)_5Si_3$ in the present case), then, if the ratio of y in the compound divided by y in the solution phase equals $1-x_*$ (the solution-compound tie lines radiate from pure j), then the left side of Equation 10 reduces to $RT\ln x/x_o$. This eliminates the entropic advantage of the solution phase over the compound phase as regards solubility. Examination of Table 27, which tabulates the requisite parameters, reveals the reasons for the solubility behavior displayed in Figures 9 and 10. First, the Ti-Si-Zr case (corresponding to additions of Zr to Ti-Si) is the only instance where negative values of $E_{ij} + E_{ik} - E_{jk}$ are obtained. In addition, this is the only case where extensive solubility of the metal addition in the compound is indicated (i.e., $(Ti,Zr)_5Si$). Both factors tend to reduce the solubility of silicon in titanium with increasing zirconium content.

V. PREDICTION OF MISCIBILITY GAPS IN BCC TITANIUM-BASE ALLOYS

Body centered cubic titanium-base alloys are being considered as structural materials because of their excellent formability and their wide range of temperature stability. Although experimental studies of the stability of bcc titanium-base alloys have been carried out at low temperatures (i.e., below 600°K), equilibrium is not always attained unless special efforts are expended. As a consequence, the possible formation of miscibility gaps in these alloys at low temperatures has not been considered widely. Such reactions could be of significance if components made of such alloys were used (or stored) for extended periods of time in the 300-600°K range with the expectation that no structural changes were going to take place. Conversely, recognition of such reactions could provide means for strengthening such alloys via spinodal reactions. Before extending this description to calculation of the above noted ternary diagrams, it is of interest to point out that the previous calculation of titanium phase diagrams (26, 1) characterized the Ti-Mo, Ti-V, Ti-Ta,and Ti-Cb binary systems by positive interaction parameters which are given in Table 25. These parameters lead to miscibility gap formation where the gap critical temperature is the interaction parameter divided by 2R for the simple description being employed here. In addition, this simple description implies a symmetrical miscibility gap. These restrictions can be removed if more complex solution models are employed (1, p. 205). Nevertheless, application of the present simple description yields the calculated diagrams shown in Figure 11 which include prediction of metastable miscibility gaps in the bcc phase. Thus solute segregation in the bcc phase is predicted (26). This behavior has recently been observed in several titanium alloys (57, 58). Recent measurements of the activity of titanium (59-62) in the bcc solution of the Ti-V and Ti-Mo systems (59, 60)

yielded values of B = 1800 and B = 2900 respectively. Although these values support the predicted values (26) shown in Table 25 as far as sign and magnitude are concerned, the Ti-Mo value of B = 2900 seems too large. Singhal and Worrell (63) have reported negative deviations from ideality in Ta-W, Cb-Mo and Ta-Mo corresponding to B = -6400, -8800 and -10,400 cal/g at. respectively. These results are in keeping with B = -3178 suggested for Cr-V (1, p. 188). An independent analysis of the Cb-Mo-Cr ternary detailed in Section VII yields a value of B = -5500 for Cb-Mo which offers some support for the Singhal-Worrell result (63). These findings will be employed below to consider the stability of bcc solid solutions in ternary titanium alloys.

Before turning to a detailed calculation of ternary titanium systems, it is instructive to consider the conditions for the formation of isolated miscibility gaps (1, p. 299). Such gaps can occur in systems where at least one of the interaction parameters is negative above the temperature where the gaps vanish in the binary components. Table 26 considers the Ti-Cb-Mo, Ti-Mo-V and Ti-Cb-V bcc phases employing the bcc interaction parameters for the titanium binary components listed in Table 25 and assuming identical values of B = -5500 for Cb-Mo, Mo-V and Cb-V. In all three cases, isolated gaps are calculated with rather high summit temperatures. Such gaps have not been heretofore reported in the literature and will be discussed in detail below. In order to provide some confidence in the calculation, it should be noted that the isolated gap in the fcc phase of the Cu-Ni-Au system (64) occurs near 1273°K, at 20 a/o Cu, 60 a/o Ni and 20 a/o Au. Current thermochemical data for the component binary systems (48, 49) suggest interaction parameters of -5200, 2800 and 4400 cal/g at. respectively for Cu-Au, Cu-Ni and Au-Ni. Thus, the predicted summit conditions are 1264°K, at 17 a/o Cu, 50 a/o Ni and 33 a/o Au in reasonable agreement with the observed results quoted above.

The predicted ternary miscibility gaps in Ti-Cb-Mo, Ti-Mo-V, and Ti-Cb-V based on the description of Table 26 are displayed in Figures 12-14. The calculations are based on the assumption that Mo-V and Cb-V exhibit the same negative interaction parameter as Cb-Mo (i.e., B = -5500). The lower right corner of Figure 12 shows the calculated miscibility gaps for Ti-Cb-Mo derived on this basis. The remaining portions of Figure 12 illustrate the results which are obtained if the Mo-V, Mo-Cb and V-Cb bcc phases are treated as ideal solutions (i.e., B = 0). Comparison of the calculated Ti-Cb-Mo gaps in the lower part of Figure 12 for the cases B(Mo-Cb) = 0 and B(Mo-Cb) = -5500 shows that the latter value leads to much more extensive gap stability.

Figure 13 shows the calculated bcc/bcc + hcp phase boundaries in the Ti-V-Mo and Ti-Cb-V systems computed on the basis of B(Mo-V) = E(Mo-V) = B(Cb-V) = E(Cb-V) = 0 as a function of temperature compared with observed phase boundaries at 300°K in Ti-V-Mo (65) and 870°K in Ti-Cb-V (66). The marked divergence for Ti-Mo-V suggests that the observed 300°K section represents equilibrium near 800°K rather than equilibrium at 300°K. The bulging bcc/bcc + hcp boundary which characterizes the observed Ti-V-Cb diagram at 870°K shown in the lower right corner of Figure 13 is indicative of negative values for B(Cb-V).

Figure 14 shows the calculated bcc/bcc + hcp boundaries which have been calculated for B(Mo-Cb) = E(Mo-Cb) = 0 (upper left corner) and B(Mo-Cb) = E(Mo-Cb) = -5500 cal/g at. in the lower left and right corners. The upper right corner displays the observed bcc/bcc + hcp boundary (67), which is in better agreement with the ideal Mo-Cb description than the description of Mo-Cb based on negative interaction parameters shown in the lower part of Figure 14. Nevertheless, it should be noted that the Ti-Mo and Ti-Cb edge values for the bcc/bcc + hcp boundaries displayed in the "observed" diagram at 870°K differ substantially from the collated results to Ti-Mo and Ti-Cb (44-46) which are reflected in the cal-

culated portions of Figure 14 and in Figure 11.

The complex configuration of the bcc/bcc + hcp boundary shown in the lower half of Figure 14 results from the interaction of the hexagonal phase and the isolated bcc miscibility gap. These equilibria have not been observed. However, the fact that it has not been observed could well reflect the fact that no one has looked for it! In summary, the calculations presented here suggest that metastable miscibility gap formation in the bcc phase of titanium alloy systems can occur. Due to the low temperatures at which these reactions are expected to occur, their attainment may be impeded by kinetic factors or competitive reactions. However, further elucidation of the energetics of these reactions will undoubtedly lead to a better overall description of phase stability in titanium alloys.

VI. CALCULATION OF THE TEMPERATURE-COMPOSITION TRAJECTORY OF EUTECTOIDS IN TERNARY TITANIUM-BASE ALLOY SYSTEMS

Eutectoid reactions offer opportunities for improving mechanical properties by appropriate heat treatment. Thus, pearlite steels have been used extensively in many applications. Moreover, recent application of directional solidification techniques to eutectic solidification of alloys has yielded new opportunities for generating unusual superalloy structures exhibiting outstanding high temperature strength. Application of such methods to eutectoid reactions in titanium alloys over suitable transformation temperature ranges could produce beneficial results. As a consequence, the temperature-composition trajectories of the eutectoid decomposition of bcc solid solutions into a compound phase and solute-lean hcp phase in the Ti-Cr-Mo and Ti-Mo-Mn systems were calculated. These systems were chosen specifically because the bcc solid solution is stable in concentrated solution at low temperature.

Previous analyses of metallic systems (1,4) have made extensive use of symmetrical functions to describe the excess free energy of mixing. However, the complex nature of the current systems of interest requires that more general forms be considered along the lines presented in Equations (209)-(212) of Reference 1 and in References 2 and 3. Accordingly, the excess free energy of solution phases will be described by Equation 11 for the i-j system, where x is the atomic fraction of j,

$$F_E = x(1-x)[(1-x)g[T] + xh[T]] \qquad (11)$$

where g[T] and h[T] are temperature dependent functions. Thus (1), the excess partial free energies of components i and j are given by Equations 12 and 13 as

$$\overline{F}_{Ei} = x^2[g[T] + (2x-1)(h[T] - g[T])] \qquad (12)$$

and

$$\overline{F}_{Ej} = (1-x)^2[g[T] + 2x(h[T] - g[T])] \qquad (13)$$

when $g[T] \equiv h[T]$, the excess free energy is symmetrical; when $g[T] = h[T]$ = constant, the solution is regular. When $g[T] = h[T] = 0$, the solution is ideal.

Two descriptions have been employed for g[T] (and h[T]). The simplest consists of the approximation

$$g[T] = g_0 + g_1 T \tag{14}$$

where g_0 and g_1 are constants. Equation 14 is employed over a limited temperature range well removed from the third law range. On the other hand, description of g[T] over a wider temperature range inclusive of 0°K requires the form of Equation 15

$$g[T] = g_2 + g_3 T^2 \; g_4 T^3 \tag{15}$$

where g_2, g_3 and g_4 are constants (2,3).

These generalized solution equations have been applied successfully to analyze the binary components of the Fe-Ni-Cr, Fe-Ni-Co, Fe-Cr-Co, and Cr-Co-Ni systems (8) as well as the Cb-Cr-Ni system (7). They permit a more detailed description of the binary system and a more accurate calculation of the ternary case. In the cases of interest here (which are summarized in Tables 28-30) the excess free energy of the bcc phase in the Ti-Cr system is given by Equation 16 as

$$F_E^{\beta} = x(1-x)[(1-x)3000 + x6000] \text{ cal/g.at.} \tag{16}$$

where x is the atomic fraction of Cr. Reference to Tables 29 and 30 shows that the Ti-Mn solution phases are regular while the Mo-Cr phases are asymmetric.

The description of the Ti-Cr system is displayed in Table 28 and Figure 16. In the previous description of this system (1), the liquid, bcc and hcp phases were treated as regular solutions with L = 1494, B = 4506 and E = 6936. In the present case, asymmetrical terms have been included such that

$$F_E^{L} = x(1-x)[(1-x)0 + x3000] \tag{17a}$$

$$F_E^{\beta} = x(1-x)[(1-x)3000 + x6000] \quad (17b)$$

and

$$F_E^{\varepsilon} = x(1-x)[(1-x)9420 + x12420] \quad (17c)$$

where x is the atom fraction of chromium in order to obtain a more precise description of the phase diagram. The current description reproduces the observed diagram to within 2 a/o and 20°K (45-47) and adequately describes the observed thermochemical properties.

Table 29 and Figure 15 display the current description of the Ti-Mn system. The liquid, bcc and hcp phases are described as regular solutions and although no thermochemical data are available to compare with the computed properties, the calculated phase diagram agrees with the observed diagram to within 3 a/o and 20°K. The present description of the Ti-Mn system will be employed to compute the eutectoid trough in Ti-Mn-Mo. Consequently, the present partial description will be adequate.

The description of the Mo-Cr system displayed in Figure 15 and Table 30 will be employed to calculate the eutectoid trough in the Ti-Mo-Cr system. The asymmetrical solution description applied to the bcc and liquid phase reproduces the observed phase diagram and thermochemical data (45-49) quite accurately.

Little data are available to provide an estimate of the interaction parameters for Mo-Mn. These parameters will be employed in the calculation of the Ti-Mn-Mo eutectoid troughs. If the methods developed earlier (1) are applied, then it is found that the large internal pressure term (e_p) for Mo-Mn cancels the negative e_o term (characteristic of Mo-Re). Thus L = B = E = 0 for this system.

Extension of the present description of asymmetric binary phases into the ternary systems has been carried out on the basis described earlier (1-3). Thus, the ternary analog of Equation 11 formulates the excess free energy of a ternary alloy with x atom fraction of chromium, y atom fraction of molybdenum and 1-x-y atom fraction of titanium as being equal to

$$x(1-x-y)(1-y)^{-1}((1-x-y)g[T]+xh[T])+y(1-x-y)(1-x)^{-1}((1-x-y)\ell[T]+ym[T])$$
$$+xy(x+y)^{-1}(xn[T]+yp[T])$$

where g[T] and h[T] refer to the Ti-Cr system, ℓ[T] and m[T] refer to the Ti-Mo system and n[T] and p[T] refer to the Cr-Mo system.

The free energy of the ternary compound phases in the systems of interest is formulated along the lines of Equations (291) and (292) of Reference 1, allowing for the variation in compound stoichiometry (2,3). Thus, consideration of a compound ψ with a base θ which runs between $i_{(1-x_*^1)}{}^j x_*^1$ and $j_{x_*}{}^k{}_{(1-x_*)}$ and having a general composition $i_{z_\psi}{}^j x_\psi{}^k{}_{(1-x_\psi-z_\psi)}$ is defined as follows.

$$p = (x_*-x_*^1)/(1-x_*)$$

$$x_\psi = x_*^1 + y_\psi p,\ z_\psi = 1-x_*^1 - y_\psi(1+p),\ y_\psi = 1-x_\psi - z_\psi \qquad (18)$$

Thus, the free energy of the compound ψ is

$$F^\psi = z_\psi F_i^\theta + x_\psi F_j^\theta + y_\psi F_k^\theta + (1-(y_\psi/x_\psi))\Delta F_A \qquad (19)$$
$$+ (y_\psi/(1-x_\psi))\Delta F_B + RT(y_\psi \ell n y_\psi + z_\psi \ell n z_\psi - (1-x_\psi)\ell n(1-x_\psi))$$

where

$$\Delta F_A = x_*^1(1-x_*^1)[(1-x_*^1)L_{ij} + x_*^1 L_{ij} - C_{ij}^\psi] \text{ cal/g.at.} \qquad (20)$$

and

$$\Delta F_B = x_*(1-x_*)[x_* L_{jk} + (1-x_*)L_{kj} - C_{jk}^\psi] \text{ cal/g.at.} \qquad (21)$$

where the L and C values in Equations 20 and 21 are defined for the component binary systems. These equations permit calculation of all compound/solution phase interactions. The solution phase interactions are carried out along the lines indicated earlier (1) on a pairwise basis. After each pairwise calculation has been completed, the results are combined to yield the most stable configuration.

The analyses of the Ti-Mo, Ti-Mn, Ti-Cr, Mo-Cr and Mo-Mn binary systems coupled with the description of the tetragonal TiMn and Laves type $TiCr_2$ phases given in Table 31 generate the $\beta/\varepsilon/\lambda$ and $\beta/\varepsilon/\tau$ equilibria shown in Figures 17-20. These figures also

show the reported experimental results taken from the collation of Molchanov (70). In the Ti-Cr-Mo case shown in Figures 17 and 18, the calculated trajectory of the $\beta/\varepsilon/\lambda$ eutectoid is shown between 920°K where it starts on the TiCr edge) and 600°K as it nears the Ti-Mo edge. Figure 18 compares the calculated and observed sections at 873°K thus providing confirmation for the calculated trajectory. It should be noted that the difference between the calculated and observed $\beta/\beta+\lambda$ boundaries at 1173°K and 1573°K in the Ti-Cr-Mo ternary system are comparable to the differences in the Ti-Cr binary where the calculated values accurately reflect the most recent experimental results (45-47).

The $\beta/\varepsilon/\tau$ calculations in Ti-Mo-Mn shown in Figures 19 and 20 compare well with the observed results (70) at 823°K, 1023°K and 1223°K. Figure 19 shows the trajectory of the $\beta/\varepsilon/\tau$ eutectoid which starts on the Ti-Mn edge at 815°K and moves toward the Ti-Mo edge as the temperature is lowered.

VII. CALCULATION OF THE Cb-Cr-Zr, Cb-Cr-Hf, Cb-Cr-Mo and Cb-Ti-Zr PHASE DIAGRAMS

Development of oxidation resistant columbium-base alloys which can be used at high temperatures has been hampered by limited phase diagram and thermochemical data. Accordingly, analyses of the component binary systems of the Cb-Cr-Zr, Cb-Cr-Hf, Cb-Cr-Mo and Cb-Ti-Zr phase diagrams were performed. The results, shown in Tables 32 and 33, were synthesized to yield the binary and ternary phase diagrams shown in Figures 21-29. The Cb-Cr binary system, which was previously analyzed on the basis of regular solutions (14), with predicted values of L = 780, B = 6120 and C = 18,000 cal/g.at., respectively, is characterized by a slightly more complex description in Table 33. The present description is in good agreement with recent phase diagram (69) and thermochemical data (71). The description of the Hf-Cb given in Table 32 is exactly the same as that employed earlier (1) and yields the phase diagram shown in Figure 23 which is in excellent agreement with recent observations by Carpenter, et. al. (72).

The earlier description of L = 4297, B = 6934 and E = 6934 cal./g.at. (1) for the Zr-Cb system has been revised as shown in Table 32 to provide a more accurate calculation of the miscibility gap maximum and monotectoid temperatures.

Figures 25 and 26 show calculated isothermal sections and limited experimental results (73) for the Cb-Cr-Zr case. The $ZrCr_2$-$CbCr_2$ quasi-binary system exhibits nearly linear behavior (74) in accordance with the present description. Figure 27 shows several calculated Cb-Cr-Hf sections which are qualitatively similar to the Cb-Cr-Zr cases in Figures 25 and 26.

The Cb-Cr-Mo system provides an interesting case since extensive phase equilibria and oxidation data are available (75-77).*

---

*It should be noted that the compilation (77) incorrectly reports the results at 1200°C (75) in weight percent when the original results (75) were given in atomic percent.

As indicated earlier, the Cb-Cr case is supported by experimental data on the heat of formation of $CbCr_2$ (71). In addition, the calculated miscibility gap in Mo-Cr with a maximum calculated at 1153°K is in agreement with thermochemical data. It is not possible to infer interaction parameters for the Cb-Mo system directly from the phase diagram. Application of estimation procedures developed and applied uniformly to all the transition metals yield small positive interaction parameters for the Cb-Mo case. Recently, Singhal and Worrell (63) reported thermochemical data for Ta-W, Cb-Mo and Ta-Mo at 1473°K. The bcc solutions in these systems can be approximated by regular solution parameters -6400, -8800 and -10400 cal/g.at. respectively. In order to evaluate the Singhal-Worrell result, which is somewhat unexpected,* an analysis of the bcc phase in the Mo-Cb-Cr system was performed as shown in Figures 28 and 29. The critical feature in this analysis was the miscibility gap which is observed at 1273°K (76,77) and 1473°K (75,77). Reference to the experimental 1273°K and 1473°K panels in Figure 28 shows that the miscibility gap extends far over to the Mo-Cr edge. This observation strongly suggests that the interaction parameter for the bcc phase in Mo-Cb is a large negative quantity supporting the Singhal-Worrell result. This conclusion stems from the fact that if $B \cong 4600$ for Mo-Cr, then the gap maximum occurs at 1157°K. In the Nb-Cr case, B = 5500, hence the gap maximum occurs at 1383°K. If the Mo-Cb system were characterized by B = 0, then no gap would be stable in Mo-Cr-Cb at 1473°K, and at 1273°K the gap would be covered by the $\beta + \lambda$ equilibria. Thus, negative values of B for Mo-Cb are implied leading to an isolated gap at high temperatures with a summit temperature above 1473°K (see pp. 299-300 of Reference 1). If a value of B = -8800 is chosen for Mo-Cb in keeping with the Singhal-Worrell result, the miscibility gap extends

*It should be noted that the compilation (77) incorrectly reports the results at 1200°C (75) in weight percent when the original results (75) were given in atomic percent.

far into the ternary at 1273°K and 1473°K. Reduction in magnitude to B = -5500 yields the results shown in Figures 28 and 29 which show conformity between the calculated and observed miscibility gaps at 1273°K and 1473°K. In addition, it should be noted that B = -3178 for Cr-V which is the analogue of Mo-Cb (i.e., Table XXI, p. 188 of Reference 1).

On this basis the interaction parameter for the bcc phase in Mo-Cb was set equal to -5500 cal/g.at. The value L = -7100 is based on the bcc/liquid equilibrium in Mo-Cb. Comparison of the calculated and observed bcc/liquid equilibria at 2650°K and 2400°K shown in Figure 29 yields reasonable agreement. Thus, the present description provides a means for calculating the entire ternary phase diagram and the thermochemical properties. The summit conditions corresponding to the peak of the isolated miscibility gap are 1626°K, 21 a/o Mo and 50 a/o Cr. This description could be employed in performing a detailed analysis of the oxidation behavior of Cb-Cr-Mo alloys (76).

Figure 29 shows a final check on the Ti-Zr, Ti-Cb and Cb-Zr values in Table 32. Here the calculated Zr-Ti-Cb section at 843°K is in excellent agreement with the observed section (78).

VIII. PREDICTION OF EUTECTIC TROUGHS AND MINIMUM MELTING POINTS IN THE COLUMBIUM-ALUMINUM-CHROMIUM SYSTEM

Fabrication of in-situ composites by means of controlled directional solidification has produced a new family of high strength materials for application at high temperatures. While rational application of this method depends on extensive phase diagram data (i.e. location of eutectic compositions, solid-liquid tie lines, curves of twofold saturation, etc.), such information is presently not available for most three-component systems. It is virtually nonexistent for systems containing four or more elements. Recently (2), the Cb-Ni-Cr system was calculated in detail in order to demonstrate application of the computational method to a problem of current interest. Comparison with limited experimental data was found to yield good results (2). The present prediction of the eutectic troughs and minimum melting points in the high temperature region of the Cb-Al-Cr system (bounded by Cr-Cb-$CbAl_3$-Cr_2Al_3) is designed to illustrate how detailed information is provided by the method for application to a system of potential interest.

The Cb-Al system is displayed in Figure 30 and Table 34. No thermochemical measurements are available for comparison with the calculations which describe the liquid and bcc phases as being regular solutions. Apart from the distortions produced by treating the Cb_3Al and Cb_2Al phases as line compounds, the computed diagram agrees with the observed diagram (47) to within 30°K and 3 a/o.

The present description of the Cr-Al system is shown in Table 35 and Figure 30. The bcc and liquid phases are described as regular solutions as indicated in Table 35. The aluminum-rich part of the diagram is complicated by a series of compound phases with melting points below 1200°K which should not influence the calculation of the liquidus surface or the isothermal sections above 1200°K. The foregoing descriptions of Cb-Cr, Cb-Al and Cr-Al are used to calculate the Cr-Cb-Al diagram by using the description of Cb-Al-Cr counterphases shown in Table 36. The results are com-

pared with limited experimental data (78,79) in Figures 31-33. Before considering the calculated results and their implications, it is instructive to note a discrepancy in the experimental results obtained at 1273°K (79), 1473°K (80) and 1773°K (80) concerning the σ and W phases. As shown in Figure 31, the experimental 1273°K study (79) suggests that the Cb_3Al (W) phase and the Cb_2Al (σ) phase both propagate into the ternary at constant Cb, i.e. $Cb_3(Al,Cr)$ (W) and $Cb_2(Al,Cr)$(σ). By contrast, the experimental 1473°K study (80) suggests that these phases propagate at constant Al, i.e. as $Al(Cb,Cr)_3$ and $Al(Cb,Cr)_2$. At 1773°K the same investigators (80) display the ternary σ phase as $Al(Cb,Cr)_2$ in agreement with their results at 1473°K. However, the stoichiometry of the W phase is represented to be between $Cb_3(Al,Cr)$ and $Al(Cb,Cr)_3$. In view of this conflicting information, initial consideration of both σ and W phases was carried out using the constant Cb and the constant Al trajectories. By comparing the initial results with the experimental findings at 1273°K, 1473°K and 1773°K, it was concluded that the best description resulted by treating the W phase as $Cb_3(Al,Cr)$ and the σ phase as $Al(Cb,Cr)_2$. This description is displayed in Table 36.

The liquidus projection shown in Figure 32 yields the minimum melting point within the confines of the Cr-Cb-$CbAl_3$-Cr_2Al_3 composition space at 1590°K and 54 a/o Al, 34 a/o Cr and 12 a/o Cb. It is possible that such a composition might provide rather interesting properties since the 1473°K section suggests that this composition would consist of a $CbAl_3$ precipitate in a matrix of a 55 Cr, 40 Al, 5 Cb. Such a composite could combine unusual strength and oxidation resistance. In particular, if the $CbAl_3$ phase could be unidirectionally solidified to yield an in-situ composite, then the 55 Cr, 40 Al, 5 Cb matrix could provide a means for obtaining high strength and oxidation resistance.

The liquidus projection in Figure 32 shows the quasi-binary eutectic between Cr_2Al_2(ρ) and $CbAl_3$(τ) at 1630°K and 63 a/o Al, 30 a/o Cr and 7 a/o Cb.

Comparison of the calculated and observed sections at 1273°K and 1473°K yields good results. However, the 1773°K section shows a discrepancy in that the λ-τ quasi-binary reported in the experimental study is not stable in the calculations. In view of the thermochemistry of the component binary systems (i.e. Cb-Al and Cr-Al exhibit substantial free energies of formation, while Cb-Cr exhibits free energies of formation which are barely negative) and the observed 1700°K peritectic in Cr-Al near $Cr_{0.55}Al_{0.45}$ (see liquidus projection) there is substantial reason to question the stable λ-τ quasi-binary shown in the experimental 1773°K section.

IX. CALCULATION OF THE EFFECTS OF CHROMIUM AND NICKEL ADDITIONS ON THE METAL-METAL CARBIDE EUTECTIC IN THE IRON-CARBON-TITANIUM SYSTEM

Metal-metal carbide composites which have been fabricated by means of controlled directional solidification techniques have been found to exhibit attractive high temperature properties. Since little or no data exist concerning the melting characteristics of multicomponent metal-metal carbide systems, the current computational methods have been applied to deal with the Fe-TiC "basis ternary." As a subsequent step, the effects of chromium and nickel additions to the iron matrix phase have been calculated by an approximate method in order to evaluate the effect of these additions on the composition of the metal-metal carbide eutectic.

In order to carry out this analysis of the Fe-C-Ti-Cr-Ni system, a total of ten binary phase diagrams (Fe-Ti, Fe-C, Fe-Ni, Fe-Cr, Ti-C, Ti-Ni, Ti-Cr, Ni-C, Cr-C and Ni-Cr) must be described. Reference 3 deals with Fe-Ni, Fe-Cr and Ni-Cr, while Ti-Cr is detailed in Section VI. The remaining six binary systems are considered below.

The description of the Fe-Ti system is summarized in Table 37. Figure 34 shows the computed phase diagram which results from combining the lattice stability parameters (1) with the description in Table 37. The free energy difference between bcc and hcp iron given in Table 37 is shown graphically in Reference 1. The numerical description in Table 37 conforms with the earlier results (1). Numerical formulation of the free energy differences between bcc, hcp, fcc, and liquid iron has been presented (3). The computed diagram is in good agreement with the reported diagram (45-47) and the temperature for martensitic bcc→hcp reactions on cooling titanium-rich alloy computed along the lines described in Section III is in agreement with the measured M_s-composition curve (28).

Table 38 summarizes the description of the Ti-Ni system. Lattice stability values for nickel presented earlier (1) were modified (14) and are given for convenience in Table 38. Figure 34

shows the resulting phase diagram which compares well with observations (45-47). This system was analyzed previously based on a regular solution model (1). The present description which allows for additional details provides a more accurate description. Moreover, the temperature for martensitic bcc→hcp reactions on cooling titanium-rich alloys computed along the lines described earlier is in agreement with the measured M_S versus composition curve (28).

Table 39 and Figure 35 summarize the present description of the Ni-C system which has been developed with cognizance of the observed phase diagram (45-47) and recent results on carbon solubility in fcc nickel (82) and the metastable fcc-liquid-Ni_3C eutectic (83). Although the positional entropy of the interstitial fcc solid solution of carbon in nickel (84) should not be equated with that of a substitutional solid solution, which is the procedure employed here, the errors are small in the solution range of interest (i.e. less than 2 a/o C) and are compensated for by the excess free energy terms in Table 39. This computational procedure was employed to take advantage of existing computer software which is available for substitutional solution interactions.

The free energy difference between the graphitic (g) and liquid forms of carbon are estimated on the basis of the most recent measurements of the graphite/vapor/liquid triple point (85,86) and an analysis of the entropy difference between the liquid and graphitic forms of carbon (87) which has been updated to reflect the most recent values of the entropy of fusion of the diamond cubic forms of Si and Ge (1). The lattice stability of bcc and fcc carbon and the graphitic and liquid forms of Ni, Cr, Ti and Fe have been estimated on the basis of the present analyses of Ni-C, Cr-C, Ti-C and Fe-C.

Table 40 and Figure 36 summarize the current description of the Cr-C system which is treated on the basis of simple regular solutions. As in the Ni-C case, the positional entropy of the interstitial solution of carbon in bcc iron should not be calculated on the same basis as a substitution solid solution. However, since

the range of interest does not exceed 2 a/o the resulting errors are not large. The computed results are in good agreement with the recent thermochemical data of Kulkarni and Worrell (88) and the phase diagram given by Rudy (69).

Table 41 and Figure 37 display the present description of the Ti-C system in which the NaCl type titanium carbide phase which is stable over a range of composition between 40 and 50 a/o C. The present simple formulation treats this phase as a line compound $Ti_{0.56}C_{0.44}(\sigma)$ (at which the maximum melting point is observed (69)) and characterizes the bcc, liquid and graphite phases as regular solutions. It should be noted that a more detailed description of the titanium carbide (σ) phase can be developed by applying the Schottky-Wagner model to allow for stoichiometric deviations. This procedure has been applied to the Ti-C system (87). However, in the present case where interest is focussed on the Ti-Fe-C-Cr-Ni liquidus surface, the present simple line compound formulation should suffice.

The description of the iron-carbon system given in Table 42 yields the calculated Fe-C phase diagram shown in Figure 38 as well as the thermochemical properties which are compared with observation (89) in Tables 42-44. The current description also provides an adequate calculation of the austenite/martensite reactions in iron-carbon alloys (84). As in the case of the Ni-C, Cr-C and Ti-C systems described earlier, the bcc, fcc and liquid solutions are treated as substitutional solutions to take advantage of existing computer software. Table 43 shows that serious errors are not introduced by this procedure since the range of composition is restricted. In the case of liquid solutions, Table 44 shows that deviations occur at the higher carbon levels. However, these deviations appear to be well within the experimental scatter of various individual investigations (90).

The foregoing description of the binary phase diagrams has been employed to compute the liquidus boundaries shown in Figure 39. In these calculations, the quasi-binary calculation

Fe-$Ti_{0.56}C_{0.44}$ versus liquid yields the diagram in the upper left corner. Expanded compositional views at 1700°K and 1600°K which include the bcc(α), fcc(γ) and Fe_2Ti(λ) phases suggest quasi-binary eutectic formation between the $Ti_{0.56}C_{0.44}$(σ) phase and the bcc phase with a eutectic near 1680°K and a composition of 0.91(Fe) + 0.09($Ti_{0.56}C_{0.44}$). Figure 40 shows a vertical section displaying the calculated eutectic temperature and composition.

Jellinghaus (91) has reported the results of an experimental study of the Fe-C-Ti system. Before considering his results with reference to the present ternary calculations shown in Figure 39, it is important to note that he reports the melting point of Fe_2Ti(λ) as 1540°Cor 1813°K. This temperature is 110°C higher than the value of 1430°C (1703°K) given in Elliot's compilation (46) and 73°K higher than the calculated melting point (1740°K) shown in Figure 34. In addition, the temperature of the liquid/bcc/Fe_2Ti eutectic reported by Jellinghaus (91) is approximately 100°K higher than that given by Elliot (46) and Figure 34. Jellinghaus reports a quasi-binary eutectic between liquid, Fe_2Ti(λ) and titanium carbide at 1733°K at a composition of 53 a/o Fe, 37 a/o Ti, 10 a/o C and a melting point minimum for liquid→bcc iron-carbon-titanium + Fe_2Ti + titanium carbide at 1600°K at 80 a/o Fe, 6 a/o C, 14 a/o Ti. These results are not in keeping with the calculations shown in Figure 39 due to the above mentioned discrepancy in the melting point of Fe_2Ti. The present calculations place the quasi-binary between Fe_2Ti and $Ti_{0.56}C_{0.44}$ near the 1735°K and 66 a/o Fe, 33 a/o Ti, 1 a/o C. Moreover, Figure 39 does not indicate a melting point minimum for liquid→bcc iron-carbon-titanium + Fe_2Ti + titanium carbide.

Jellinghaus (91) has heated mixtures of 90 a/o Fe-5 a/o C-5 a/o Ti, 85 a/o Fe- 7.5 a/o C-7.5 a/o Ti, 80 a/o Fe-10 a/o C-10 a/o Ti, etc. to determine the minimum melting temperature. Microstructural results were employed to fix the temperature and composition of the liquid→bcc iron-carbon-titanium + titanium carbide reaction. The above mentioned experiments indicate the critical

composition between 90 Fe-10($Ti_{0.5}C_{0.5}$) and 85 Fe-15($Ti_{0.5}C_{0.5}$) with the critical temperature between 1400°C and 1470°C. These findings are in reasonable agreement with the predicted results shown in Figure 40 which correspond to 91 Fe(Ti,C)-9 ($Ti_{0.56}C_{0.44}$).

Extension of the present calculations to the Fe-C-Ti-Ni-Cr case requires solution of five component equilibrium equations. Although sufficient thermochemical information is available to perform such an analysis, computational systems are not available. However, an approximate calculation can be carried out if it is assumed that equilibrium between a liquid containing Fe, C, Ti, Ni and Cr and $Ti_{0.56}C_{0.44}$ on the one hand and the same liquid and a solid Fe-Ni-Cr alloy on the other hand is constrained by the following set of conditions,

$$y = (1-x_*)q \ , \ x = x_*q \ , \ u = u_o(1-q) \ , \text{ and } v = v_o(1-q) \quad (22)$$

where x is the atomic fraction of carbon, y is the atomic fraction of titanium, u is the atomic fraction of nickel and v is the atomic fraction of chromium, $x_* = 0.44$ (i.e. the atomic fraction of carbon in $Ti_{0.56}C_{0.44}$) and q is the composition variable along the join between $Fe_{(1-u_o-v_o)}Ni_{u_o}Cr_{v_o}$. Thus in Figure 40 $u_o = v_o = 0$ and q represents the fraction of $Ti_{0.56}C_{0.44}$ at the boundary of the liquid field. If q_1 is the liquid boundary in equilibrium with the iron-rich phase and q_2 is the liquid boundary in equilibrium with $Ti_{0.56}C_{0.44}(\sigma)$ then

$$q_1 = q_2 = q_E \text{ when } T = T_E \quad (23)$$

The remaining constraints required to obtain an approximate solution are that we can neglect the solubility of iron, nickel and chromium in σ and titanium and carbon in $Fe_{(1-u_o-v_o)}Ni_{u_o}Cr_{v_o}$. The errors introduced by assuming the validity of both these constraints will be discussed after presentation of the results of this computation.

Under these circumstances, the free energy of the five-component liquid is given by Equation 24 as

$$F^L = (1-q)[F_1+E_1] + q[F_2+E_2] + RT(q\ell nq+(1-q)\ell n(1-q)) + q(1-q)[E_3-E_2-E_1] \quad (24)$$

where

$$F_1 = (1-u_o-v_o)F^L_{Fe} + u_oF^L_{Ni} + v_oF^L_{Cr} + RT[(1-u_o-v_o)\ell n(1-u_o-v_o)+u_o\ell nu_o+v_o\ell nv_o] \quad (25)$$

$$F_2 = x_*F^L_C+(1-x_*)F^L_{Ti}+RT[(1-x_*)\ell n(1-x_*)+x_*\ell nx_*] \quad (26)$$

$$E_1 = u_o(1-u_o-v_o)L_{Fe-Ni}+v_o(1-u_o-v_o)L_{Fe-Cr}+u_ov_oL_{Ni-Cr} \quad (27)$$

$$E_2 = x_*(1-x_*)L_{C-Ti} \quad (28)$$

and

$$E_3 = x_*(1-u_o-v_o)L_{Fe-C}+(1-u_o-v_o)(1-x_*)L_{Fe-Ti}+u_ox_*L_{C-Ni} +v_ox_*L_{C-Cr}+u_o(1-x_*)L_{Ti-Ni}+v_o(1-x_*)L_{Ti-Cr} \quad (29)$$

In these equations F^L_{Fe}, F^L_{Ni}, F^L_{Cr}, F^L_C and F^L_{Ti} are the free energies of the liquid forms of pure Fe, Ni, Cr, C and Ti. The L parameters are the regular solution interaction parameters for the liquid phase in the binary systems designated. Thus, Tables 40 and 41 and Reference 3 indicate that $L_{C-Cr} = -33{,}000$, $L_{C-Ti} = -42{,}000$, $L_{Fe-Cr} = 4970 - 2.5T$ and $L_{Ni-Cr} = -2000$ cal./g.at. respectively.

Examination of Tables 28, 37, 38, 39, 43 and Reference 3 shows that the Ti-Cr, Fe-Ti, Ti-Ni, C-Ni, Fe-C, and Fe-Ni liquids are not symmetrical. In these cases the appropriate L value is the value nearest the iron component (i.e. in Fe-Ti, Fe-C) or the average of the values listed. Thus, Equation 24 is an explicit function of q and T.

In similar fashion the free energy of $Fe_{(1-u_o-v_o)}Ni_{u_o}Cr_{v_o}$ is given by

$$F^\phi = (1-u_o-v_o)F^\phi_{Fe}+u_oF^\phi_{Ni}+v_oF^\phi_{Cr}+u_o(1-u_o-v_o)\Phi_{Fe-Ni} +v_o(1-u_o-v_o)\Phi_{Fe-Cr} + u_ov_o\Phi_{Ni-Cr} +RT((1-u_ov_o)\ell n(1-u_ov_o) + u_o\ell nu_o+v_o\ell nv_o) \quad (30)$$

where ϕ is the stable form of the alloy $Fe_{(1-u_o-v_o)}Ni_{u_o}Cr_{v_o}$ (i.e. bcc or fcc) at the temperature in question and Φ_{Fe-Ni}, etc. is the interaction parameter of the ϕ phase in the binary system indicated. Finally, the free energy of the compound phase F^{Ψ} is given by Equation 31 as

$$F^{\Psi} = (1-x_*)F^{\theta}_{Ti} + x_* F^{\theta}_{C} + x_*(1-x_*)[L_{C-Ti} - C] \quad (31)$$

where $x_* = 0.44$, $\Psi = \sigma$ and θ refers to the fcc base phase for titanium carbide phase as shown in Table 41. In the case at hand, $C = 104{,}000 - 13.4T$ cal/g.at.

The conditions for equilibrium can now be specified to define $q_1[T]$ and $q_2[T]$ by means of Equations 32 and 33.

$$F^{\phi} = [F^{L} - q\partial F^{L}/\partial q] \text{ at } q = q_1 \quad (32)$$

and

$$F^{\Psi} = [F^{L} + (1-q)\partial F^{L}/\partial q] \text{ at } q = q_2 \quad (33)$$

Substituting Equations 24-31 into Equations 32 and 33 yields the following explicit results

$$0 = RT\ell n(1-q_1) + q_1^2[E_3 - E_2 - E_1] + Q_1 \quad (34)$$

and

$$0 = RT\ell n q_1 + (1-q_1)^2[E_3 - E_2 - E_1] + Q_2 \quad (35)$$

where

$$Q_1 = (1-u_o-v_o)\Delta F^{\phi\to L}_{Fe} + u_o\Delta F^{\phi\to L}_{Ni} + v_o\Delta F^{\phi\to L}_{Cr} + u_o(1-u_o-v_o)(L_{Fe-Ni} - \Phi_{Fe-Ni}) + v_o(1-u_o-v_o)(L_{Fe-Cr} - \Phi_{Fe-Cr}) + u_o v_o(L_{Ni-Cr} - \Phi_{Ni-Cr}) \quad (36)$$

and

$$Q_2 = x_*\Delta F^{\theta\to L}_{C} + (1-x_*)\Delta F^{\theta\to L}_{Ti} + x_*(1-x_*)C + RT[x_*\ell n x_* + (1-x_*)\ell n(1-x_*)] \quad (37)$$

Equations 34 and 35 can be solved explicitly for q_1 and q_2 at each temperature and the eutectic is located by applying Equa-

tion 23. Table 45 contains the results.

The first entry shows the value of T_E and q_E generated by the approximate solution for the case of $u_o = v_o = 0$. These values are to be compared with $T_E = 1680$, $q_E = 0.09$ shown in Figure 40. Thus, the approximate result yields a lower eutectic temperature and a slightly higher composition. Nevertheless, these values are still comparable with the experimental findings of Jellinghaus (91). In the present case, the errors introduced by assuming zero solubility of Ti and C in iron and zero solubility in $Ti_{0.56}C_{0.44}$ do not appear to be important. This circumstance is probably due to the fact that the free energy of formation of titanium carbide is much more negative than any other binary compounds in the systems of interest. The results in Table 45 are calculated with ϕ = bcc for iron and all of the iron-chromium alloys as well as the alloys containing 10Ni-30Cr, 10Ni-40Cr and 20Ni-30Cr. The calculations indicate that chromium additions to iron tend to increase q_E while nickel additions increase q_E. Combined additions of nickel and chromium yield the lowest values of T_E.

X. CALCULATION OF THE ACTIVITY OF METALLIC COMPONENTS IN SOLUTION PHASES

The thermochemical descriptions of the systems provided in the foregoing sections permit explicit calculation of the chemical activities of each component. In particular, if a_i^α is the activity of component i in the α solution relative to the β form of pure i, then,

$$RT\ell n a_i^\alpha = \bar{F}_i^\alpha - F_i^\beta = RT\ell n(1-x-y) + \Delta F_i^{\beta\to\alpha} + \bar{F}_{Ei}^\alpha \qquad (38)$$

Similar equations can be written for the j and k components based on the definitions displayed in Equations 236-239 of Reference 1. In the present description, the asymmetric description presented above Equation 17 yields the following results for $\bar{F}_{Ei}^\alpha$, $\bar{F}_{Ej}^\alpha$ and $\bar{F}_{Ek}^\alpha$ where

$$w = g[T] + \ell[T] - n[T]$$
$$r = h[T] - g[T]$$
$$s = m[T] - \ell[T]$$
$$t = p[T] - n[T]$$

$$\bar{F}_{Ei}^\alpha = x^2 g[T] + y^2 \ell[T] + xyw + rx^2\left[\frac{x(2-y)}{(1-y)^2} - 1\right] + sy^2\left[\frac{y(2-x)}{(1-x)^2} - 1\right] - t\frac{xy^2}{(x+y)} \qquad (39)$$

$$\bar{F}_{Ej}^\alpha = (1-x)^2 g[T] + y^2 \ell[T] - y(1-x)w + r\left[\frac{x(2-y)}{(1-y)^2} + \frac{(2-3x-2y)}{x(1-y)} - 1\right]x^2 + sy^2\left[\frac{y}{1-x} - 1\right] + t\frac{y^2}{(x+y)^2}[y(1-x) - x^2] \qquad (40)$$

and

$$\bar{F}_{Ek}^\alpha = x^2 g[T] + (1-y)^2 \ell[T] - x(1-y)w + r\left[\frac{x}{1-y} - 1\right]x^2 + sy^2\left[\frac{y(2-x)}{(1-x)^2} + \frac{(2-3y-2x)}{y(1-x)} - 1\right] + \frac{txy}{(x+y)^2}[2x+y-xy-y^2] \qquad (41)$$

REFERENCES

1. L. Kaufman and H. Bernstein, Computer Calculation of Phase Diagrams, Academic Press, New York (1970).

2. L. Kaufman and H. Nesor, Conference on In-Situ Composites, F. D. Lemkey and E. R. Thompson Eds., September 1972, Lakeville, Connecticut (proceedings to be published).

3. L. Kaufman and H. Nesor, International Symposium in Thermodynamics of Alloys, Munster, West Germany (1972)(to be published in Zeit. f. Metallkunde).

4. L. Kaufman and H. Nesor, Proceedings of the Second International Conference on Titanium, Cambridge, Massachusetts, May 1972, R. I. Jaffee Ed., Met. Soc. A.I.M.E., New York, New York.

5. V. Heine, Phase Stability in Metals and Alloys, P. S. Rudman, J. Stringer and R. I. Jaffee Eds., McGraw-Hill (1967) p. 111.

6. L. Kaufman, Progress in Material Science (1969) 14, pp. 57, 58.

7. V. Heine and D. Weaire, Solid State Physics (1970) 24, pp. 433-439.

8. J. Inglesfield, International Symposium on Metallurgical Chemistry, O. Kubaschewski Ed., London (1971) HMSO, p. 185.

9. L. Kaufman, Ibid (Discussion) p. 347.

10. R. M. Pick, J. Phys. (France) (1967) 28, 539.

11. R. W. Shaw, J. Phys. C., (1969) 2, 2335, (Proc. Phys. Soc.).

12. D. G. Pettifor, J. Phys. C.: Solid State Physics (1970) 3, 367.

13. D. G. Pettifor, International Symposium on Metallurgical Chemistry, O. Kubaschewski Ed., London (1971) HMSO, p. 191.

14. L. Kaufman, Ibid, p. 373.

15. E. W. Collings and J. C. Ho, The Science, Technology and Application of Titanium, R. I. Jaffee and N. Promisel Eds., Pergamon (1970) p. 331.

16. E. S. Fisher and D. Dever, Ibid, p. 373.

17. I. I. Kornilov, Ibid, p. 407.

18. A. D. McQuillan, Ibid (Discussion), p. 421.

19. R. I. Jaffee, Ibid (Discussion), p. 421.

20. N. V. Ageev and L. A. Petrova, Ibid, p. 809.

21. W. Hume-Rothery, Progress in Material Science (1967) 13, 229.

22. J. R. Mihalisin, C. G. Bieber and R. T. Grant, Tr. Met. Soc. A.I.M.E. (1968) 242 2414.

23. L. Kaufman, Acta Met. (1959) 7, 575.

24. L, Kaufman, Phase Stability in Metals and Alloys, P. S. Rudman, J. Stringer and R. I. Jaffee Eds., McGraw-Hill (1967) p. 125.

25. H. Kaneko and Y. C. Huang, J. Japan. Inst. of Metals (1963) 27, 387.

26. L. Kaufman and H. Bernstein, The Science, Technology and Application of Titanium, R. I. Jaffee and N. Promisel Eds., Pergamon (1970) p. 361.

27. K. S. Jepson, A. R. G. Brown and J. Gray, Ibid, p. 677.

28. Y. C. Huang, S. Suzuki, H. Kaneko and T. Sato, Ibid, p. 691.

29. L. Kaufman, Energetics in Metallurgical Phenomena, W. Mueller Ed., Gordon Breach Science Publishers, New York, (1967) 3, 53.

30. C. Hammond and P. M. Kelley, The Science, Technology and Application of Titanium, R. I. Jaffee and N. Promisel Eds., Pergamon (1970) p. 659.

31. M. J. Blackburn, Ibid, p. 633.

32. L. N. Guseva, L. A. Petrova and I. A. Ogloblina, Dokl. Akad. Nauk SSSR (1969) 185, 799 (Tr. Sov. Phys. Dokl. (1969)) 14, 367.

33. R. H. Ericksen, R. Taggart and D. H. Polonis, Tr. Met. Soc. A.I.M.E. (1969) 245, 359.

34. L. Kaufman, E. V. Clougherty and R. J. Weiss, Acta Met. (1963) 11, 323.

35. A. P. Miodownik, International Symposium on Metallurgical Chemistry, O. Kubaschewski Ed., London (1971) HMSO, p. 233.

36. I. Ansara, Ibid, p. 403.

37. H. Harvig, T. Nishizawa and B. Uhrenius, Ibid, p. 431.

38. J. F. Counsell, E. B. Lees and P. J. Spencer, Ibid, p. 451.

39. J. F. Counsell and O. Kubaschewski, Ibid, p. 649.

40. C. H. P. Lupis and H. Gaye, Ibid, p. 469.

41. K. A. Gschneider and R. B. Griffin, Met. Tr. (1971) 2, 2525.

42. N. A. Vanderpuye and A. P. Miodownik, The Science, Technology and Application of Titanium, R. I. Jaffee and N. Promisel Eds., Pergamon (1970) p. 719.

43. J. F. Breedis and L. Kaufman (1971) 2, 2359.

44. L. Bidwell, AFML (Private Communication).(See also P. Ehrlich, Zeit. Anorg. Chem. (1949) 249 1.)

45. M. Hansen and K. Anderko, Constitution of Binary Alloys, McGraw-Hill, New York (1958).

46. R. P. Elliot, Ibid, First Supplement (1965).

47. F. A. Shunk, Ibid, Second Supplement (1968).

48. R. Hultgren, R. L. Orr, P. D. Anderson and K. K. Kelley, Selected Values of Thermodynamic Properties of Metals and Alloys, John Wiley (1963).

49. R. Hultgren, et. al., Supplement to Selected Values of Thermodynamic Properties of Metals and Alloys, University of California (Berkeley) (1966-1971).

50. D. B. Hunter, Tr. Met. Soc. A.I.M.E. (1966) 236, 900.

51. B. Predel and D. W. Stein, Acta Met. (1972) 20, 515.

52. D. Clark, K. S. Jepson and C. J. Lewis, J. Inst. Metals (1962-1963) 91, p. 197.

53. M. J. Blackburn, Tr. Met. Soc. A.I.M.E. (1967) 239, p. 1200.

54. F. A. Crossley, Ibid (1968) 242, p. 726.

55. M. J. Blackburn, Ibid (1968) 242, p. 728.

56. H. L. Gegel and M. Hoch, Proceedings of the Second International Conference on Titanium, Cambridge, Massachusetts, May 1972, R. I. Jaffee Ed., Met. Soc. A.I.M.E., New York.

57. G. H. Narayaman and T. F. Archibold, Tr. Met. Soc. A.I.M.E. (1970) 1, p. 2281.

58. J. C. Williams, B. S. Hickman and D. H. Leslie, Met. Trans. (1971) 2, p. 477.

59. E. J. Rolinski, M. Hoch anc C. Oblinger, Met. Trans. (1971) 2, p. 2613.

60. M. Hoch and R. Viswanathan, Met. Trans. (1971) 2, p. 2765.

61. J. V. Hackworth, M. Hoch and H. L. Gegel, Met. Tr. (1971) 2, p. 1799.

62. E. J. Rolinski, M. Hoch and C. J. Oblinger, Met. Tr. (1972) 3, p. 1413.

63. S. C. Singhal and W. L. Worrell, International Symposium on Metallurgical Chemistry, O. Kubaschewski Ed., HMSO, London (1971) p. 149.

64. J. L. Meijering, Philips Research Reports (1950) 5, p. 333.

65. I. I. Kornilov and R. S. Polyakova, Izvest. Akad. Nauk S.S.S.R. Otdel. Tekh. Nauk Met. I. Toplivo (1961) 4, 76 (Report 183, DMIC, Battelle-Columbus (1963) p (162-1)-63).

66. Report 152, DMIC, Battelle-Columbus (1961) p. 113 (Office of Technical Services PB 171421).

67. I. I. Kornilov, Zhur. neorg. Khim. (1958) 3, 879 (Report 152, DMIC, Battelle-Columbus (1961) p. 105--Office of Technical Services PB 171421).

68. M. J. Pool, R. Speiser and G. St. Pierre, Tr. Met. Soc. A.I.M.E. (1967) 239, p. 1180.

69. E. Rudy, Compendium of Phase Diagram Data, AFML-TR-65-2, Part V, 1969, Wright-Patterson Air Force Base, Ohio.

70. Ye. K. Molchanov, Atlas of Diagrams of State of Titanium Alloys, Translated from the Russian by Foreign Technology Division, Wright-Patterson Air Force Base, Ohio, FTD-MT-65-387, August 1967.

71. J. F. Martin, F. Muller and O. Kubaschewski, Tr. Faraday Soc. (1970) 66, p. 1065.

72. R. W. Carpenter, C. T. Liu and P. G. Mardon, Met. Trans. (1971) 2, p. 125.

73. M. M. Savel'eva and N. V. Grum-Grzhimaylo, Iz. Akad. Nauk S.S.S.R., Metally (1969) 1, p. 224.

74. I. I. Kornilov, S. P. Alisova and P. B. Budberg, Iz. Akad. Nauk S.S.S.R., Neorg. Mater. (1965) 1, p. 2205.

75. M. I. Zakharova and D. A. Prokoshkim, Iz. Akad. Nauk S.S.S.R., Otdel. Tekh Nauk Met. I. Topliva (1961) 4, 59.

76. H. J. Goldschmidt and J. A. Brandt, J. L. C. M. (1961) 3, p. 44.

77. DMIC Report 183, 7 February 1963, "Binary and Ternary Phase Diagrams of Cb, Mo, Ta and W," Battelle Memorial Institute, Columbus, Ohio.

78. Toshio Doy, Masahiro Kitada and Fumihiko Ishida, J. Japan. Inst. of Metals (1968) 32, p. 684.

79. C. R. Hunt and A. Ramon, Zeit. Metallkunde (1968) 59, p. 701.

80. V. N. Svechnikov, A. K. Schurin and G. P. Dimytreva, Nauka (1964) 104.

81. R. H. German and G. R. St. Pierre, Met. Tr. (1972) 3, 2819.

82. J. Swartz, Met. Tr. (1971) 2, 2318.

83. H. Strong, Tr. Met. Soc. A.I.M.E. (1965) 233, 643.

84. L. Kaufman, S. V. Radcliffe and M. Cohen, Decomposition of Austenite by Diffusional Processes, V. F. Zackay and H. I. Aaronson Eds., published by A.I.M.E. and Interscience Publishers, New York (1962) p. 313.

85. G. J. Schoessow, "Graphite Triple Point and Solidus-Liquidus Interface Experimentally Determined to 1000 Atmospheres," NASA CR-1148, July 1968.

86. N. S. Diaconis, E. R. Stover, J. Hook and G. J. Catalano, "Graphite Melting Behavior," AFML-TR-71-119, July 1971.

87. L. Kaufman and E. V. Clougherty, Metallurgy at High Pressures and High Temperatures, K. A. Gschneider, M. T. Hepworth and N. A. P. Parlee Eds., Metallurgical Society Conferences, Volume 22 (1964) p. 322, Gordon and Breach, New York.

88. A. D. Kulkarni and W. L. Worrell, Met. Tr. (1972) 3, 2363.

89. J. Chipman, Met. Tr. (1972) 3, 55.

90. H. Schenk, E. Steinmetz and M. Gloz, Metallurgical Chemistry, O. Kubaschewski Ed., HMSO, London (1972) p. 445.

91. W. Jellinghaus, Arch. f. d. Eisenhutt (1969) 40, 843.

TABLE 1

DEBYE TEMPERATURES AND ELECTRONIC SPECIFIC HEAT COEFFICIENTS FOR BCC AND HCP TITANIUM

H.C.P.	DEBYE TEMPERATURE ^{o}K	ELECTRONIC γ (cal/g.at.$^{o}K^{2}$)
Kaufman (1959) (23)	365	8.25×10^{-4}
Collings and Ho (1968) (15)	420	8.03×10^{-4}
BCC		
Kaufman (1959) (23)	299	5.7×10^{-4}
Collings and Ho (1968) (15)	295	17.4×10^{-4}

BCC MINUS HCP ENTROPY COMPONENTS at 1155^{o}K	Vibrational (cal/g.at.^{o}K)	Electronic (cal/g.at.^{o}K)
Kaufman (1959) (23)	+1.180	-0.294
Collings and Ho (1968) (15)	+2.110	+1.082

ENTROPY DIFFERENCE (at 1155^{o}K, cal./g.at.^{o}K) (BCC-HCP)	
Kaufman (1959) (23)	+0.89 (1.05 at 300^{o}K)
Collings and Ho (1968) (15)	+3.19 (2.25 at 300^{o}K)
OBSERVED (23)	+0.90

TABLE 2

SUMMARY OF REGULAR SOLUTION PARAMETERS FOR
THE Ti-Al, Ti-Sn, Ti-Mo, Ti-V and Mo-Mn SYSTEMS
(cal/g.at.)

	L	B	E
Ti-Al	-24100 + 10.0T	-28000 + 10.0T	-29000 + 10.0T
Ti-Sn	-18000	-21000	-21000
Ti-Mo	1560	1241	6121
Ti-V	871	2659	4084
Ti-Mn	-3000	0	+8540
Ti-Cr*	0	3000	+9420
	3000	6000	+12420

*$F_E^{\beta} = (1-x)[(1-x)3000 + x6000]$ where $x = x_{Cr}$

TABLE 3

CALCULATED M_s TEMPERATURES FOR DIFFERENT ATOM FRACTIONS OF ALLOYING ELEMENTS IN THE Ti-Al-V SYSTEM

Al	V	T°K	Al	V	T°K	Al	V	T°K
0.00	0.00	1105	0.02	0.00	1135	0.04	0.00	1163
0.00	0.01	1060	0.02	0.01	1089	0.04	0.01	1118
0.00	0.02	1015	0.02	0.02	1044	0.04	0.02	1073
0.00	0.03	970	0.02	0.03	999	0.04	0.03	1028
0.00	0.04	926	0.02	0.04	955	0.04	0.04	983
0.00	0.05	882	0.02	0.05	911	0.04	0.05	939
0.00	0.06	837	0.02	0.06	866	0.04	0.06	895
0.00	0.07	794	0.02	0.07	822	0.04	0.07	851
0.00	0.08	750	0.02	0.08	779	0.04	0.08	807
0.00	0.09	707	0.02	0.09	735	0.04	0.09	763
0.00	0.10	663	0.02	0.10	692	0.04	0.10	720
0.00	0.11	621	0.02	0.11	649	0.04	0.11	677
0.00	0.12	578	0.02	0.12	607	0.04	0.12	634
0.00	0.13	535	0.02	0.13	564	0.04	0.13	592
0.00	0.14	493	0.02	0.14	522	0.04	0.14	550
0.00	0.15	451	0.02	0.15	480	0.04	0.15	508
0.00	0.16	410	0.02	0.16	438	0.04	0.16	466
0.00	0.17	368	0.02	0.17	397	0.04	0.17	424
0.00	0.18	327	0.02	0.18	355	0.04	0.18	383
0.00	0.19	286	0.02	0.19	314	0.04	0.19	342
0.00	0.20	245	0.02	0.20	274	0.04	0.20	301
0.01	0.00	1120	0.03	0.00	1149	0.05	0.00	1177
0.01	0.01	1075	0.03	0.01	1104	0.05	0.01	1132
0.01	0.02	1030	0.03	0.02	1059	0.05	0.02	1087
0.01	0.03	985	0.03	0.03	1014	0.05	0.03	1042
0.01	0.04	940	0.03	0.04	969	0.05	0.04	997
0.01	0.05	896	0.03	0.05	925	0.05	0.05	953
0.01	0.06	852	0.03	0.06	881	0.05	0.06	908
0.01	0.07	808	0.03	0.07	837	0.05	0.07	865
0.01	0.08	765	0.03	0.08	793	0.05	0.08	821
0.01	0.09	721	0.03	0.09	750	0.05	0.09	777
0.01	0.10	678	0.03	0.10	706	0.05	0.10	734
0.01	0.11	635	0.03	0.11	663	0.05	0.11	691
0.01	0.12	592	0.03	0.12	621	0.05	0.12	648
0.01	0.13	550	0.03	0.13	578	0.05	0.13	606
0.01	0.14	508	0.03	0.14	536	0.05	0.14	563
0.01	0.15	466	0.03	0.15	494	0.05	0.15	521
0.01	0.16	424	0.03	0.16	452	0.05	0.16	479
0.01	0.17	383	0.03	0.17	411	0.05	0.17	438
0.01	0.18	341	0.03	0.18	369	0.05	0.18	397
0.01	0.19	300	0.03	0.19	328	0.05	0.19	355
0.01	0.20	260	0.03	0.20	287	0.05	0.20	315

TABLE 4

CALCULATED M_s TEMPERATURES FOR DIFFERENT ATOM FRACTIONS OF ALLOYING ELEMENTS IN THE Ti-Al-V SYSTEM

Al	V	T°K	Al	V	T°K	Al	V	T°K
0.06	0.00	1191	0.08	0.00	1218	0.10	0.00	1245
0.06	0.01	1146	0.08	0.01	1173	0.10	0.01	1199
0.06	0.02	1101	0.08	0.02	1128	0.10	0.02	1154
0.06	0.03	1056	0.08	0.03	1083	0.10	0.03	1109
0.06	0.04	1011	0.08	0.04	1038	0.10	0.04	1064
0.06	0.05	966	0.08	0.05	993	0.10	0.05	1019
0.06	0.06	922	0.08	0.06	949	0.10	0.06	975
0.06	0.07	878	0.08	0.07	905	0.10	0.07	931
0.06	0.08	834	0.08	0.08	861	0.10	0.08	887
0.06	0.09	791	0.08	0.09	817	0.10	0.09	843
0.06	0.10	748	0.08	0.10	774	0.10	0.10	800
0.06	0.11	705	0.08	0.11	731	0.10	0.11	757
0.06	0.12	662	0.08	0.12	688	0.10	0.12	714
0.06	0.13	619	0.08	0.13	646	0.10	0.13	671
0.06	0.14	577	0.08	0.14	603	0.10	0.14	629
0.06	0.15	535	0.08	0.15	561	0.10	0.15	587
0.06	0.16	493	0.08	0.16	519	0.10	0.16	545
0.06	0.17	451	0.08	0.17	478	0.10	0.17	503
0.06	0.18	410	0.08	0.18	436	0.10	0.18	462
0.06	0.19	369	0.08	0.19	395	0.10	0.19	420
0.06	0.20	328	0.08	0.20	354	0.10	0.20	379
0.07	0.00	1205	0.09	0.00	1232	0.11	0.00	1258
0.07	0.01	1159	0.09	0.01	1186	0.11	0.01	1212
0.07	0.02	1114	0.09	0.02	1141	0.11	0.02	1167
0.07	0.03	1069	0.09	0.03	1096	0.11	0.03	1122
0.07	0.04	1024	0.09	0.04	1051	0.11	0.04	1077
0.07	0.05	980	0.09	0.05	1006	0.11	0.05	1032
0.07	0.06	936	0.09	0.06	962	0.11	0.06	988
0.07	0.07	892	0.09	0.07	918	0.11	0.07	944
0.07	0.08	848	0.09	0.08	874	0.11	0.08	900
0.07	0.09	804	0.09	0.09	831	0.11	0.09	856
0.07	0.10	761	0.09	0.10	787	0.11	0.10	813
0.07	0.11	718	0.09	0.11	744	0.11	0.11	769
0.07	0.12	675	0.09	0.12	701	0.11	0.12	726
0.07	0.13	632	0.09	0.13	658	0.11	0.13	684
0.07	0.14	590	0.09	0.14	616	0.11	0.14	641
0.07	0.15	548	0.09	0.15	574	0.11	0.15	599
0.07	0.16	506	0.09	0.16	532	0.11	0.16	557
0.07	0.17	465	0.09	0.17	490	0.11	0.17	515
0.07	0.18	423	0.09	0.18	449	0.11	0.18	474
0.07	0.19	382	0.09	0.19	408	0.11	0.19	433
0.07	0.20	341	0.09	0.20	367	0.11	0.20	392

TABLE 5

CALCULATED M_s TEMPERATURES FOR DIFFERENT ATOM FRACTIONS OF ALLOYING ELEMENTS IN THE Ti-Al-V SYSTEM

Al	V	T°K	Al	V	T°K	Al	V	T°K
0.12	0.00	1270	0.14	0.00	1295	0.16	0.00	1320
0.12	0.01	1225	0.14	0.01	1250	0.16	0.01	1274
0.12	0.02	1179	0.14	0.02	1204	0.16	0.02	1228
0.12	0.03	1134	0.14	0.03	1159	0.16	0.03	1183
0.12	0.04	1089	0.14	0.04	1114	0.16	0.04	1138
0.12	0.05	1045	0.14	0.05	1069	0.16	0.05	1093
0.12	0.06	1000	0.14	0.06	1025	0.16	0.06	1049
0.12	0.07	956	0.14	0.07	981	0.16	0.07	1004
0.12	0.08	912	0.14	0.08	937	0.16	0.08	960
0.12	0.09	869	0.14	0.09	893	0.16	0.09	917
0.12	0.10	825	0.14	0.10	849	0.16	0.10	873
0.12	0.11	782	0.14	0.11	806	0.16	0.11	830
0.12	0.12	739	0.14	0.12	763	0.16	0.12	787
0.12	0.13	696	0.14	0.13	720	0.16	0.13	744
0.12	0.14	654	0.14	0.14	678	0.16	0.14	701
0.12	0.15	611	0.14	0.15	636	0.16	0.15	659
0.12	0.16	569	0.14	0.16	593	0.16	0.16	617
0.12	0.17	528	0.14	0.17	552	0.16	0.17	575
0.12	0.18	486	0.14	0.18	510	0.16	0.18	533
0.12	0.19	445	0.14	0.19	469	0.16	0.19	492
0.12	0.20	404	0.14	0.20	428	0.16	0.20	451
0.13	0.00	1283	0.15	0.00	1308	0.17	0.00	1331
0.13	0.01	1237	0.15	0.01	1262	0.17	0.01	1286
0.13	0.02	1192	0.15	0.02	1216	0.17	0.02	1240
0.13	0.03	1147	0.15	0.03	1171	0.17	0.03	1195
0.13	0.04	1102	0.15	0.04	1126	0.17	0.04	1150
0.13	0.05	1057	0.15	0.05	1081	0.17	0.05	1105
0.13	0.06	1013	0.15	0.06	1037	0.17	0.06	1060
0.13	0.07	969	0.15	0.07	993	0.17	0.07	1016
0.13	0.08	925	0.15	0.08	949	0.17	0.08	972
0.13	0.09	881	0.15	0.09	905	0.17	0.09	928
0.13	0.10	837	0.15	0.10	861	0.17	0.10	884
0.13	0.11	794	0.15	0.11	818	0.17	0.11	841
0.13	0.12	751	0.15	0.12	775	0.17	0.12	798
0.13	0.13	708	0.15	0.13	732	0.17	0.13	755
0.13	0.14	666	0.15	0.14	690	0.17	0.14	712
0.13	0.15	624	0.15	0.15	647	0.17	0.15	670
0.13	0.16	582	0.15	0.16	605	0.17	0.16	628
0.13	0.17	540	0.15	0.17	563	0.17	0.17	586
0.13	0.18	498	0.15	0.18	522	0.17	0.18	545
0.13	0.19	457	0.15	0.19	480	0.17	0.19	503
0.13	0.20	416	0.15	0.20	439	0.17	0.20	462

TABLE 6

CALCULATED M_s TEMPERATURES FOR DIFFERENT ATOM FRACTIONS OF ALLOYING ELEMENTS IN THE Ti-Al-V SYSTEM

Al	V	T°K	Al	V	T°K	Al	V	T°K
0.18	0.00	1343	0.19	0.00	1354	0.20	0.00	1366
0.18	0.01	1297	0.19	0.01	1309	0.20	0.01	1320
0.18	0.02	1252	0.19	0.02	1263	0.20	0.02	1274
0.18	0.03	1206	0.19	0.03	1218	0.20	0.03	1229
0.18	0.04	1161	0.19	0.04	1172	0.20	0.04	1184
0.18	0.05	1116	0.19	0.05	1128	0.20	0.05	1139
0.18	0.06	1072	0.19	0.06	1083	0.20	0.06	1094
0.18	0.07	1027	0.19	0.07	1039	0.20	0.07	1050
0.18	0.08	983	0.19	0.08	994	0.20	0.08	1005
0.18	0.09	939	0.19	0.09	950	0.20	0.09	961
0.18	0.10	896	0.19	0.10	907	0.20	0.10	918
0.18	0.11	852	0.19	0.11	863	0.20	0.11	874
0.18	0.12	809	0.19	0.12	820	0.20	0.12	831
0.18	0.13	766	0.19	0.13	777	0.20	0.13	788
0.18	0.14	724	0.19	0.14	735	0.20	0.14	745
0.18	0.15	681	0.19	0.15	692	0.20	0.15	703
0.18	0.16	639	0.19	0.16	650	0.20	0.16	661
0.18	0.17	597	0.19	0.17	608	0.20	0.17	619
0.18	0.18	556	0.19	0.18	566	0.20	0.18	577
0.18	0.19	514	0.19	0.19	525	0.20	0.19	536
0.18	0.20	473	0.19	0.20	484	0.20	0.20	494

TABLE 7

CALCULATED M_s TEMPERATURES FOR DIFFERENT ATOM FRACTIONS OF ALLOYING ELEMENTS IN THE Ti-Al-Mo SYSTEM

Al	Mo	T°K	Al	Mo	T°K	Al	Mo	T°K
0.00	0.00	1105	0.02	0.00	1135	0.04	0.00	1163
0.00	0.01	1024	0.02	0.01	1054	0.04	0.01	1083
0.00	0.02	941	0.02	0.02	972	0.04	0.02	1003
0.00	0.03	858	0.02	0.03	890	0.04	0.03	922
0.00	0.04	775	0.02	0.04	808	0.04	0.04	840
0.00	0.05	690	0.02	0.05	724	0.04	0.05	758
0.00	0.06	605	0.02	0.06	640	0.04	0.06	675
0.00	0.07	520	0.02	0.07	556	0.04	0.07	591
0.00	0.08	433	0.02	0.08	470	0.04	0.08	507
0.00	0.09	346	0.02	0.09	384	0.04	0.09	422
0.00	0.10	258	0.02	0.10	297	0.04	0.10	336
0.01	0.00	1120	0.02	0.11	210	0.04	0.11	249
0.01	0.01	1039	0.03	0.00	1149	0.05	0.00	1177
0.01	0.02	957	0.03	0.01	1069	0.05	0.01	1098
0.01	0.03	874	0.03	0.02	988	0.05	0.02	1018
0.01	0.04	791	0.03	0.03	906	0.05	0.03	937
0.01	0.05	707	0.03	0.04	824	0.05	0.04	856
0.01	0.06	623	0.03	0.05	741	0.05	0.05	774
0.01	0.07	538	0.03	0.06	658	0.05	0.06	691
0.01	0.08	452	0.03	0.07	573	0.05	0.07	608
0.01	0.09	365	0.03	0.08	489	0.05	0.08	524
0.01	0.10	278	0.03	0.09	403	0.05	0.09	440
			0.03	0.10	317	0.05	0.10	355
			0.03	0.11	230	0.05	0.11	269

TABLE 8

CALCULATED M_s TEMPERATURES FOR DIFFERENT ATOM FRACTIONS OF ALLOYING ELEMENTS IN THE Ti-Al-Mo SYSTEM

Al	Mo	T°K	Al	Mo	T°K	Al	Mo	T°K
0.06	0.00	1191	0.08	0.00	1218	0.10	0.00	1245
0.06	0.01	1112	0.08	0.01	1140	0.10	0.01	1167
0.06	0.02	1032	0.08	0.02	1061	0.10	0.02	1090
0.06	0.03	952	0.08	0.03	982	0.10	0.03	1011
0.06	0.04	871	0.08	0.04	902	0.10	0.04	932
0.06	0.05	790	0.08	0.05	822	0.10	0.05	853
0.06	0.06	708	0.08	0.06	741	0.10	0.06	773
0.06	0.07	625	0.08	0.07	659	0.10	0.07	692
0.06	0.08	542	0.08	0.08	577	0.10	0.08	611
0.06	0.09	458	0.08	0.09	494	0.10	0.09	529
0.06	0.10	373	0.08	0.10	410	0.10	0.10	446
0.06	0.11	288	0.08	0.11	326	0.10	0.11	363
0.06	0.12	202	0.08	0.12	241	0.10	0.12	279
0.07	0.00	1205	0.09	0.00	1232	0.11	0.00	1258
0.07	0.01	1126	0.09	0.01	1154	0.11	0.01	1181
0.07	0.02	1047	0.09	0.02	1076	0.11	0.02	1103
0.07	0.03	967	0.09	0.03	997	0.11	0.03	1026
0.07	0.04	887	0.09	0.04	917	0.11	0.04	947
0.07	0.05	806	0.09	0.05	837	0.11	0.05	868
0.07	0.06	724	0.09	0.06	757	0.11	0.06	789
0.07	0.07	642	0.09	0.07	676	0.11	0.07	708
0.07	0.08	560	0.09	0.08	594	0.11	0.08	628
0.07	0.09	476	0.09	0.09	512	0.11	0.09	546
0.07	0.10	392	0.09	0.10	428	0.11	0.10	464
0.07	0.11	307	0.09	0.11	345	0.11	0.11	381
0.07	0.12	221	0.09	0.12	260	0.11	0.12	298

TABLE 9

CALCULATED M_s TEMPERATURES FOR DIFFERENT ATOM FRACTIONS OF ALLOYING ELEMENTS IN THE Ti-Al-Mo SYSTEM

Al	Mo	T°K	Al	Mo	T°K	Al	Mo	T°K
0.12	0.00	1270	0.14	0.00	1295	0.16	0.00	1320
0.12	0.01	1194	0.14	0.01	1220	0.16	0.01	1245
0.12	0.02	1117	0.14	0.02	1144	0.16	0.02	1170
0.12	0.03	1040	0.14	0.03	1067	0.16	0.03	1094
0.12	0.04	962	0.14	0.04	990	0.16	0.04	1018
0.12	0.05	883	0.14	0.05	913	0.16	0.05	942
0.12	0.06	804	0.14	0.06	835	0.16	0.06	864
0.12	0.07	724	0.14	0.07	756	0.16	0.07	787
0.12	0.08	644	0.14	0.08	677	0.16	0.08	709
0.12	0.09	563	0.14	0.09	597	0.16	0.09	630
0.12	0.10	482	0.14	0.10	517	0.16	0.10	550
0.12	0.11	400	0.14	0.11	435	0.16	0.11	470
0.12	0.12	317	0.14	0.12	354	0.16	0.12	390
0.12	0.13	233	0.14	0.13	271	0.16	0.13	308
0.13	0.00	1283	0.15	0.00	1308	0.16	0.14	226
0.13	0.01	1207	0.15	0.01	1232	0.17	0.00	1331
0.13	0.02	1131	0.15	0.02	1157	0.17	0.01	1257
0.13	0.03	1054	0.15	0.03	1081	0.17	0.02	1182
0.13	0.04	976	0.15	0.04	1004	0.17	0.03	1107
0.13	0.05	898	0.15	0.05	927	0.17	0.04	1032
0.13	0.06	819	0.15	0.06	850	0.17	0.05	956
0.13	0.07	740	0.15	0.07	772	0.17	0.06	879
0.13	0.08	661	0.15	0.08	693	0.17	0.07	802
0.13	0.09	580	0.15	0.09	614	0.17	0.08	724
0.13	0.10	499	0.15	0.10	534	0.17	0.09	646
0.13	0.11	418	0.15	0.11	453	0.17	0.10	567
0.13	0.12	335	0.15	0.12	372	0.17	0.11	488
0.13	0.13	252	0.15	0.13	290	0.17	0.12	408
			0.15	0.14	207	0.17	0.13	327
						0.17	0.14	245

TABLE 10

CALCULATED M_s TEMPERATURES FOR DIFFERENT ATOM FRACTIONS OF ALLOYING ELEMENTS IN THE Ti-Al-Mo SYSTEM

Al	Mo	T°K	Al	Mo	T°K	Al	Mo	T°K
0.18	0.00	1343	0.19	0.00	1354	0.20	0.00	1366
0.18	0.01	1269	0.19	0.01	1281	0.20	0.01	1293
0.18	0.02	1195	0.19	0.02	1207	0.20	0.02	1219
0.18	0.03	1120	0.19	0.03	1133	0.20	0.03	1146
0.18	0.04	1045	0.19	0.04	1058	0.20	0.04	1072
0.18	0.05	970	0.19	0.05	983	0.20	0.05	997
0.18	0.06	894	0.19	0.06	908	0.20	0.06	922
0.18	0.07	817	0.19	0.07	832	0.20	0.07	846
0.18	0.08	740	0.19	0.08	755	0.20	0.08	770
0.18	0.09	662	0.19	0.09	678	0.20	0.09	693
0.18	0.10	584	0.19	0.10	600	0.20	0.10	616
0.18	0.11	505	0.19	0.11	522	0.20	0.11	538
0.18	0.12	425	0.19	0.12	443	0.20	0.12	460
0.18	0.13	345	0.19	0.13	363	0.20	0.13	381
0.18	0.14	264	0.19	0.14	283	0.20	0.14	301
			0.19	0.15	202	0.20	0.15	221

TABLE 11

CALCULATED M_s TEMPERATURES FOR DIFFERENT ATOM FRACTIONS OF ALLOYING ELEMENTS IN THE Ti-3a/oMn-Al-V SYSTEM

Al	V	T°K	Al	V	T°K	Al	V	T°K
0.00	0.00	758	0.02	0.00	792	0.04	0.00	825
0.00	0.01	716	0.02	0.01	749	0.04	0.01	782
0.00	0.02	673	0.02	0.02	707	0.04	0.02	739
0.00	0.03	631	0.02	0.03	664	0.04	0.03	697
0.00	0.04	589	0.02	0.04	622	0.04	0.04	655
0.00	0.05	547	0.02	0.05	581	0.04	0.05	613
0.00	0.06	506	0.02	0.06	539	0.04	0.06	572
0.00	0.07	464	0.02	0.07	498	0.04	0.07	530
0.00	0.08	423	0.02	0.08	457	0.04	0.08	489
0.00	0.09	383	0.02	0.09	416	0.04	0.09	449
0.00	0.10	342	0.02	0.10	375	0.04	0.10	408
0.00	0.11	302	0.02	0.11	335	0.04	0.11	368
0.00	0.12	262	0.02	0.12	295	0.04	0.12	328
0.00	0.13	222	0.02	0.13	255	0.04	0.13	288
0.01	0.00	775	0.02	0.14	216	0.04	0.14	248
0.01	0.01	732	0.03	0.00	808	0.04	0.15	209
0.01	0.02	690	0.03	0.01	766	0.05	0.00	841
0.01	0.03	648	0.03	0.02	723	0.05	0.01	798
0.01	0.04	606	0.03	0.03	681	0.05	0.02	756
0.01	0.05	564	0.03	0.04	639	0.05	0.03	713
0.01	0.06	522	0.03	0.05	597	0.05	0.04	671
0.01	0.07	481	0.03	0.06	555	0.05	0.05	629
0.01	0.08	440	0.03	0.07	514	0.05	0.06	588
0.01	0.09	399	0.03	0.08	473	0.05	0.07	546
0.01	0.10	359	0.03	0.09	432	0.05	0.08	505
0.01	0.11	319	0.03	0.10	392	0.05	0.09	465
0.01	0.12	279	0.03	0.11	351	0.05	0.10	424
0.01	0.13	239	0.03	0.12	311	0.05	0.11	384
0.01	0.14	199	0.03	0.13	272	0.05	0.12	343
			0.03	0.14	232	0.05	0.13	304
						0.05	0.14	264
						0.05	0.15	225

TABLE 12

CALCULATED M_s TEMPERATURES FOR DIFFERENT ATOM FRACTIONS OF ALLOYING ELEMENTS IN THE Ti-3a/oMn-Al-V SYSTEM

Al	V	T°K
0.06	0.00	857
0.06	0.01	814
0.06	0.02	772
0.06	0.03	729
0.06	0.04	687
0.06	0.05	645
0.06	0.06	604
0.06	0.07	562
0.06	0.08	521
0.06	0.09	480
0.06	0.10	440
0.06	0.11	399
0.06	0.12	359
0.06	0.13	319
0.06	0.14	280
0.06	0.15	240
0.07	0.00	873
0.07	0.01	830
0.07	0.02	787
0.07	0.03	745
0.07	0.04	703
0.07	0.05	661
0.07	0.06	619
0.07	0.07	578
0.07	0.08	537
0.07	0.09	496
0.07	0.10	455
0.07	0.11	415
0.07	0.12	375
0.07	0.13	335
0.07	0.14	295
0.07	0.15	256
0.07	0.16	217

Al	V	T°K
0.08	0.00	889
0.08	0.01	846
0.08	0.02	803
0.08	0.03	761
0.08	0.04	719
0.08	0.05	677
0.08	0.06	635
0.08	0.07	594
0.08	0.08	552
0.08	0.09	512
0.08	0.10	471
0.08	0.11	431
0.08	0.12	390
0.08	0.13	350
0.08	0.14	311
0.08	0.15	271
0.09	0.00	904
0.09	0.01	861
0.09	0.02	819
0.09	0.03	776
0.09	0.04	734
0.09	0.05	692
0.09	0.06	650
0.09	0.07	609
0.09	0.08	568
0.09	0.09	527
0.09	0.10	486
0.09	0.11	446
0.09	0.12	406
0.09	0.13	366
0.09	0.14	326
0.09	0.15	287
0.09	0.16	247
0.09	0.17	209

Al	V	T°K
0.10	0.00	919
0.10	0.01	877
0.10	0.02	834
0.10	0.03	791
0.10	0.04	749
0.10	0.05	707
0.10	0.06	666
0.10	0.07	624
0.10	0.08	583
0.10	0.09	542
0.10	0.10	501
0.10	0.11	461
0.10	0.12	421
0.10	0.13	381
0.10	0.14	341
0.10	0.15	302
0.10	0.16	263
0.10	0.17	224
0.10	0.18	185
0.10	0.19	147
0.10	0.20	108
0.11	0.00	935
0.11	0.01	892
0.11	0.02	849
0.11	0.03	807
0.11	0.04	764
0.11	0.05	722
0.11	0.06	681
0.11	0.07	639
0.11	0.08	598
0.11	0.09	557
0.11	0.10	516
0.11	0.11	476
0.11	0.12	436
0.11	0.13	396
0.11	0.14	356
0.11	0.15	317
0.11	0.16	277
0.11	0.17	238

TABLE 13

CALCULATED M_s TEMPERATURES FOR DIFFERENT ATOM FRACTIONS OF ALLOYING ELEMENTS IN THE Ti-3a/oMn-Al-V SYSTEM

Al	V	T°K
0.12	0.00	950
0.12	0.01	907
0.12	0.02	864
0.12	0.03	821
0.12	0.04	779
0.12	0.05	737
0.12	0.06	695
0.12	0.07	654
0.12	0.08	613
0.12	0.09	572
0.12	0.10	531
0.12	0.11	491
0.12	0.12	450
0.12	0.13	410
0.12	0.14	371
0.12	0.15	331
0.12	0.16	292
0.12	0.17	253
0.13	0.00	964
0.13	0.01	921
0.13	0.02	879
0.13	0.03	836
0.13	0.04	794
0.13	0.05	752
0.13	0.06	710
0.13	0.07	669
0.13	0.08	627
0.13	0.09	586
0.13	0.10	546
0.13	0.11	505
0.13	0.12	465
0.13	0.13	425
0.13	0.14	385
0.13	0.15	346
0.13	0.16	306
0.13	0.17	268

Al	V	T°K
0.14	0.00	979
0.14	0.01	936
0.14	0.02	893
0.14	0.03	851
0.14	0.04	808
0.14	0.05	766
0.14	0.06	725
0.14	0.07	683
0.14	0.08	642
0.14	0.09	601
0.14	0.10	560
0.14	0.11	520
0.14	0.12	479
0.14	0.13	439
0.14	0.14	400
0.14	0.15	360
0.14	0.16	321
0.14	0.17	282
0.15	0.00	993
0.15	0.01	950
0.15	0.02	908
0.15	0.03	865
0.15	0.04	823
0.15	0.05	781
0.15	0.06	739
0.15	0.07	697
0.15	0.08	656
0.15	0.09	615
0.15	0.10	574
0.15	0.11	534
0.15	0.12	493
0.15	0.13	453
0.15	0.14	414
0.15	0.15	374
0.15	0.16	335
0.15	0.17	296
0.15	0.18	257

Al	V	T°K
0.16	0.00	1008
0.16	0.01	965
0.16	0.02	922
0.16	0.03	879
0.16	0.04	837
0.16	0.05	795
0.16	0.06	753
0.16	0.07	712
0.16	0.08	670
0.16	0.09	629
0.16	0.10	588
0.16	0.11	548
0.16	0.12	507
0.16	0.13	467
0.16	0.14	428
0.16	0.15	388
0.16	0.16	349
0.16	0.17	310
0.16	0.18	271
0.17	0.00	1022
0.17	0.01	979
0.17	0.02	936
0.17	0.03	893
0.17	0.04	851
0.17	0.05	809
0.17	0.06	767
0.17	0.07	725
0.17	0.08	684
0.17	0.09	643
0.17	0.10	602
0.17	0.11	562
0.17	0.12	521
0.17	0.13	481
0.17	0.14	441
0.17	0.15	402
0.17	0.16	363
0.17	0.17	323
0.17	0.18	285

TABLE 14

CALCULATED M_s TEMPERATURES FOR DIFFERENT ATOM FRACTIONS OF ALLOYING ELEMENTS IN THE Ti-3a/oMn-Al-V SYSTEM

Al	V	T°K	Al	V	T°K	Al	V	T°K
0.18	0.00	1036	0.19	0.00	1049	0.20	0.00	1063
0.18	0.01	993	0.19	0.01	1006	0.20	0.01	1020
0.18	0.02	950	0.19	0.02	963	0.20	0.02	977
0.18	0.03	907	0.19	0.03	921	0.20	0.03	934
0.18	0.04	865	0.19	0.04	878	0.20	0.04	892
0.18	0.05	823	0.19	0.05	836	0.20	0.05	850
0.18	0.06	781	0.19	0.06	794	0.20	0.06	808
0.18	0.07	739	0.19	0.07	753	0.20	0.07	766
0.18	0.08	698	0.19	0.08	711	0.20	0.08	725
0.18	0.09	657	0.19	0.09	670	0.20	0.09	683
0.18	0.10	616	0.19	0.10	629	0.20	0.10	643
0.18	0.11	575	0.19	0.11	589	0.20	0.11	602
0.18	0.12	535	0.19	0.12	548	0.20	0.12	562
0.18	0.13	495	0.19	0.13	508	0.20	0.13	521
0.18	0.14	455	0.19	0.14	468	0.20	0.14	482
0.18	0.15	415	0.19	0.15	429	0.20	0.15	442
0.18	0.16	376	0.19	0.16	389	0.20	0.16	403
0.18	0.17	337	0.19	0.17	350	0.20	0.17	363
0.18	0.18	298	0.19	0.18	312	0.20	0.18	325
0.18	0.19	260	0.19	0.19	273	0.20	0.19	286

TABLE 15

CALCULATED M_s TEMPERATURES FOR DIFFERENT ATOM FRACTIONS OF ALLOYING ELEMENTS IN THE Ti-8a/oCr-Al-Mo SYSTEM

Al	Mo	T°K
0.00	0.00	288
0.01	0.00	308
0.01	0.01	221
0.02	0.00	327
0.02	0.01	241
0.03	0.00	347
0.03	0.01	261
0.04	0.00	366
0.04	0.01	281
0.05	0.00	385
0.05	0.01	300
0.05	0.02	215
0.06	0.00	404
0.06	0.01	320
0.06	0.02	235
0.07	0.00	423
0.07	0.01	339
0.07	0.02	255
0.08	0.00	441
0.08	0.01	358
0.08	0.02	275
0.09	0.00	460
0.09	0.01	377
0.09	0.02	294
0.09	0.03	210
0.10	0.00	478
0.10	0.01	396
0.10	0.02	314
0.10	0.03	230
0.11	0.00	496
0.11	0.01	415
0.11	0.02	333
0.11	0.03	250
0.12	0.00	514
0.12	0.01	433
0.12	0.02	352
0.12	0.03	270
0.13	0.00	532
0.13	0.01	451
0.13	0.02	370
0.13	0.03	289
0.13	0.04	207
0.14	0.00	549
0.14	0.01	469
0.14	0.02	389
0.14	0.03	308
0.14	0.04	226
0.15	0.00	567
0.15	0.01	487
0.15	0.02	408
0.15	0.03	327
0.15	0.04	246
0.16	0.00	584
0.16	0.01	505
0.16	0.02	426
0.16	0.03	346
0.16	0.04	265
0.17	0.00	601
0.17	0.01	523
0.17	0.02	444
0.17	0.03	365
0.17	0.04	285
0.17	0.05	204
0.18	0.00	617
0.18	0.01	540
0.18	0.02	462
0.18	0.03	383
0.18	0.04	304
0.18	0.05	224
0.19	0.00	634
0.19	0.01	557
0.19	0.02	479
0.19	0.03	401
0.19	0.04	323
0.19	0.05	243
0.20	0.00	650
0.20	0.01	574
0.20	0.02	497
0.20	0.03	419
0.20	0.04	341
0.20	0.05	262

TABLE 16

CALCULATED M_s TEMPERATURES FOR DIFFERENT ATOM FRACTIONS OF ALLOYING ELEMENTS IN THE Ti-Mo-Al-Sn SYSTEM

0.0330 Al 0.0025 Sn	
Mo	T°K
0.00	1153
0.01	1073
0.02	992
0.03	910
0.04	828
0.05	746
0.06	662
0.07	578
0.08	493
0.09	408
0.10	322
0.11	235

0.0660 Al 0.0050 Sn	
Mo	T°K
0.00	1199
0.01	1120
0.02	1041
0.03	961
0.04	880
0.05	799
0.06	717
0.07	635
0.08	551
0.09	468
0.10	383
0.11	298
0.12	212

0.0990 Al 0.0075 Sn	
Mo	T°K
0.00	1243
0.01	1166
0.02	1088
0.03	1009
0.04	930
0.05	850
0.06	770
0.07	689
0.08	608
0.09	525
0.10	443
0.11	359
0.12	275

0.1320 Al 0.0100 Sn	
Mo	T°K
0.00	1285
0.01	1209
0.02	1132
0.03	1055
0.04	978
0.05	900
0.06	821
0.07	742
0.08	662
0.09	581
0.10	500
0.11	418
0.12	336
0.13	253

0.1550 Al 0.0125 Sn	
Mo	T°K
0.00	1313
0.01	1238
0.02	1162
0.03	1086
0.04	1010
0.05	933
0.06	855
0.07	777
0.08	698
0.09	619
0.10	539
0.11	458
0.12	377
0.13	295
0.14	213

TABLE 17

SUMMARY OF FREE ENERGY DIFFERENCES FOR SILICON, GALLIUM AND TIN USED IN PHASE DIAGRAM CALCULATIONS
(All Units in cal/g.at.)

$\Delta F_{Ga}^{\rho\rightarrow L}=1335-4.41T$ $\Delta F_{Sn}^{\tau\rightarrow L}=1720-3.41T$ $\Delta F_{Si}^{\delta\rightarrow L}=12100-7.17T$

$\Delta F_{Ga}^{\rho\rightarrow \beta}=1335-2.41T$ $\Delta F_{Sn}^{\tau\rightarrow \beta}=1720-1.91T$ $\Delta F_{Si}^{\delta\rightarrow \beta}=10600-4.67T$

$\Delta F_{Ga}^{\rho\rightarrow \varepsilon}=835-1.69T$* $\Delta F_{Sn}^{\tau\rightarrow \varepsilon}=1620-1.81T$ $\Delta F_{Si}^{\delta\rightarrow \varepsilon}=12100-4.27T$

TABLE 18

SOLUTION AND COMPOUND PARAMETERS FOR THE Ti-Be and Zr-Be SYSTEMS

Solution Phases

Phase	Symbol	Regular Solution Interaction Parameter (Cal/g.at.) Ti-Be	Zr-Be
Liquid	L	-9000	-10000
bcc	β	0	+ 2000
hcp	ε	+6000(or +10,000)	+10000

Compound Phases

Phase	Symbol ψ	x_*(at.fr.Be)	Base Phase θ	Compound Parameter (cal/g.at.)
$Ti_{1/3}Be_{2/3}$	ϕ	0.667	α	17,230
$T_{1/4}Be_{3/4}$	ρ	0.750	α	26,000-3.4T
$Ti_{2/19}Be_{17/19}$	δ	0.895	β	70,300-27.0T
$Ti_{1/13}Be_{12/13}$	ξ	0.923	β	86,900-35.7T
$Zr_{1/3}Be_{2/3}$	η	0.667	β	12,800-2.2T
$Zr_{1/6}Be_{5/6}$	μ	0.833	β	35,800-11.9T
$Zr_{2/19}Be_{17/19}$	δ	0.895	β	62,800-23.7T
$Zr_{1/14}Be_{13/14}$	ω	0.929	β	96,800-38.9T

*B. Predel and D. W. Stein (51) estimate $\Delta H_{Ga}^{\rho\rightarrow\alpha}$ = 2000 $\pm$ 1000 cal/g.at.

TABLE 19

CALCULATION OF FREE ENERGY OF FORMATION OF
TITANIUM-BERYLLIUM AND ZIRCONIUM-BERYLLIUM COMPOUNDS

$$F^{\psi} = (1-x_*)\, F^{\theta}_{Me} + x_*\, F^{\theta}_{Be} + x_*\,(1-x_*)\,(L-C^{\psi})$$

$$\Delta F_f{}^{\psi} = F^{\psi} - (1-x_*)\, F^{o}_{Me} - x_*\, F^{o}_{Be}$$

$F^{o}_{Zr}=F^{\varepsilon}_{Zr}$ for $T \leq 1155^{o}K$;

$F^{o}_{Zr}=F^{\beta}_{Zr}$ for $1155^{o}K \leq T \leq 2125^{o}K$;

$F^{o}_{Zr}=F^{L}_{Zr}$ for $T \geq 2125^{o}K$;

$F^{o}_{Ti}=F^{\varepsilon}_{Ti}$ for $T \leq 1155^{o}K$

$F^{o}_{Ti}=F^{\beta}_{Ti}$ for $1155^{o}K \leq T \leq 1940^{o}K$

$F^{o}_{Ti}=F^{L}_{Ti}$ for $T \geq 1940^{o}K$

$F^{o}_{Be}=F^{\varepsilon}_{Be}$ for $T \leq 1528^{o}K$

$F^{o}_{Be}=F^{\beta}_{Be}$ for $1528^{o}K \leq T \leq 1556^{o}K$

$F^{o}_{Be}=F^{L}_{Be}$ for $T \geq 1566^{o}K$

Compound	x_* (at fr. Be)	ΔF_f(at 300°K) (cal/g.at.)	ΔF_f (at 1300°K) (cal/g.at.)
$Ti_{1/3}Be_{2/3}$	(ϕ)(0.667)	-5240 + 0.29T	-5590 + 0.59T
$Ti_{1/4}Be_{3/4}$	(ρ)(0.750)	-6015 + 0.96T	-6275 + 1.19T
$Ti_{2/19}Be_{17/19}$	(δ)(0.895)	-6360 + 1.81T	-6470 + 1.90T
$Ti_{1/13}Be_{12/13}$	(ξ)(0.923)	-5730 + 1.81T	-5810 + 1.88T
$Zr_{1/3}Be_{2/3}$	(η)(0.667)	-3980 - 0.29T	-4330 + 0.01T
$Zr_{1/6}Be_{5/6}$	(μ)(0.833)	-5280 + 0.90T	-5450 + 1.05T
$Zr_{2/19}Be_{17/19}$	(δ)(0.895)	-5750 + 1.05T	-5860 + 1.59T
$Zr_{1/14}Be_{13/14}$	(ω)(0.929)	-5950 + 1.84T	-6030 + 1.90T

TABLE 20

SUMMARY OF PARAMETERS EMPLOYED FOR DESCRIBING THE Ti-Si and Zr-Si SYSTEMS

Solution Phases

Phase	Symbol	Regular Solution Interaction Parameter (cal/g.at.)	
		Ti-Si	Zr-Si
Liquid	L	-52,000	-50,000
bcc	β	-45,000	-40,000
hcp	ε	-60,000+13.2T	-40,000

Compound Phases

(Base Phase θ is the bcc β phase)

Phase	Symbol	Compound Parameter C^{ψ} (Cal/g.at.)	Phase	Symbol	Compound Parameter C^{ψ} (Cal/g.at.)
$Ti_{5/8}Si_{3/8}$	ξ	47,000-10.0T	$Zr_{5/8}Si_{3/8}$	ξ	48,400-10.9T
$Ti_{1/2}Si_{1/2}$	ω	34,000- 7.2T	$Zr_{3/5}Si_{2/5}$	σ	48,700-10.6T
$Ti_{1/3}Si_{2/3}$	ϕ	30,000- 6.2T	$Zr_{6/11}Si_{5/11}$	μ	48,200- 9.7T
$Zr_{3/4}Si_{1/4}$	τ	37,900- 9.5T	$Zr_{1/2}Si_{1/2}$	ω	49,000-10.8T
$Zr_{2/3}Si_{1/3}$	π	46,900-10.4T	$Zr_{1/3}Si_{2/3}$	ρ	43,200-13.7T

TABLE 21

CALCULATION OF FREE ENERGY OF FORMATION OF
Ti-Si and Zr-Si COMPOUNDS

$$F^{\psi} = (1-x_*)\ F^{\theta}_{Me} + x_*\ F^{\theta}_{Si} + x_*\ (1-x_*)(L-C^{\psi})$$

$$\Delta F^{\psi}_f = F^{\psi} - (1-x_*)\ F^{o}_{Me} - x_* F^{o}_{Si}$$

$$F^{o}_{Si} = F^{\delta}_{Si} \text{ for } T \leq 1688^{o}K$$

$$F^{o}_{Si} = F^{L}_{Si} \text{ for } T \geq 1688^{o}K$$

Compound	x_* (at.fr.Si)	ΔF_f(at 300°K) (cal/g.at.)	ΔF_f(at 1300°K) (cal/g.at.)
$Ti_{5/8}Si_{3/8}$	ξ(0.375)	-19,100+0.25T	-19,500+0.59T
$Ti_{1/2}Si_{1/2}$	ω(0.500)	-15,700-0.99T	-16,200-0.54T
$Ti_{1/3}Si_{2/3}$	ϕ(0.667)	-10,600-2.33T	-11,300-1.73T
$Zr_{3/4}Si_{1/4}$	τ(0.250)	-13,500-0.07T	-13,800+0.61T
$Zr_{2/3}Si_{1/3}$	π(0.333)	-17,300+0.15T	-18,000+0.75T
$Zr_{5/8}Si_{3/8}$	ξ(0.375)	-18,400+0.24T	-19,000+0.80T
$Zr_{3/5}Si_{2/5}$	σ(0.400)	-18,800+0.13T	-19,500+0.67T
$Zr_{6/11}Si_{5/11}$	μ(0.455)	-19,000-0.20T	-19,500+0.29T
$Zr_{1/2}Si_{1/2}$	ω(0.500)	-18,900-0.07T	-19,500+0.36T
$Zr_{1/3}Si_{2/3}$	ρ(0.667)	-13,300-0.37T	-13,600-0.07T

TABLE 22

EQUATIONS FOR SOLUBILITY OF SILICON AND BERYLLIUM IN THE HCP AND BCC FORMS OF TITANIUM AND ZIRCONIUM

(Equations apply for small values of solute concentrations below 1.5% or 0.015 at.fr.)

Be in hcp Ti :

$$4.575\ T \log x = -13{,}869 + 0.43T$$

or

$$4.575\ T \log x = -17{,}869 + 0.43T$$

Be in hcp Zr :

$$4.575\ T \log x = -15{,}980 - 0.45T$$

Si in hcp Ti :

$$4.575\ T \log x = -1411 - 8.79T$$

Si in hcp Zr :

$$4.575\ T \log x = -24{,}300 + 4.03T$$

Si in bcc Ti :

$$4.575\ T \log x = -16{,}875 + 6.25T$$

Si in bcc Zr :

$$4.575\ T \log x = -25{,}925 + 7.13T$$

TABLE 23

SUMMARY OF PARAMETERS EMPLOYED FOR DESCRIBING THE Ti-Al, Ti-Ga and Ti-Sn SYSTEMS

Solution Phases

Phase	Symbol	Regular Solution Interaction Parameter (cal/g.at.)		
		Ti-Al	Ti-Ga	Ti-Sn
Liquid	L	-24,100+10.0T	-10,000	-18,000
bcc	β	-28,000+10.0T	-13,000	-21,000
hcp	ε	-29,000+10.0T	-13,800	-21,000
fcc	α	-24,200+10.0T	-	-

Compound Phases

Phase	Symbol	x_* at.fr.	Base Phase θ	Compound Parameter C^{ψ} (cal/g.at.)
$Ti_{3/4}Al_{1/4}$	ξ	0.250 (Al)	ε	7800 + 4.0T
$Ti_{3/4}Ga_{1/4}$	ξ	0.250 (Ga)	ε	7000 + 4.5T
$Ti_{3/4}Sn_{1/4}$	ξ	0.250 (Sn)	ε	6600 + 6.0T
$Ti_{2/3}Ga_{1/3}$	η	0.333 (Ga)	ε	8900 + 4.2T
$Ti_{2/3}Sn_{1/3}$	η	0.333 (Sn)	ε	9300 + 3.64T
$Ti_{1/2}Al_{1/2}$	γ	0.500 (Al)	α	20,000 - 2.28T
$Ti_{1/4}Al_{3/4}$	δ	0.750 (Al)	ε	25,000 - 4.50T

TABLE 24

CALCULATION OF FREE ENERGY OF FORMATION OF
Ti-Aℓ, Ti-Ga and Ti-Sn COMPOUNDS

$$F^{\psi} = (1-x_*)F^{\theta}_{Ti} + x_*F^{\theta}_{Me} + x_*(1-x_*)(L-C^{\psi})$$

$$\Delta F^{\psi}_f = F^{\psi} - (1-x_*)F^{o}_{Ti} - x_*F^{o}_{Me}$$

Ti-Aℓ Solid Solution (hcp)

$$F^{\varepsilon} = (1-x)F^{\varepsilon}_{Ti} + xF^{\varepsilon}_{A\ell} + RT(x\ell nx + (1-x)\ell n(1-x)) + (-29{,}000 + 10.0T)x(1-x)$$

$$\Delta F_f = F^{\varepsilon} - (1-x)F^{o}_{Ti} - xF^{o}_{A\ell}$$

$F^{o}_{Ga} = F^{\rho}_{Ga}$ for $T \leq 302^{o}K$; $F^{o}_{Sn} = F^{\tau}_{Sn}$ for $286 \leq T \leq 504^{o}K$

$F^{o}_{Ga} = F^{L}_{Ga}$ for $T \geq 302^{o}K$; $F^{o}_{Sn} = F^{L}_{Sn}$ for $T \geq 504^{o}K$

$F^{o}_{A\ell} = F^{\alpha}_{A\ell}$ for $T \leq 930^{o}K$; $F^{o}_{A\ell} = F^{L}_{A\ell}$ for $T \geq 930^{o}K$

Compound	x_* (at.fr.Me)	$\Delta F_f(300^{o}K)$ (cal/g.at.)	$\Delta F_f(1300^{o}K)$ (cal/g.at.)
hcp solid solution	ε(0.120)	-2900 + 0.38T	-2670 + 0.29T
Ti_3Al	ξ(0.250)	-5660 + 1.02T	-7400 + 2.49T
TiAl	γ(0.500)	-10,600 + 3.07T	-12,400 + 4.90T
$TiAl_3$	δ(0.750)	-8200 + 3.04T	-10,400 + 5.00T
Ti_3Ga	ξ(0.250)	-3000 - 1.26T	-3900 + 0.10T
Ti_2Ga	η(0.333)	-3900 - 1.48T	-4800 + 0.02T
Ti_3Sn	ξ(0.250)	-4200 - 1.58T	-5000 - 0.50T
Ti_2Sn	η(0.333)	-5510 - 1.41T	-6210 - 0.28T

MEASURED HEAT OF FORMATION AT $300^{o}K$

hcp solid solution	ε(0.120Aℓ)	-3400 ± 500
$Ti_3A\ell$	ξ(0.250Aℓ)	-6000 ± 500
TiAℓ	γ(0.500Aℓ)	-9000 ± 500
$TiA\ell_3$	δ(0.750Aℓ)	-8700 ± 500

TABLE 25

REGULAR SOLUTION PARAMETERS FOR THE
Liquid(L), HCP(E) and BCC(B) PHASES

System	L	E	B	$T_c^{\beta}=B/2R$
		(cal/g.at.)		°K
Ti-Zr	-746	+2090	+894	225
Ti-V	+871	+2659	+2659	669
Ti-Cb	+3125	+3125	+3125	786
Ti-Ta	+2779	+2790	+2790	702
Ti-Mo	+1560	+3671	+1241	312
Mo-Cb	-7100	-5500	-5500	
Aℓ-Sn	2800	2800	2800	
Aℓ-Ga	400	400	400	

TABLE 26

CALCULATED SUMMIT CONDITIONS FOR THE BCC
ISOLATED MISCIBILITY GAPS IN THE Ti-Cb-Mo,
Ti-Mo-V and Ti-Cb-V SYSTEMS

System	Interaction Parameters	Summit Conditions
Ti-Cb-Mo	3125, 1241, -5500	935°K, Ti=0.500, Mo=0.164
Ti-Mo-V	2659, 1241, -5500	859°K, Ti=0.500, Mo=0.185
Ti-Cb-V	3125, 2659, -5500	1076°K, Ti=0.500, V=0.229

TABLE 27

INPUT PARAMETERS FOR CALCULATION OF THE SOLUBILITY OF BERYLLIUM AND SILICON in HCP TITANIUM-ZIRCONIUM ALLOYS

(All units in cal/g.at.)

i	j	k	ψ	x_*	E_{ij}	E_{ik}	$-E_{jk}$	$-E_{ik}/x_*$
Ti	Si	Zr	Ti_5Si_3	0.375	-60,300+13.2T	+2091	+40,000	-5576
Ti	Be	Zr	$TiBe_2$	0.667	+10,000	+2091	-10,000	-3560
Zr	Si	Ti	Zr_3Si	0.250	-40,000	+2091	+60,300-13.2T	-8364
Zr	Be	Ti	$ZrBe_2$	0.667	+10,000	+2091	-10,000	-3560

System	$(E_{ij} + E_{ik} - E_{jk})$(at 800°K)
Ti-Si-Zr	-8049
Ti-Be-Zr	+2091
Zr-Si-Ti	+12,231
Zr-Be-Ti	+2091

TABLE 28

SUMMARY OF EXCESS FREE ENERGY AND COMPOUND PARAMETERS FOR THE Ti-Cr SYSTEM
(cal/g.at., °K)

Liquid (L)	0	for $1600 \leq T \leq 2200$°K
	3000	for $1600 \leq T \leq 2200$°K
BCC (β)	3000	for $600 \leq T \leq 2200$°K
	6000	for $600 \leq T \leq 2200$°K
HCP (ε)	9420	for $600 \leq T \leq 1200$°K
	12420	for $600 \leq T \leq 1200$°K

Compound	Structure	Base	Compound Parameter
$TiCr_2$	Laves Phase	hcp	7900 + 3.1T

Comparison of Calculated and Observed (68) Thermochemical Properties

	ΔH_f(300°K)	ΔS_f(300°K)	ΔF_f(1550°K)
$Ti_{0.333}Cr_{0.667}$	+30(calc.)	+0.69(calc.)	-920(calc.)
			-900±300(obs.)

Excess Free Energy of bcc phase at 1523°K

x	(calc.)	(obs.)	x	(calc.)	(obs.)
0.10	300	400	0.60	1150	1280
0.20	580	680	0.70	1070	1020
0.30	820	980	0.80	860	820
0.40	1010	1180	0.90	510	480

TABLE 29

SUMMARY OF EXCESS FREE ENERGY AND COMPOUND PARAMETERS FOR THE Ti-Mn SYSTEM
(cal/g.at., °K)

$\Delta F_{Mn}^{\beta \rightarrow L} = 3500 - 2.3T$; $\Delta F_{Mn}^{\beta \rightarrow \varepsilon} = 800 + 0.52T$ for $300 \leq T \leq 1600°K$ (1,43)

Liquid (L)	-3000	for $1300 \leq T \leq 2000°K$
	-3000	for $1300 \leq T \leq 2000°K$
BCC (β)	0	for $600 \leq T \leq 2000°K$
	0	for $600 \leq T \leq 2000°K$
HCP (ε)	+8540	for $600 \leq T \leq 1200°K$
	+8540	for $600 \leq T \leq 1200°K$

Compound	Structure	Base	Compound Parameter
TiMn (τ)	tetragonal	β	700 + 3.27T
$TiMn_2$ (λ)	Laves Phase	ε	4000 + 6.3T

Calculated Thermochemical Properties of Compound Phases (at 300°K)

	ΔH_f	ΔS_f
$Ti_{0.50}Mn_{0.50}$	+45	0.17
$Ti_{0.333}Mn_{0.667}$	-210	+1.13

TABLE 30

SUMMARY OF EXCESS FREE ENERGY
PARAMETERS FOR THE Mo-Cr SYSTEM
(cal/g.at., °K)

Liquid (L)	$3000 - 1.4T$	for $2000 \leq T \leq 3000°K$
	$6100 - 2.7T$	for $2000 \leq T \leq 3000°K$
BCC (β)	$5100 - 1.4T$	for $300 \leq T \leq 2700°K$
	$8200 - 2.7T$	for $300 \leq T \leq 2700°K$

Comparison of Calculated and Observed
Thermochemical Properties (obs. ref. 49)

Atomic fraction Chromium	H_E^β		S_E^β		F_E^β(1471°K)	
	(calc)	(obs)(±100)	(calc)	(obs)(±0.10)	(calc)	(obs)(±100)
0.10	487	495	0.138	0.103	284	343
0.20	915	963	0.266	0.236	524	615
0.30	1266	1345	0.376	0.356	713	821
0.40	1521	1600	0.461	0.451	843	958
0.50	1663	1725	0.513	0.463	908	1023
0.60	1670	1710	0.523	0.478	901	1021
0.70	1526	1555	0.485	0.475	813	922
0.80	1212	1244	0.390	0.342	638	741
0.90	710	745	0.231	0.203	370	446

Calculated Miscibility Gap Summit = 1153°K, 0.617 Cr.

Observed Miscibility Gap Summit = 1150°K, 0.61 Cr.

TABLE 31

DESCRIPTION OF COUNTERPHASES IN THE

Ti-Mo-Cr AND Ti-Mo-Mn SYSTEMS

Stable Compound Phase	Counter Phase	Base Phase	Counter Phase Compound Parameter
TiMn (τ)	Ti_3Mo	β	1500 (cal/g.at.)
$TiCr_2$ (λ)	$MoCr_2$	ε	0

TABLE 32

SUMMARY OF SOLUTION AND COMPOUND PARAMETERS
FOR COMPONENTS OF Cb-Cr-Zr, Cb-Cr-Hf, Mo-Cr-Cb
AND Zr-Ti-Cb SYSTEMS
(cal/g.at. °K)

System	L	B	E	Compound	x_*	Base	Parameter
Cb-Zr	1500	4400	8000	----	----	----	----
	1500	4400	8000	----	----	----	----
Zr-Cr	-2000	6000	9000	Laves(λ)	0.667	ε	16,300
	-2000	6000	9000				
Cb-Hf	3219	5137	5137	----	----	----	----
	3219	5137	5137				
Hf-Cr	0	6000	9000	Laves(λ)	0.667	ε	17,200
	0	6000	9000				
Mo-Cb	-7100	-5500	-5500	----	----	----	----
	-7100	-5500	-5500				
Ti-Cb	3121	3125	3125	----	----	----	----
	3121	3125	3125				
Ti-Zr	-746	+2090	+894	----	----	----	----
	-746	+2090	+894	----	----	----	----
Cb-Cr	1400	5400	5400	Laves(λ)	0.667	ε	17,200
	1400	7000	7000				+1.0T
Mo-Cr	(3000 -1.4T)	(5100 -1.4T)	(5100 -1.4T)	----	----	----	----
	(6100 -2.7T)	(8200 -2.7T)	(8200 -2.7T)				

TABLE 33

SUMMARY OF EXCESS FREE ENERGY AND COMPOUND PARAMETERS FOR THE Cb-Cr SYSTEM
(cal/g.at., °K)

Liquid (L)	1400 for $1500 \leq T \leq 2800$°K
	1400 for $1500 \leq T \leq 2800$°K
FCC (α)	5400 for $1200 \leq T \leq 2000$°K
	7000 for $1200 \leq T \leq 2000$°K
BCC (β)	5400 for $1200 \leq T \leq 2000$°K
	7000 for $1200 \leq T \leq 2000$°K

Compound	Structure	Base	Compound Parameter
$CbCr_2$ (λ)	Laves Phase	hcp	17,200 + 1.0T

Comparison of Calculated and Observed Thermochemical Properties at 300°K

	ΔH_f	ΔS_f
$Cb_{0.333}Cr_{0.667}$	-1670 (calc.)	-0.15 (calc.)
	-1670 ± 250 (obs 70)	-0.12 ± 0.15 (obs 70)

TABLE 34

SUMMARY OF EXCESS FREE ENERGY AND COMPOUND PARAMETERS FOR THE Cb-Al SYSTEM
(cal/g.at. °K)

Liquid (L)	-11000 for $1400 \leq T \leq 2800$°K
	-11000 for $1400 \leq T \leq 2800$°K
BCC (β)	-12000 for $1200 \leq T \leq 2500$°K
	-12000 for $1200 \leq T \leq 2500$°K

Compound	Structure	Base	Compound Parameter
Cb_3Al (W)	beta tungsten	bcc	8100 + 3.0T
Cb_2Al (σ)	sigma	bcc	10100 + 2.0T
$CbAl_3$ (t)	b.c. tetrag ($TiAl_3$)	hcp	41400 - 8.0T

Calculated Thermochemical Properties
at 300°K

	ΔH_f	ΔS_f
$Cb_{0.750}Al_{0.250}$	-2980	+0.85
$Cb_{0.667}Al_{0.333}$	-3880	+0.83
$Cb_{0.250}Al_{0.750}$	-8460	-1.38

TABLE 35

SUMMARY OF EXCESS FREE ENERGY AND COMPOUND PARAMETERS FOR THE Cr-Al SYSTEM (cal/g.at., °K)

Liquid (L)	-11,100 for $1500 \leq T \leq 2200$°K
	-11,100 for $1500 \leq T \leq 2200$°K
BCC (β)	-14,400 for $600 \leq T \leq 2200$°K
	-14,400 for $600 \leq T \leq 2200$°K

Compound	Structure	Base	Compound Parameter
$Cr_{0.65}Al_{0.35}$(T)	tetrag. $C11_b$ ($MoSi_2$)	bcc	5000 + 4.25 T
$Cr_{0.40}Al_{0.60}$(ρ)	rhomb. $D8_{10}$	bcc	11500 + 1.80 T

Comparison of Calculated and Observed Thermochemical Properties (obs. ref. 49)

Excess Integral Free Energy of Mixing of BCC Phase at 1273°K

a/o Al		
10	-1200(calc.)	-1312 ± 250(obs)
20	-2115 (calc.)	-2360 ± 250(obs)
30	-2750(calc.)	-3138 ± 250(obs)
40	-3078(calc.)	-3573 ± 250(obs)

	ΔH_f(300°K)	ΔS_f(300°K)	ΔF_f(1273°K)
$Cr_{0.65}Al_{0.35}$	-2820(calc.)	+1.37(calc.)	
	-2600 ± 250(obs)		
$Cr_{0.40}Al_{0.60}$	-3980(calc.)	+1.12(calc.)	-5405(calc.)
	-3600 ± 250(obs)		-5685 ± 250(obs)

TABLE 36

DESCRIPTION OF COUNTERPHASES IN

THE Cb-Al-Cr SYSTEM

Stable Compound Phase	Counter Phase	Base Phase	Counter Phase Compound Parameter
$CbAl_3$ (τ)	$CbCr_3$	ε	0
Cr_2Al_3 (ρ)	Cb_2Al_3	β	0
Cb_3Al (W)	Cb_3Cr	β	0
Cb_2Al (σ)	Cr_2Al	β	0
$CbCr_2$ (λ)	Al_3Cb	ε	41,300 - 8.0T

TABLE 37

SUMMARY OF EXCESS FREE ENERGY AND
COMPOUND PARAMETERS FOR THE Fe-Ti SYSTEM
(cal/g.at., °K)

$$\Delta F_{Fe}^{bcc \rightarrow hcp} = 1125 - 1.656 \times 10^{-3} T^2 + 1.298 \times 10^{-6} T^2 \text{ for } T \leq 1150°K$$
$$= -300 + 1.0T \text{ for } T \geq 1150°K$$

Liquid	-15,000 for $1400 \leq T \leq 2000°K$
	-11,000 for $1400 \leq T \leq 2000°K$
BCC	-11,000 for $700 \leq T \leq 2000°K$
	- 5,500 for $700 \leq T \leq 2000°K$
HCP	+ 7,900 for $T \leq 1200$
	+ 7,900 for $T \leq 1200$
FCC	- 8,000 for $1000 \leq T \leq 1800$
	- 2,500 for $1000 \leq T \leq 1800$

Compound	Structure	Base	Compound Parameter
Fe_2Ti	Laves Phase	hcp	14,000
FeTi	CsCl	bcc	6400 + 0.18T

Comparison of Calculated and
Observed Thermochemical Properties at 300°K

	ΔH_f	ΔS_f
$Fe_{0.50}Ti_{0.50}$	-4330 (calc.)	+0.48 (calc.)
	-4850 ± 500 (obs.) (49)	
$Fe_{0.667}Ti_{0.333}$	-5380 (calc.)	+0.26 (calc.)

TABLE 38

SUMMARY OF EXCESS FREE ENERGY AND COMPOUND PARAMETERS FOR THE Ti-Ni SYSTEM

(cal/g.at., °K)

$\Delta F_{Ni}^{bcc \rightarrow fcc}$ = -1330 + 0.25T for $T \geq 900°K$

= -940 - 0.74167 x $10^{-3}T^2$ + 0.5555 x $10^{-6}T^3$ for $T \leq 1200°K$

Liquid	-27,000 + 7.0T -45,000 + 13.0T	HCP	-10,600 + 7.0T -10,600 + 7.0T
FCC	-21,600 + 7.0T -43,600 + 13.0T	BCC	-18,600 + 7.0T -39,200 + 13.0T

Compound	Structure	Base	Compound Parameter
Ti_2Ni	fcc (Fd3m)	fcc	-2000 + 5.00T
TiNi	CsCl	bcc	+2200 + 4.05T
$TiNi_3$	hexagonal	hcp	+6700 + 3.21T

Comparison of Calculated and Observed Thermochemical Properties

	ΔH_f[300°K]	ΔS_f[300°K]
$Ti_{0.667}Ni_{0.333}$	-6350(calc.)-6400±500(obs.49)	-0.89 (calc.)
$Ti_{0.50}Ni_{0.50}$	-8580(calc.)-8100±500(obs.49)	-1.22 (calc.)
$Ti_{0.250}Ni_{0.750}$	-8660(calc.)-8300±500(obs.49)	-1.78 (calc.)

x_{Ni}	F_E^L[1873°K]		S_E^L[1873°K]	
	(calc.)	(obs.)(81)	(calc.)	(obs.)(81)
0.1	-1330	-1300	-0.68	-0.53
0.2	-2320	-2500	-1.31	-1.12
0.3	-3340	-3600	-1.85	-1.66
0.4	-3980	-4300	-2.26	-2.08
0.5	-4320	-4600	-2.50	-2.40
0.6	-4310	-4400	-2.56	-2.67
0.7	-3920	-3900	-2.35	-2.56
0.8	-3050	-3100	-1.89	-2.14
0.9	-1790	-1900	-1.12	-1.39

TABLE 39

SUMMARY OF EXCESS FREE ENERGY AND COMPOUND PARAMETERS FOR THE Ni-C SYSTEM

$\Delta F_C^{g \to L}$ = 27,300 - 6.5T ; $\Delta F_C^{fcc \to L}$ = -5,800 - 3.0T

$\Delta F_{Me}^{g \to L}$ = -6.0T, Me = Ti,Cr,Fe,Ni $\Delta F_C^{bcc \to L}$ = -7,800 - 3.0T

Liquid	-26,000 + 10.2T	1500 $\leq$ T $\leq$ 4400°K
	-23,800 + 3.67T	1500 $\leq$ T $\leq$ 4400°K
FCC	-19,000 + 1.03T	T $\leq$ 1600°K
	-26,000 + 16.18T	T $\leq$ 1600
Graphite	10,000	T $\leq$ 4400°K
	10,000	T $\leq$ 4400°K

Compound	Structure	Base	Compound Parameter
Ni_3C	rhombohedral	fcc	14,000 + 6.2T

Comparison of Calculated and Observed Thermochemical Properties at 300°K

	ΔH_f	ΔS_f
$Ni_{0.75}C_{0.25}$	+1025 (calc.)	+0.44 (calc.)

TABLE 40

SUMMARY OF EXCESS FREE ENERGY AND
COMPOUND PARAMETERS FOR THE Cr-C SYSTEM

Liquid	-33,000	$1700 \leq T \leq 4400°K$
	-33,000	$1700 \leq T \leq 4400°K$
BCC	-32,000	$T < 2200°K$
	-32,000	$T \leq 2200$
Graphite	10,000	$T < 4400°K$
	10,000	$T \leq 4400°K$

Compound	Structure	Base	Compound Parameter
$Cr_{23}C_6$	Complex fcc	bcc	27,400 - 0.78T
Cr_7C_3	Hexagonal	bcc	33,900 - 1.36T
Cr_3C_2	Orthorhombic	bcc	39,200 - 2.18T

Comparison of Calculated and Observed
Thermochemical Properties

	ΔH_f	ΔS_f
$Cr_{0.793}C_{0.207}$	-2650 (calc.)	0.60 (calc.)
	-2655 (obs.)(88)	0.63 (obs.)(88)
$Cr_{0.70}C_{0.30}$	-3520 (calc.)	0.76 (calc.)
	-3520 (obs.)(88)	0.87 (obs.)(88)
$Cr_{0.60}C_{0.40}$	-3290 (calc.)	0.88 (calc.)
	-3280 (obs.)(88)	0.88 (obs.)(88)

TABLE 41

SUMMARY OF EXCESS FREE ENERGY AND
COMPOUND PARAMETERS FOR THE Ti-C SYSTEM
(cal/g.at.)

Liquid	-42,000	for	$1600 \leq T \leq 4400°K$
	-42,000		$1600 \leq T \leq 4400°K$
BCC	-50,000	for	$T \leq 2000°K$
	-50,000		$T \leq 2000°K$
Graphite	20,000	for	$T \leq 4400°K$
	20,000		$T \leq 4400°K$

Compound	Structure	Base	Compound Parameter
$Ti_{0.56}C_{0.44}$	NaCl	fcc	104,000 - 13.4T

Comparison of Calculated and Observed
Thermochemical Properties

	ΔH_f	ΔS_f
$Ti_{0.56}C_{0.44}$	-20,960 (calc.)	-1.76 (calc.)
$Ti_{0.5}C_{0.5}$	-22,000 (obs.)(49)	-1.44 (obs.)(49)

TABLE 42

SUMMARY OF EXCESS FREE ENERGY AND
COMPOUND PARAMETERS FOR THE Fe-C SYSTEM
(cal/g.at.)

Liquid	-21,900 + 2.52T	$1200 \leq T \leq 4400°K$
	-37,300 + 11.70T	$1200 \underline{\leq} T \underline{\leq} 4400°K$
FCC	-22,600 - 0.70T	$300 \leq T \leq 2000$
	-37,100 + 1.39T	$300 \underline{\leq} T \underline{\leq} 2000$
BCC	- 8,400 - 9.04T	$300 \leq T \leq 2000$
	-22,900 - 6.95T	$300 \underline{\leq} T \underline{\leq} 2000$
Graphite	10,000	$T \leq 4400$
	10,000	$T \underline{\leq} 4400$

Compound	Structure	Base	Compound Parameter
Fe_3C	orthorhombic	FCC	14,800 + 3.67T

Comparison of Calculated and Observed
Thermochemical Properties

	ΔH_f	ΔS_f
$Fe_{0.75}C_{0.25}$	(1000--1400°K)	(1000--1400°K)
	672 (calc.)	0.660 (calc.)
	671 (obs.) (89)	0.656 (obs.) (89)
	(300°K)	(300°K)
	1700 (calc.)	1.64 (calc.)
	1496 (obs.) (89)	1.02 (obs.) (89)

(Solubility of C in bcc phase in equilibrium with Fe_3C, x = at.fr.)

RTlnx = -19,885 + 6.00T (calc.)
-18,485 + 3.95T (obs.) (89)

TABLE 43

COMPARISON OF CALCULATED AND OBSERVED
THERMOCHEMICAL PROPERTIES OF THE Fe-C SYSTEM
(observed values in parentheses) (89)

Activity of Carbon in Austenite Relative to Graphite

T°K	Atom Fraction Carbon					
	0.000001	0.02	0.04	0.06	0.08	(0.10)
1000	0.00002381	0.5960	1.507	----	----	----
	(0.00002398)	(0.5989)	(1.510)	----	----	----
1100	0.00001473	0.3630	0.9027	1.697	----	----
	(0.00001482)	(0.3640)	(0.9021)	(1.692)	----	----
1200	0.000009871	0.2402	0.5889	1.091	1.809	2.829
	(0.000009921)	(0.2404)	(0.5873)	(1.085)	(1.799)	(2.824)
1300	0.000007035	0.1693	0.4103	0.7506	1.228	1.894
	(0.000007066)	(0.1692)	(0.4084)	(0.7453)	(1.219)	(1.887)
1400	0.000005262	0.1255	0.3010	0.5448	0.8810	1.342
	(0.000005282)	(0.1253)	(0.2993)	(0.5400)	(0.8736)	(1.337)
1500	0.000004092	0.09678	0.2302	0.4126	0.6607	0.9962
	(0.000004105)	(0.09651)	(0.2284)	(0.4085)	(0.6544)	(0.9910)
1600	0.000003283	0.07711	0.1820	0.3236	0.5137	----
	(0.000003292)	(0.07682)	(0.1804)	(0.3200)	(0.5082)	----
1700	0.000002704	0.06310	0.1479	0.2611	----	----
	(0.000002710)	(0.06281)	(0.1465)	(0.2579)	----	----
1800	0.000002275	0.05280	0.1230	----	----	----
	(0.000002279)	(0.05252)	(0.1217)	----	----	----

TABLE 44

COMPARISON OF CALCULATED AND OBSERVED
THERMOCHEMICAL PROPERTIES OF THE Fe-C SYSTEM
(observed values in parentheses)(89)

Activity of Carbon in Liquid Fe-C Relative to Graphite

T°K	Atom Fraction Carbon					
	0.000001	0.04	0.08	0.12	0.16	0.20
1500	0.0000008260	0.05111	0.1561	0.3528	0.6992	1.281
	(0.0000008260)	(0.04783)	(0.1430)	(0.3331)	(0.7200)	(1.536)
1600	0.0000007376	0.04508	0.1357	0.3016	0.5867	1.053
	(0.0000007376)	(0.04213)	(0.1242)	(0.2845)	(0.6042)	(1.264)
1700	0.0000006674	0.04036	0.1199	0.2627	0.5026	0.8860
	(0.0000006674)	(0.03767)	(0.1096)	(0.2475)	(0.5176)	(1.064)
1800	0.0000006107	0.03658	0.1074	0.2327	0.4379	0.7599
	(0.0000006107)	(0.03410)	(0.0981)	(0.2187)	(0.4511)	(0.9137)
1900	0.0000005641	0.03350	0.0974	0.2081	0.3872	0.6623
	(0.0000005641)	(0.03120)	(0.0888)	(0.1958)	(0.3989)	(0.7970)
2000	0.0000005251	0.03095	0.0892	0.1884	0.3466	0.5852
	(0.0000005251)	(0.02880)	(0.0812)	(0.1772)	(0.3571)	(0.7048)

TABLE 45

RESULTS OF APPROXIMATE CALCULATION OF
QUASI-BINARY EUTECTIC TEMPERATURE AND COMPOSITIONS
FOR TITANIUM CARBIDE-IRON ALLOY COMPOSITES

Iron Alloy	Eutectic Temperature (°K)	Eutectic Composition (fraction $Ti_{0.56}Co_{0.44}$)*
Fe	1582	0.1045
$Fe_{0.90}Cr_{0.10}$	1568	0.1063
$Fe_{0.80}Cr_{0.20}$	1561	0.1096
$Fe_{0.70}Cr_{0.30}$	1561	0.1142
$Fe_{0.60}Cr_{0.40}$	1567	0.1201
$Fe_{0.50}Cr_{0.50}$	1579	0.1273
$Fe_{0.90}Ni_{0.10}$	1568	0.0978
$Fe_{0.80}Ni_{0.10}Cr_{0.10}$	1546	0.0971
$Fe_{0.70}Ni_{0.10}Cr_{0.20}$	1516	0.0942
$Fe_{0.80}Ni_{0.20}$	1555	0.0917
$Fe_{0.70}Ni_{0.20}Cr_{0.10}$	1533	0.0911
$Fe_{0.70}Ni_{0.30}$	1544	0.0872
$Fe_{0.60}Ni_{0.10}Cr_{0.30}$	1555	0.1080
$Fe_{0.60}Ni_{0.20}Cr_{0.20}$	1504	0.0883
$Fe_{0.60}Ni_{0.30}Cr_{0.10}$	1523	0.0866
$Fe_{0.60}Ni_{0.40}$	1537	0.0842
$Fe_{0.50}Ni_{0.10}Cr_{0.40}$	1573	0.1167
$Fe_{0.50}Ni_{0.20}Cr_{0.30}$	1468	0.0835
$Fe_{0.50}Ni_{0.30}Cr_{0.20}$	1496	0.0838
$Fe_{0.50}Ni_{0.40}Cr_{0.10}$	1518	0.0834
$Fe_{0.50}Ni_{0.50}$	1535	0.0824

*i.e., this specification signifies that for an iron alloy with 10 a/o Cr and 20 a/o Ni the eutectic occurs at 1533°K at a composition corresponding to 0.9089 [$Fe_{0.70}Ni_{0.20}Cr_{0.10}$] plus 0.0911 [$Ti_{0.56}Co_{0.44}$].

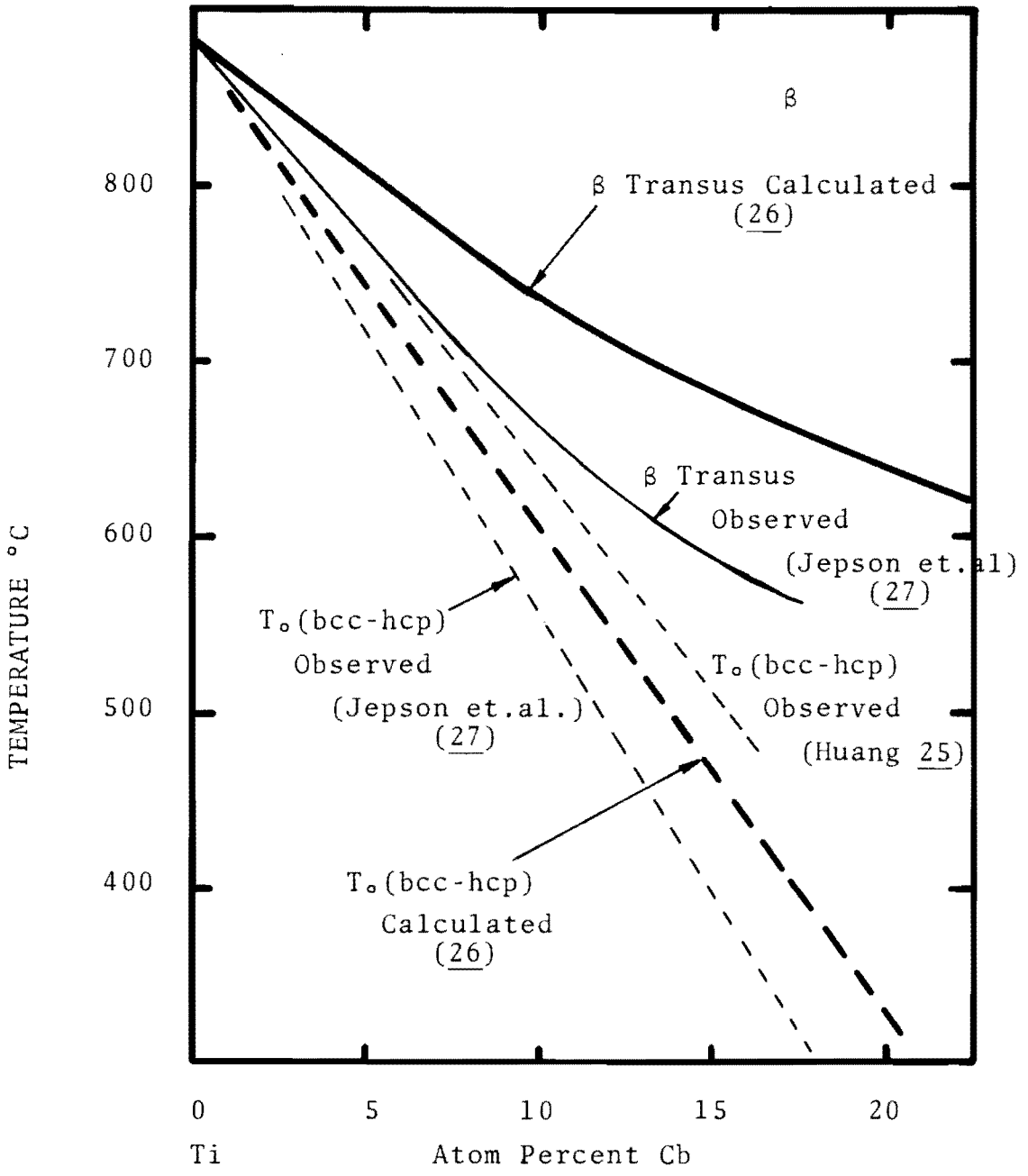

Figure 1 Observed and Calculated Transformation Temperatures in the Ti-Cb System

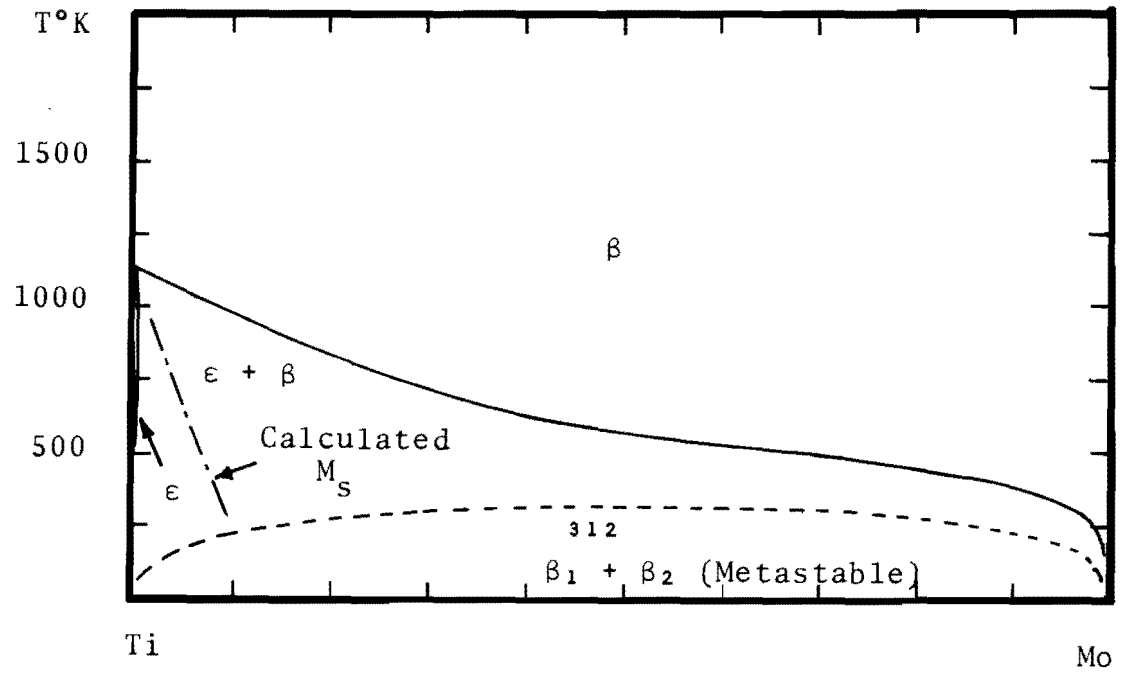

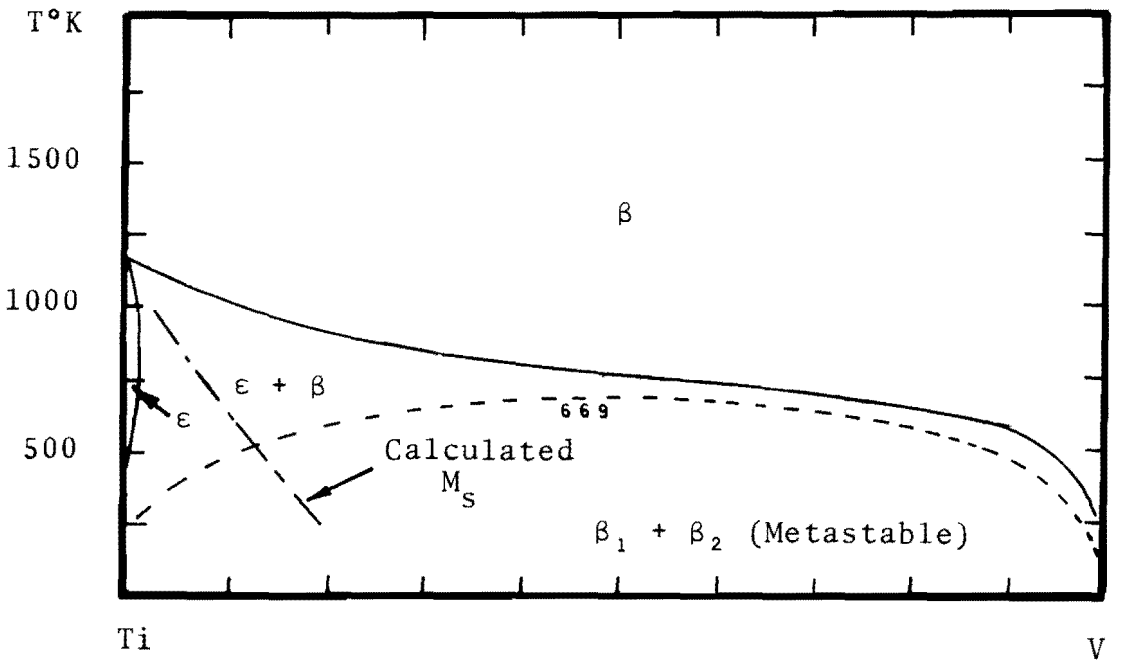

Figure 2. Calculated Partial Ti-Mo and Ti-V Phase Diagrams.

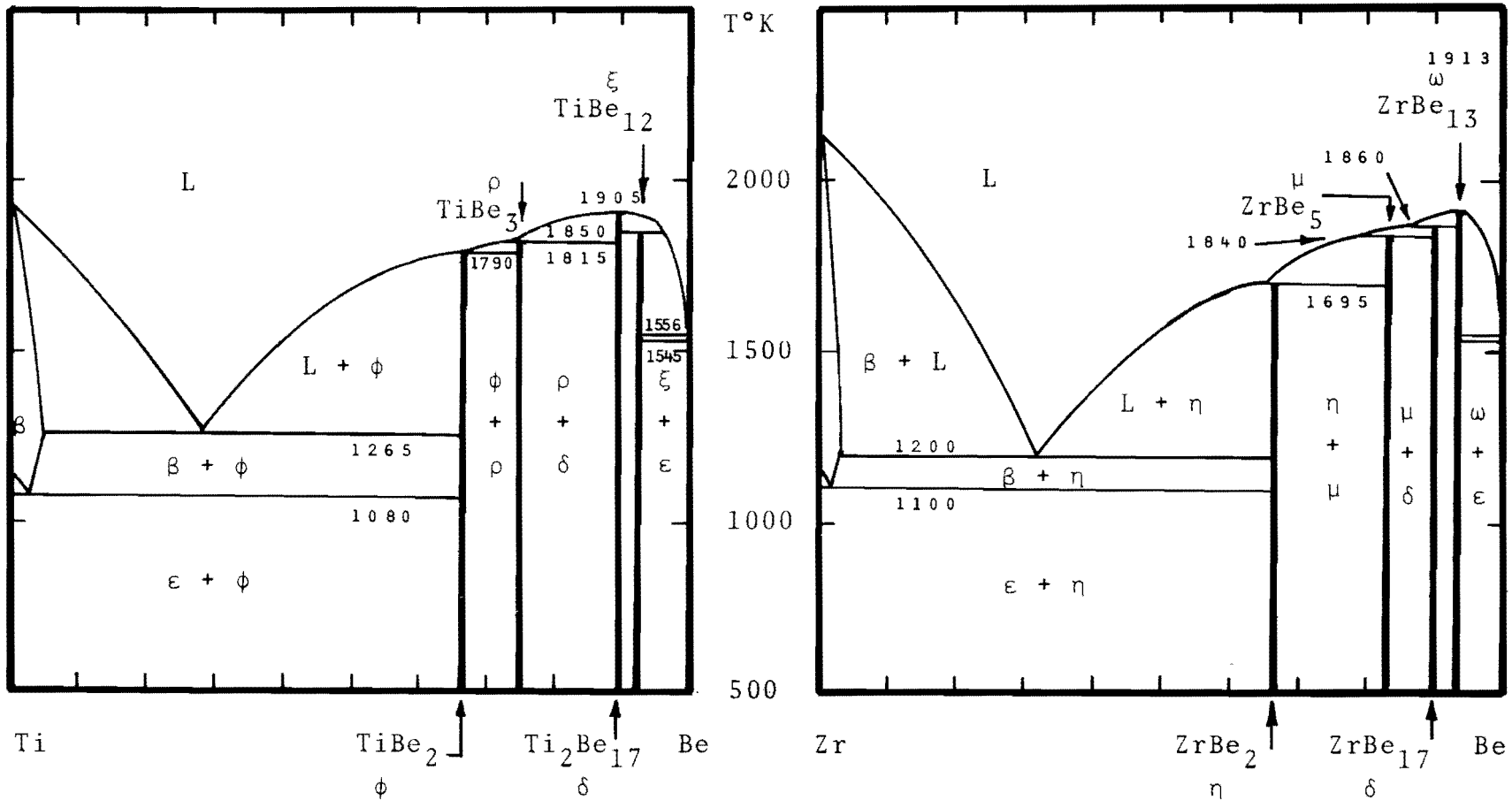

Figure 3. Calculated Ti-Be and Zr-Be Phase Diagrams

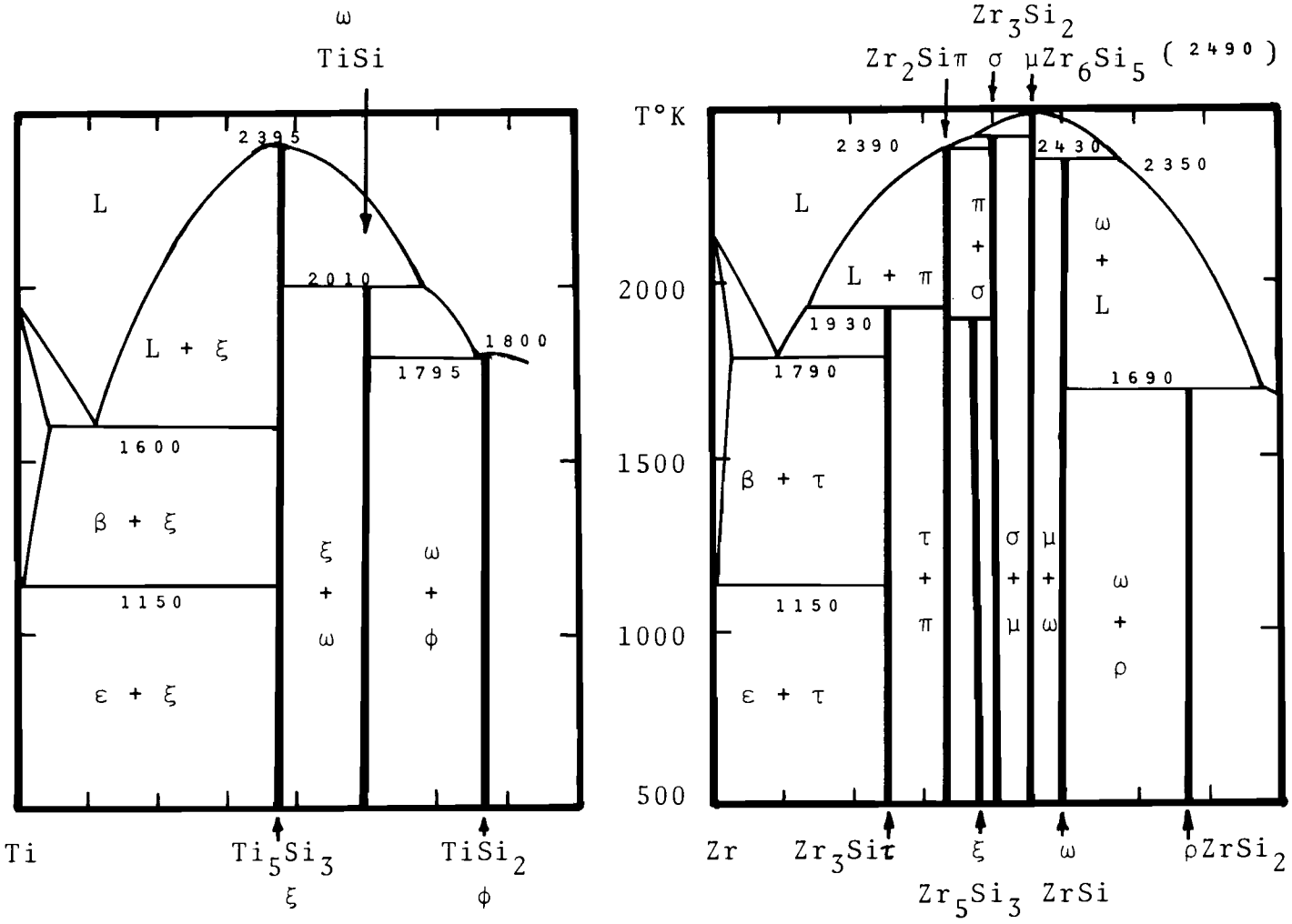

Figure 4. Calculated Partial Ti-Si and Zr-Si Phase Diagrams

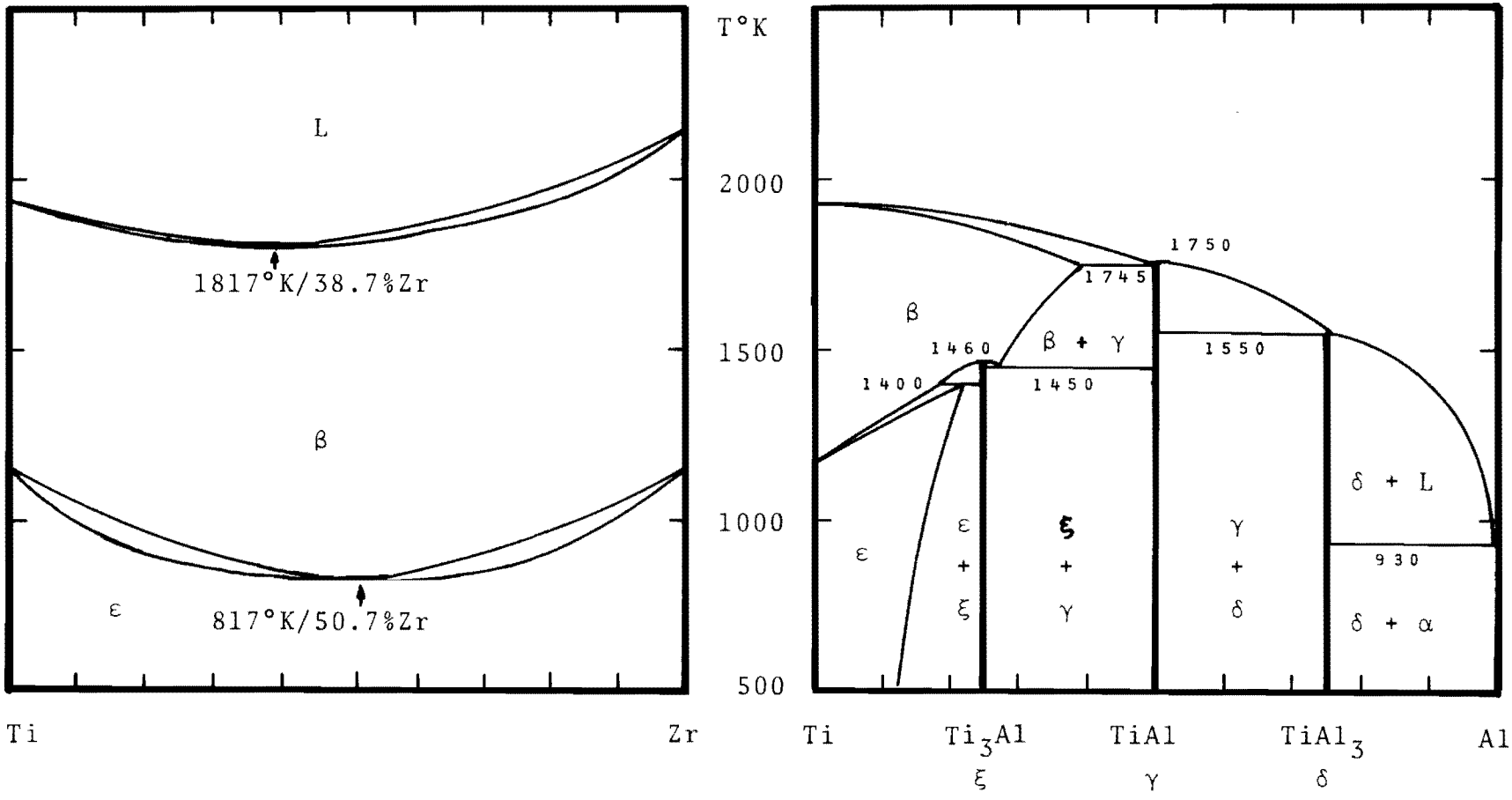

Figure 5. Calculated Ti-Zr and Ti-Al Phase Diagrams

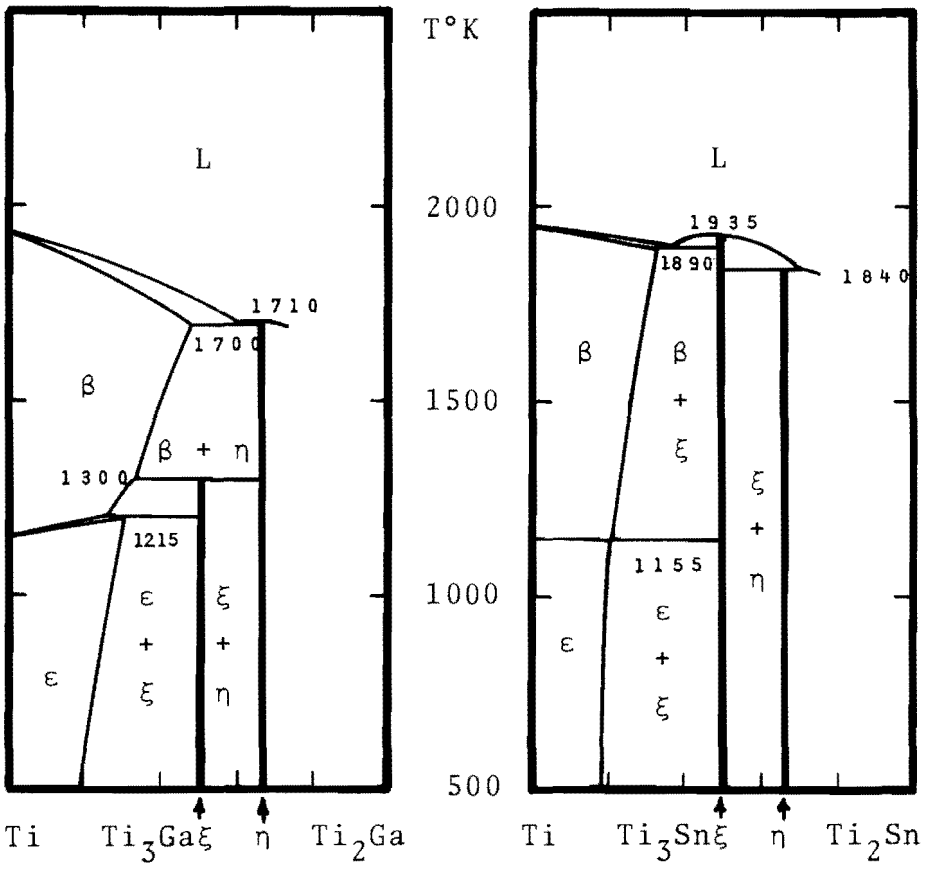

Figure 6. Calculated Partial Ti-Ga and Ti-Sn Phase Diagrams

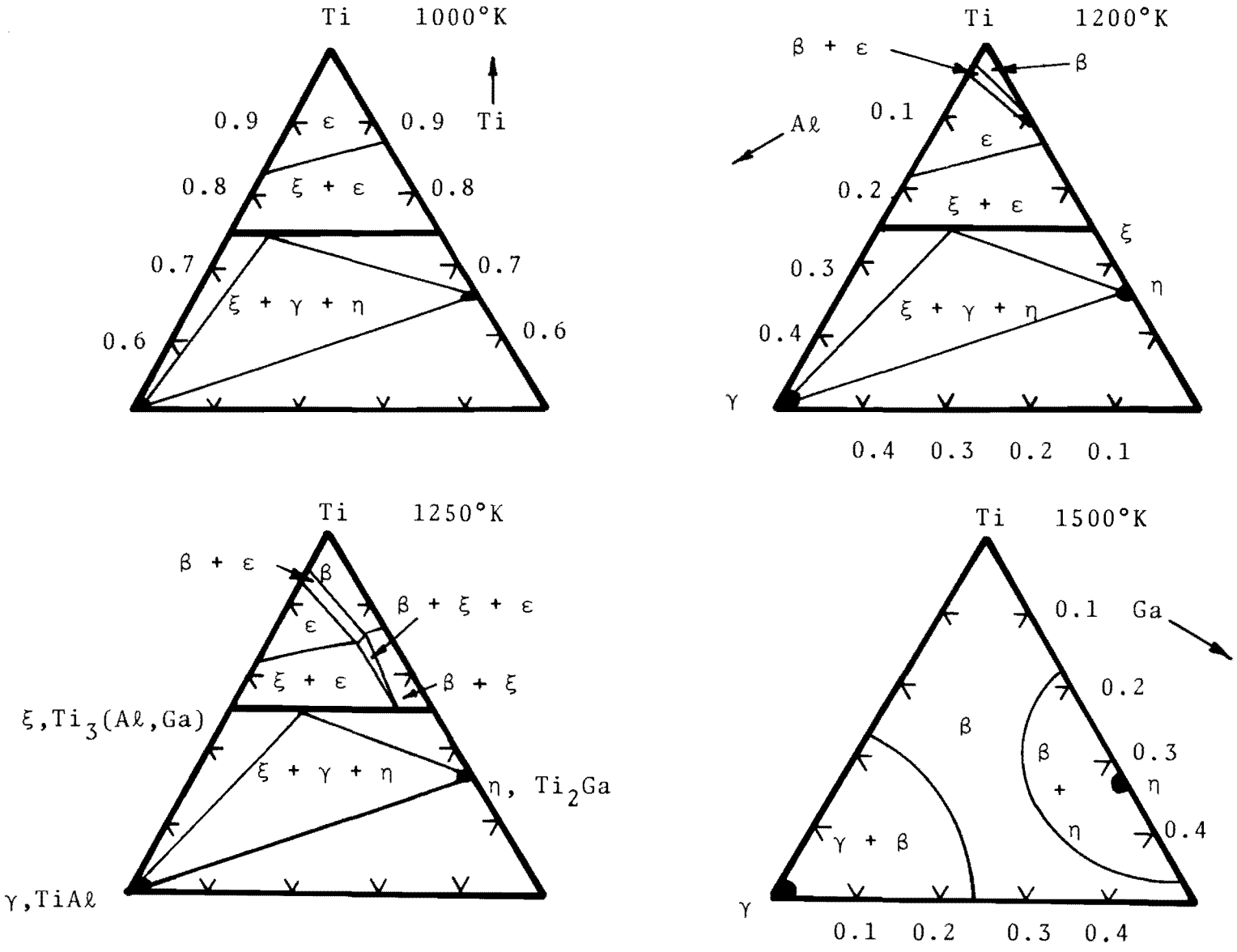

Figure 7. Calculated Partial Isothermal Sections in the Ti-Ga-Aℓ System

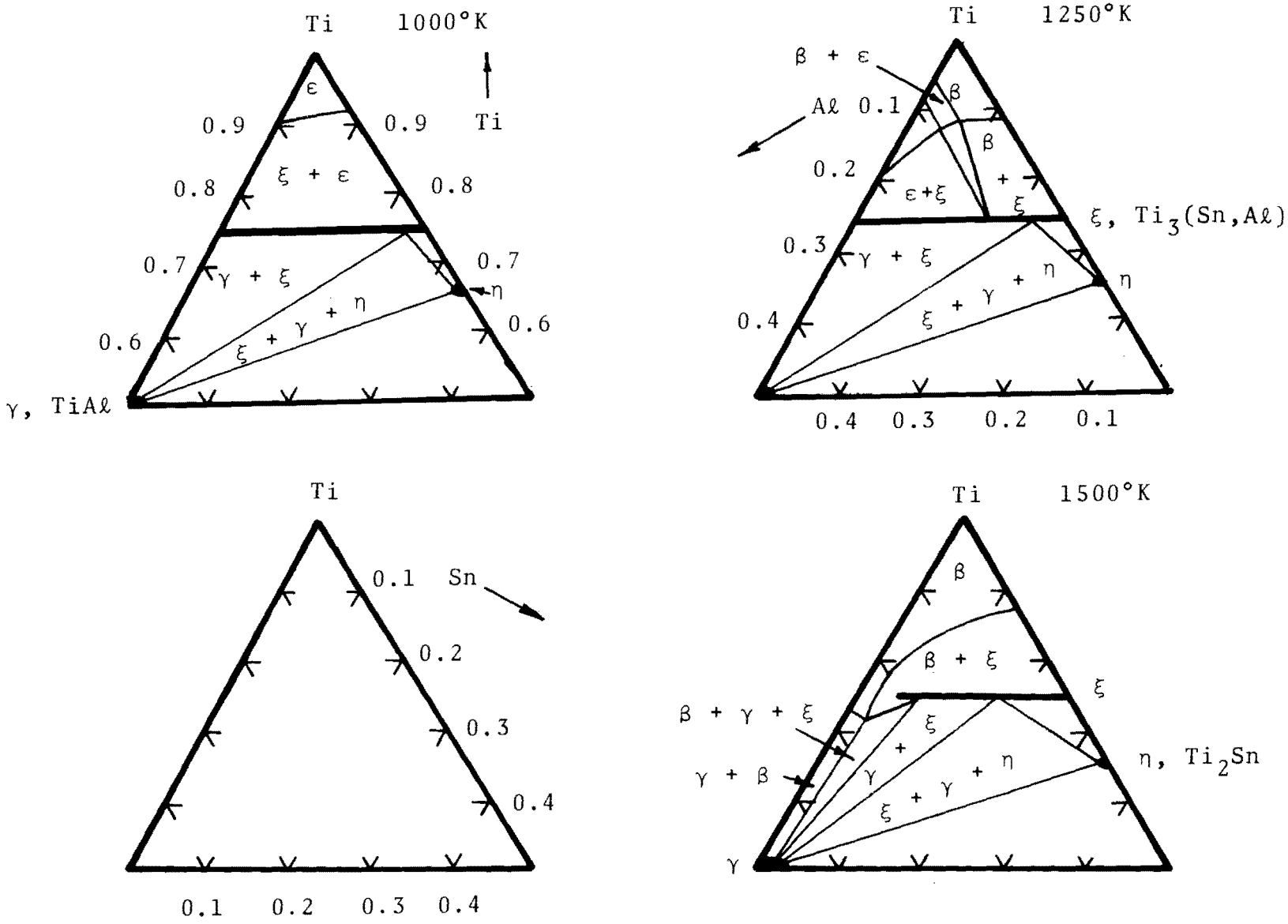

Figure 8 Calculated Partial Isothermal Sections in the Ti-Sn-Al System

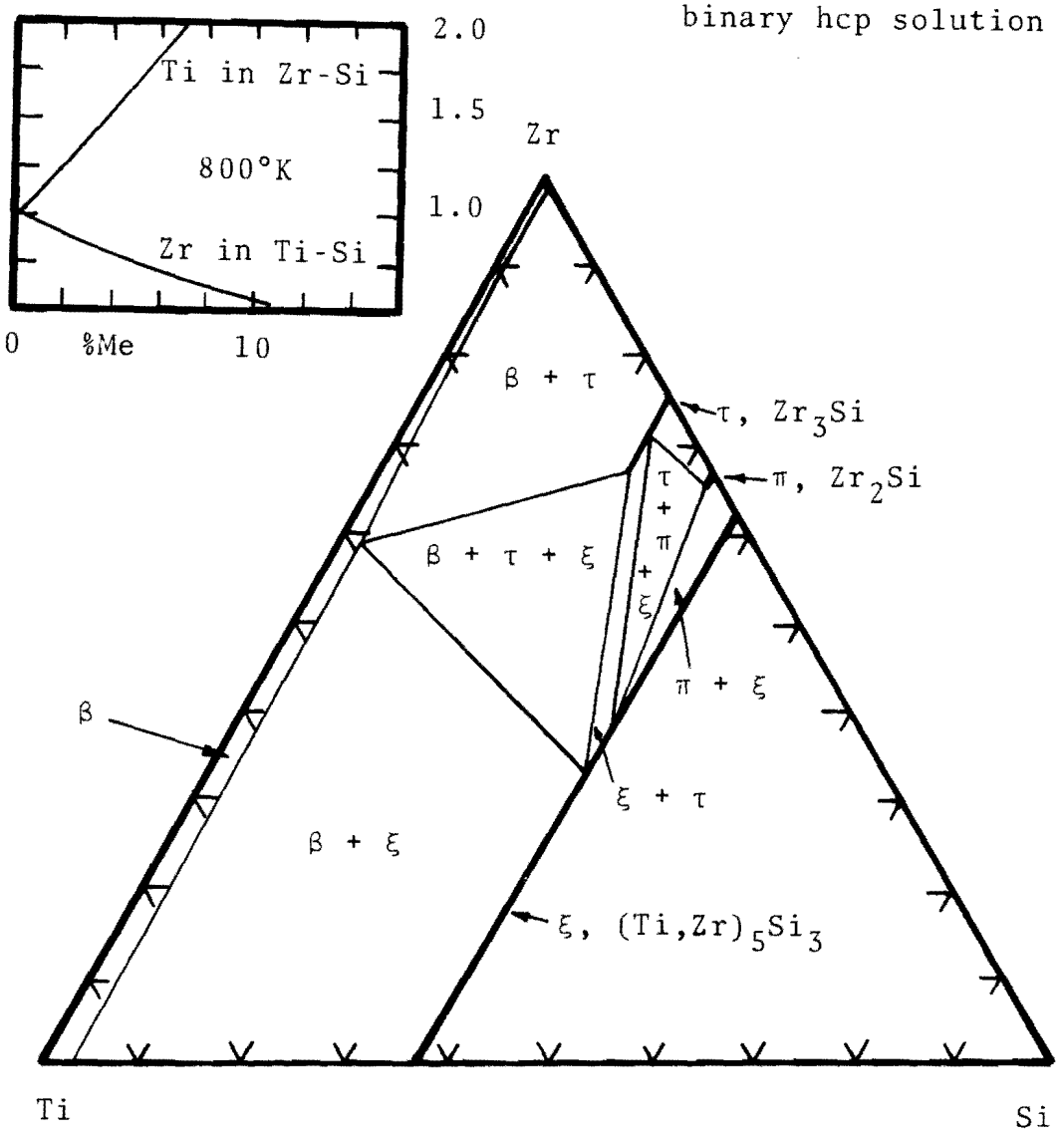

Figure 9 Calculated Partial Isothermal Section in the Zr-Si-Ti System at 1500°K

Insert shows calculated ratio of beryllium solubility in the hcp ternary solution divided by beryllium solubility in hcp binary solution

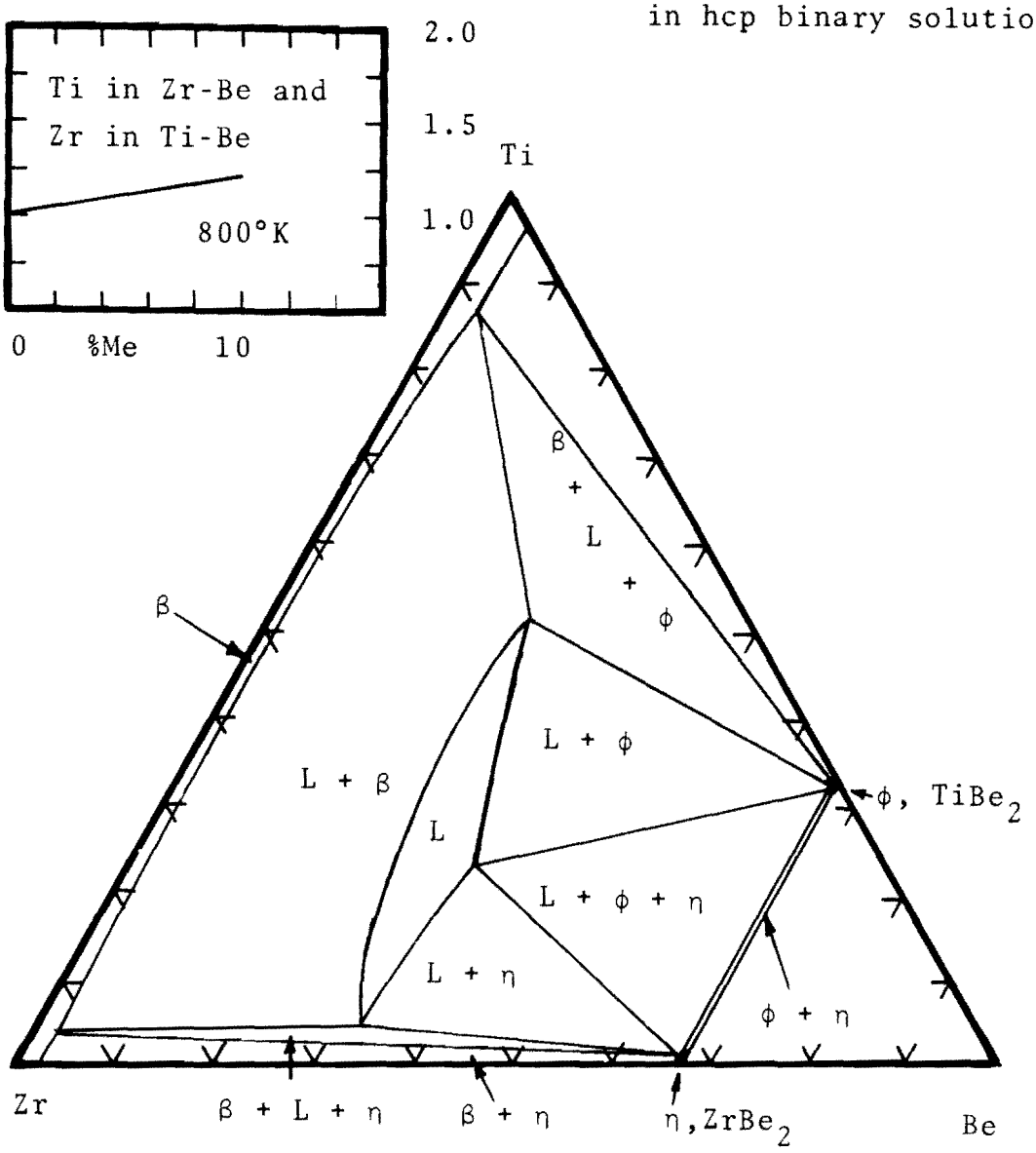

Figure 10 Calculated Partial Isothermal Section in the Ti-Be-Zr System at 1180°K

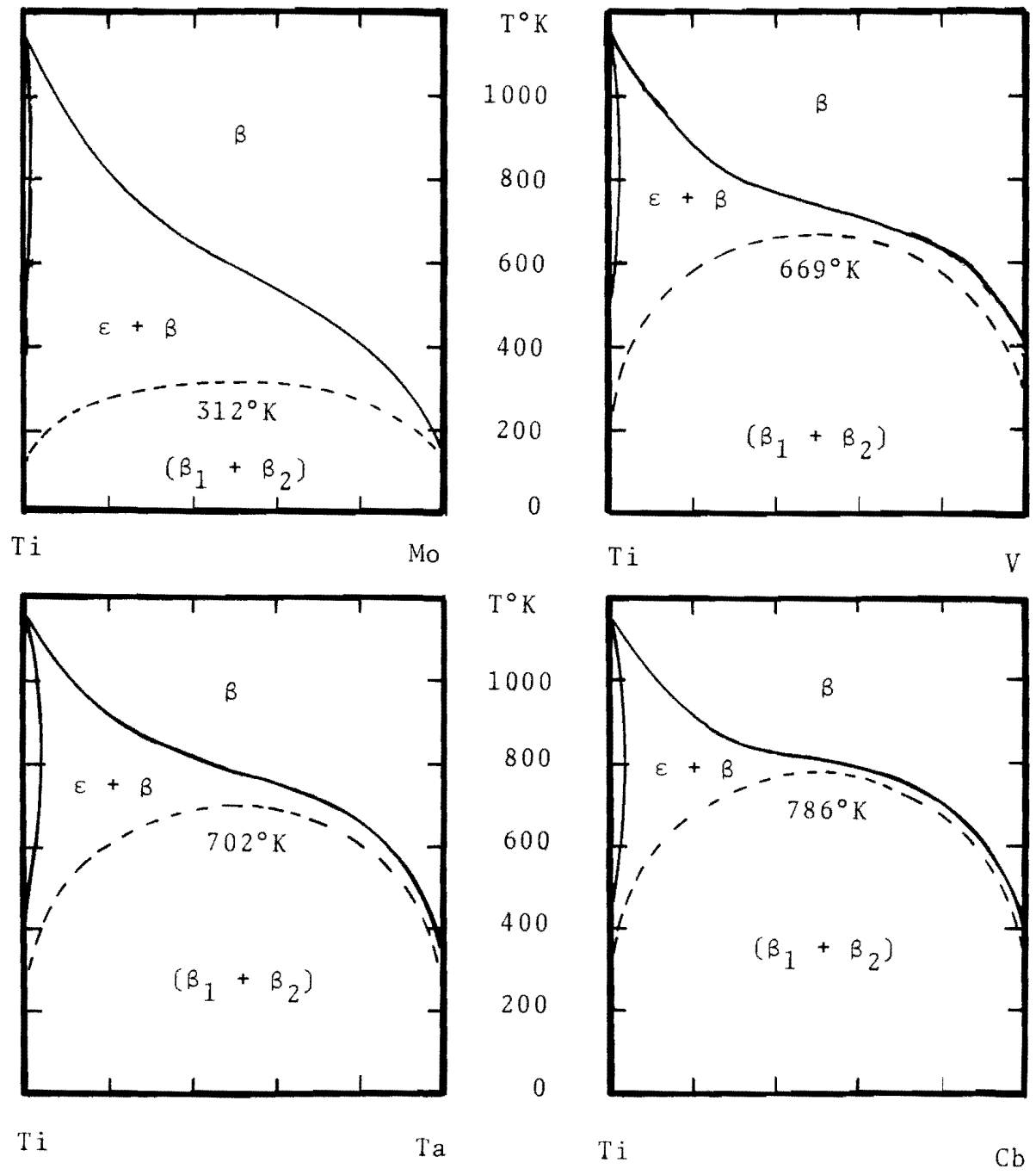

Figure 11 Calculated BCC/HCP Equilibria and Metastable BCC Miscibility Gaps in Binary Titanium Systems

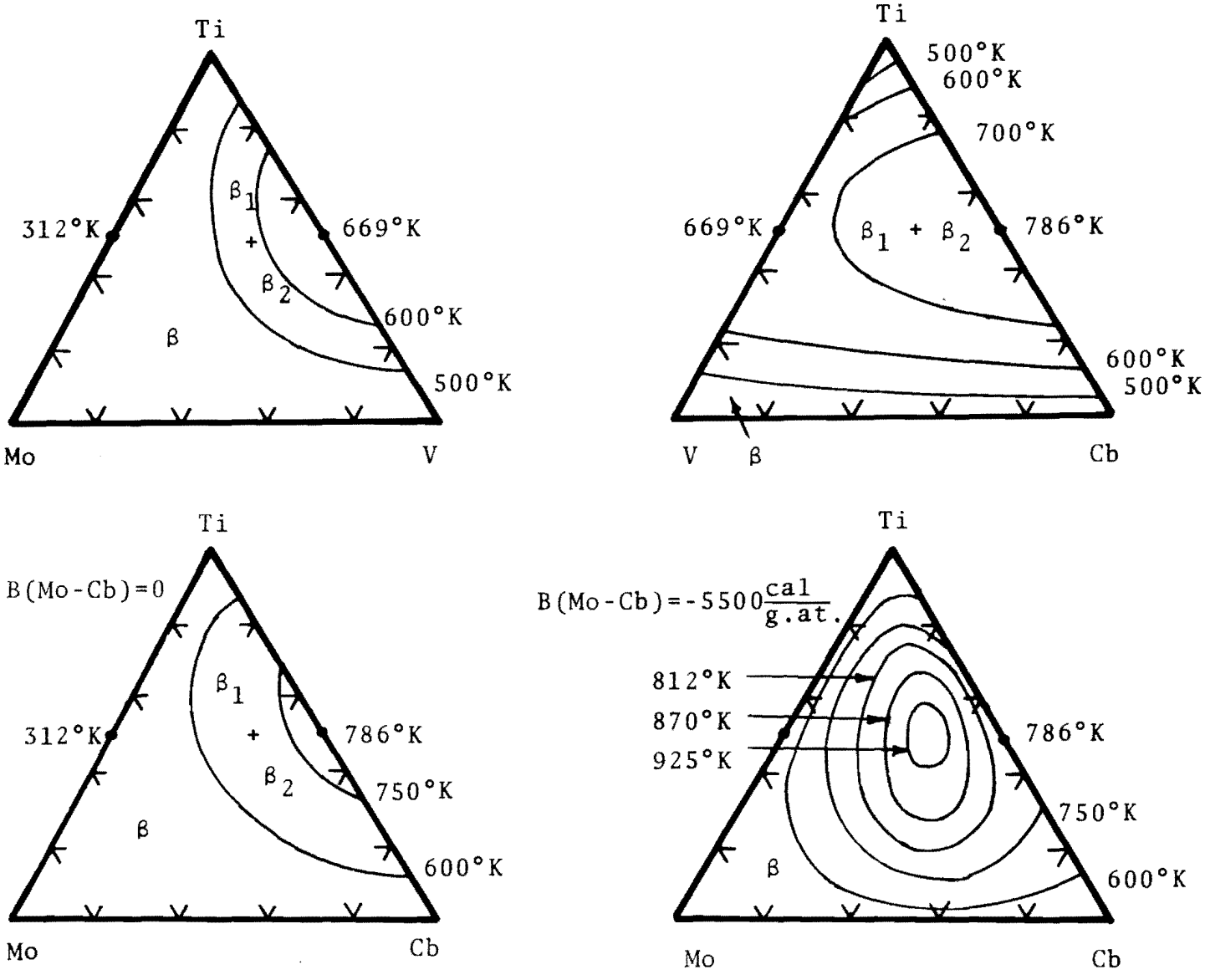

Figure 12 Calculated Miscibility Gaps in the BCC Phase of the Ti-V-Mo, Ti-Cb-V and Ti-Cb-Mo Systems

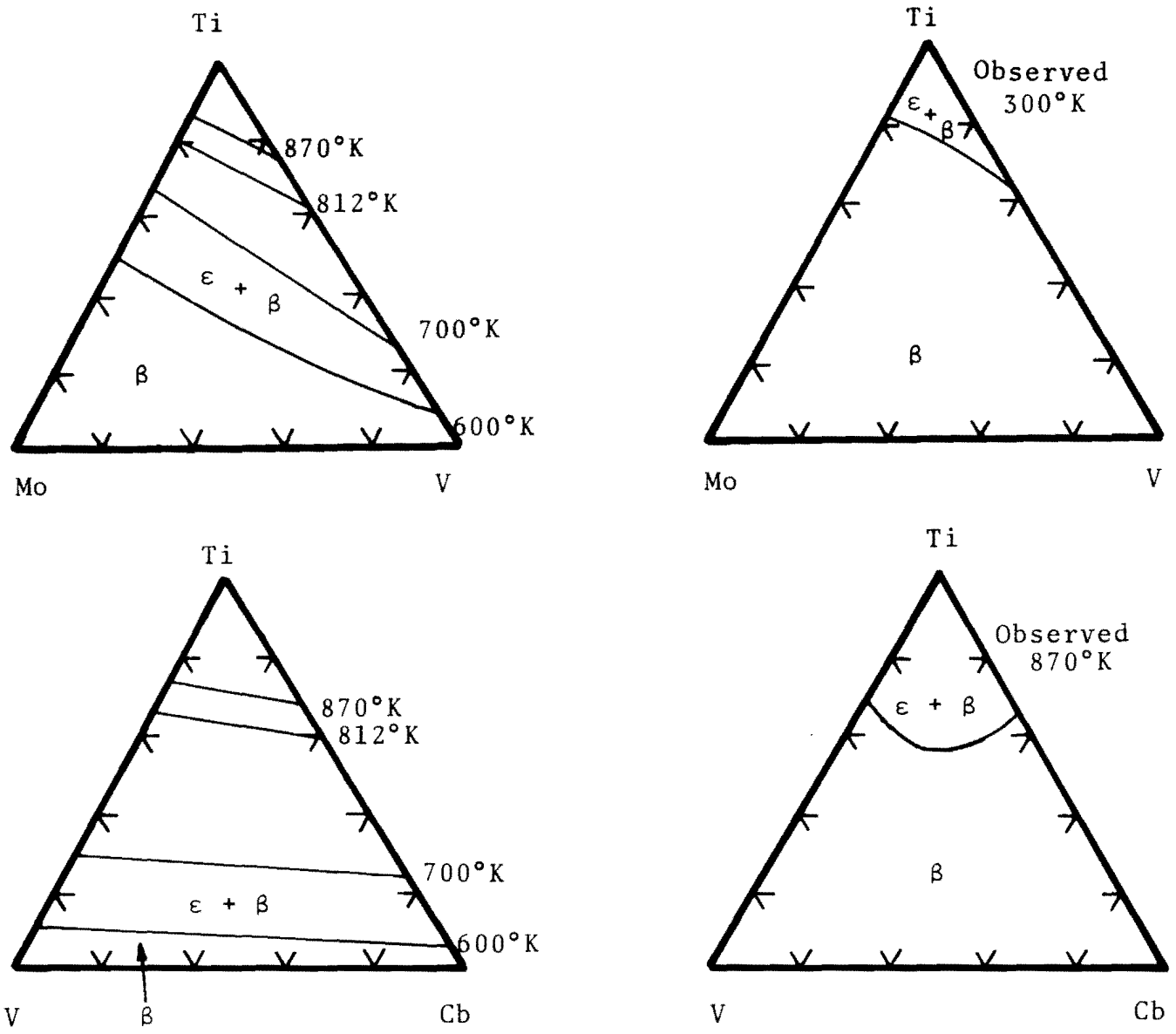

Figure 13 Calculated and Observed BCC/(HCP + BCC) Phase Boundaries in the Ti-V-Mo and Ti-Cb-V Systems

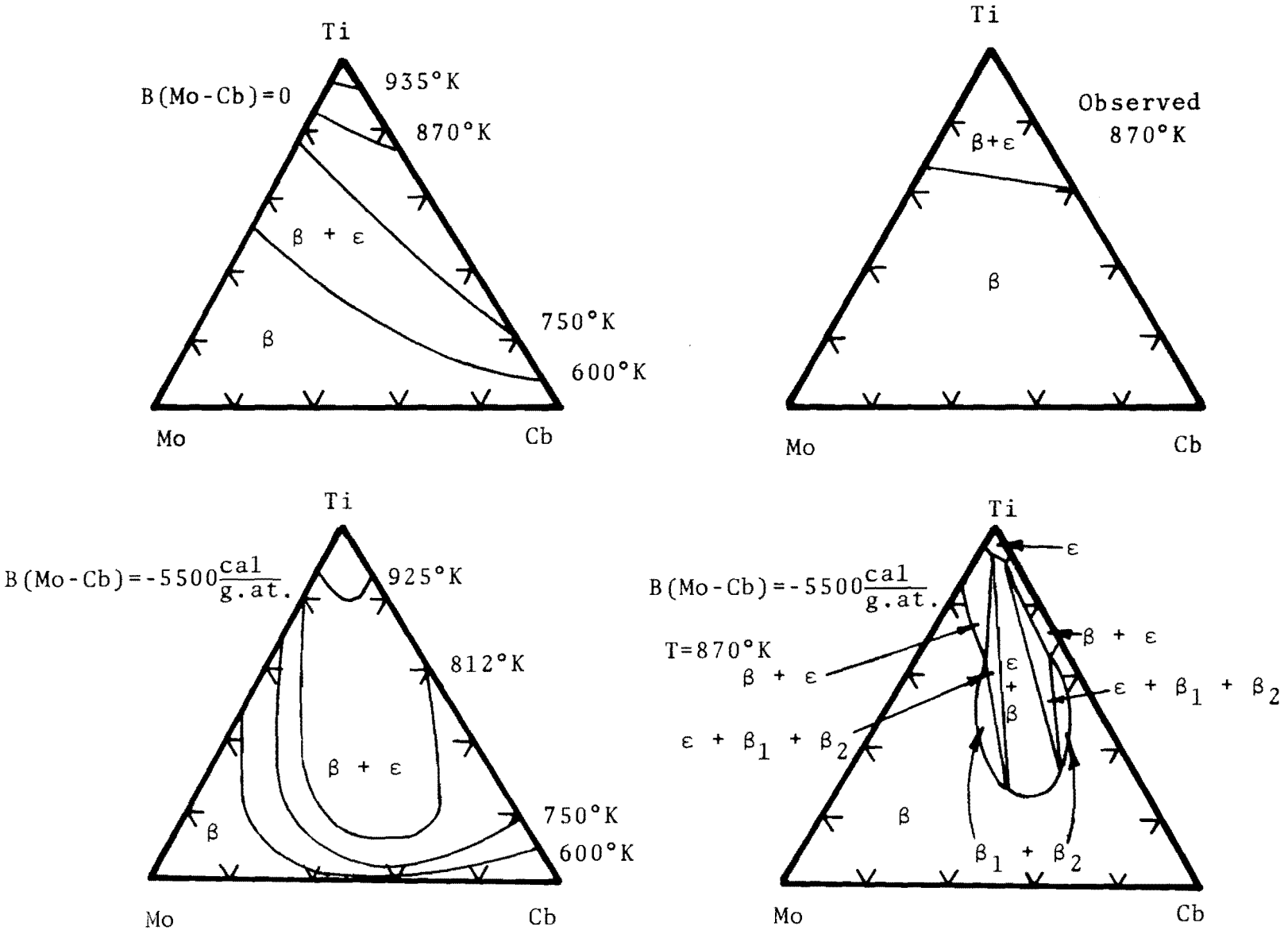

Figure 14 Calculated BCC/(BCC + HCP) Phase Boundaries in the Ti-Cb-Mo System. Observed Boundary at 870°K shown in the upper right corner

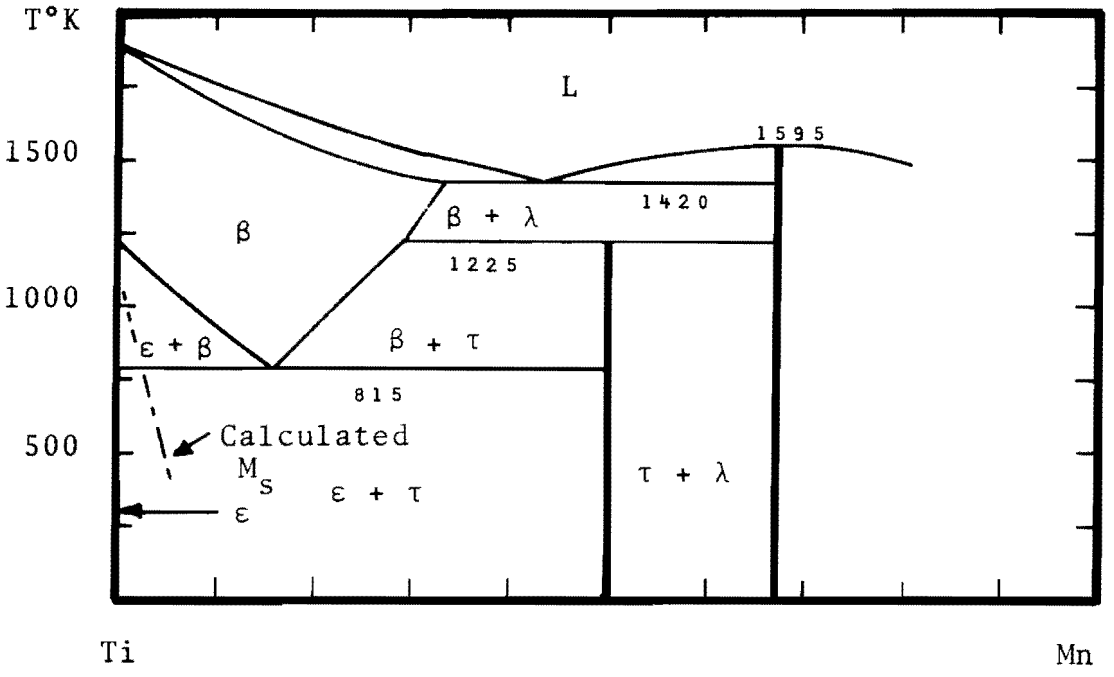

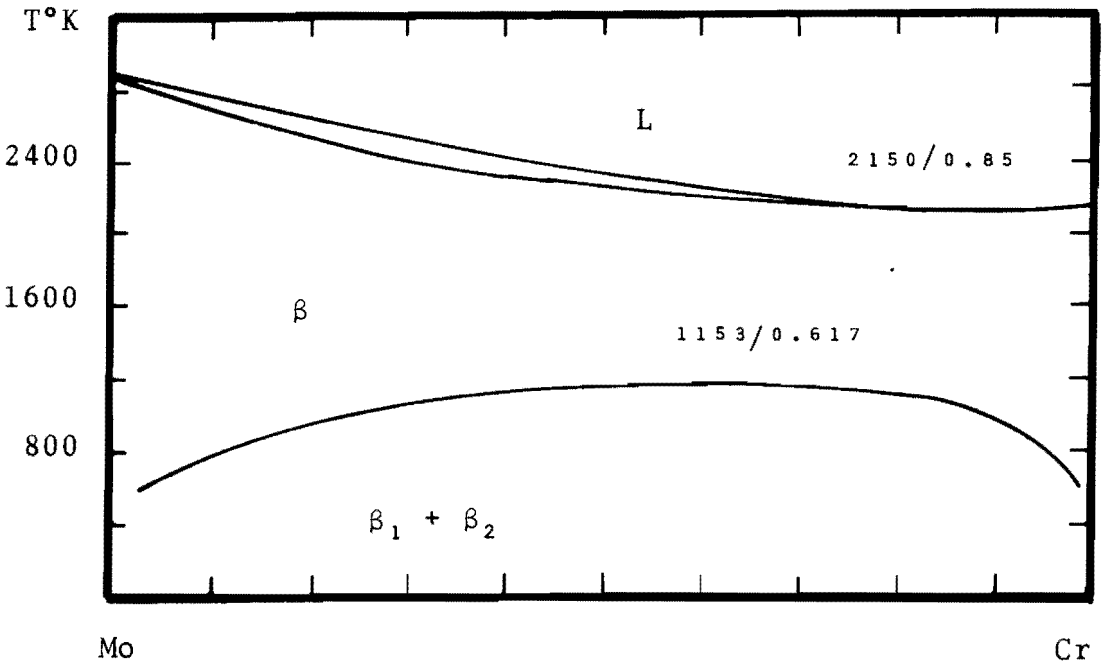

Figure 15 Calculated Partial Ti-Mn and Mo-Cr Phase Diagrams.

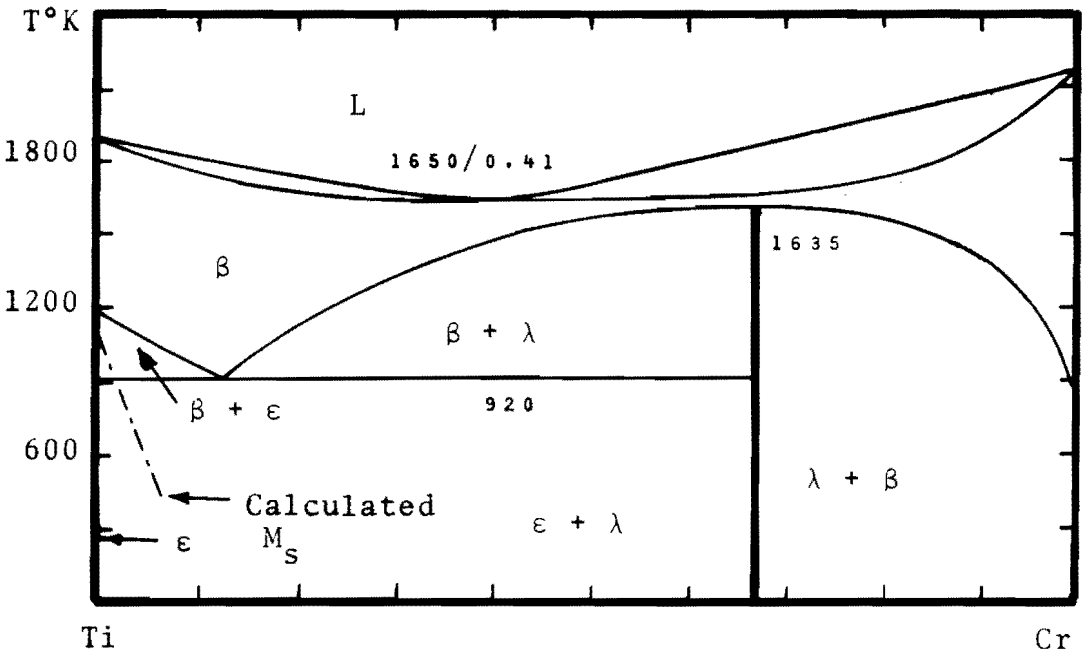

Figure 16. Calculated Partial Cr-Al and Ti-Cr Phase Diagrams.

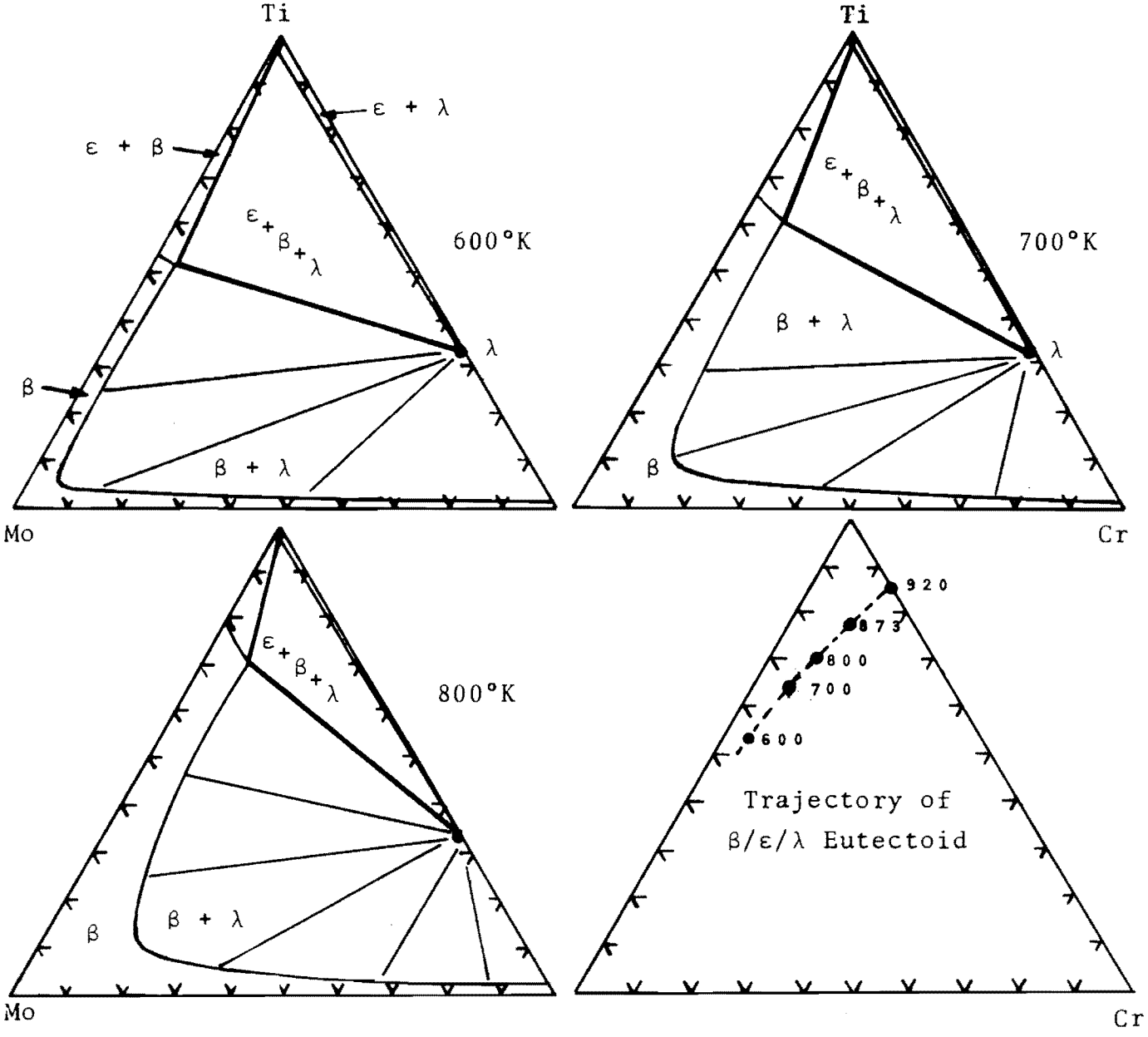

Figure 17. Calculated BCC/HCP/Laves Phase Equilibria in the Ti-Cr-Mo System.

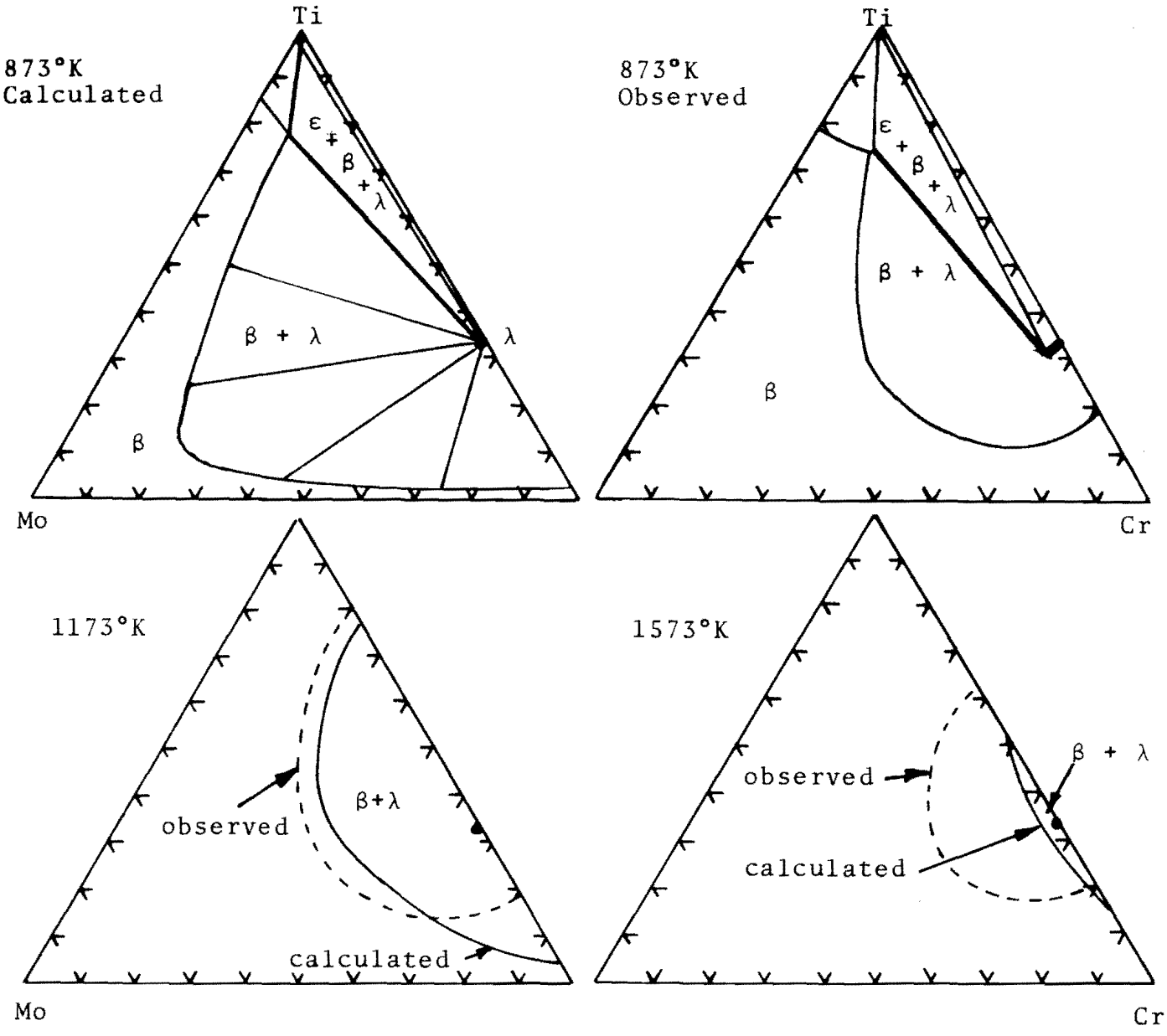

Figure 18. Calculated and Observed Isothermal Sections in the Ti-Cr-Mo System at 873, 1173 and 1573°K.

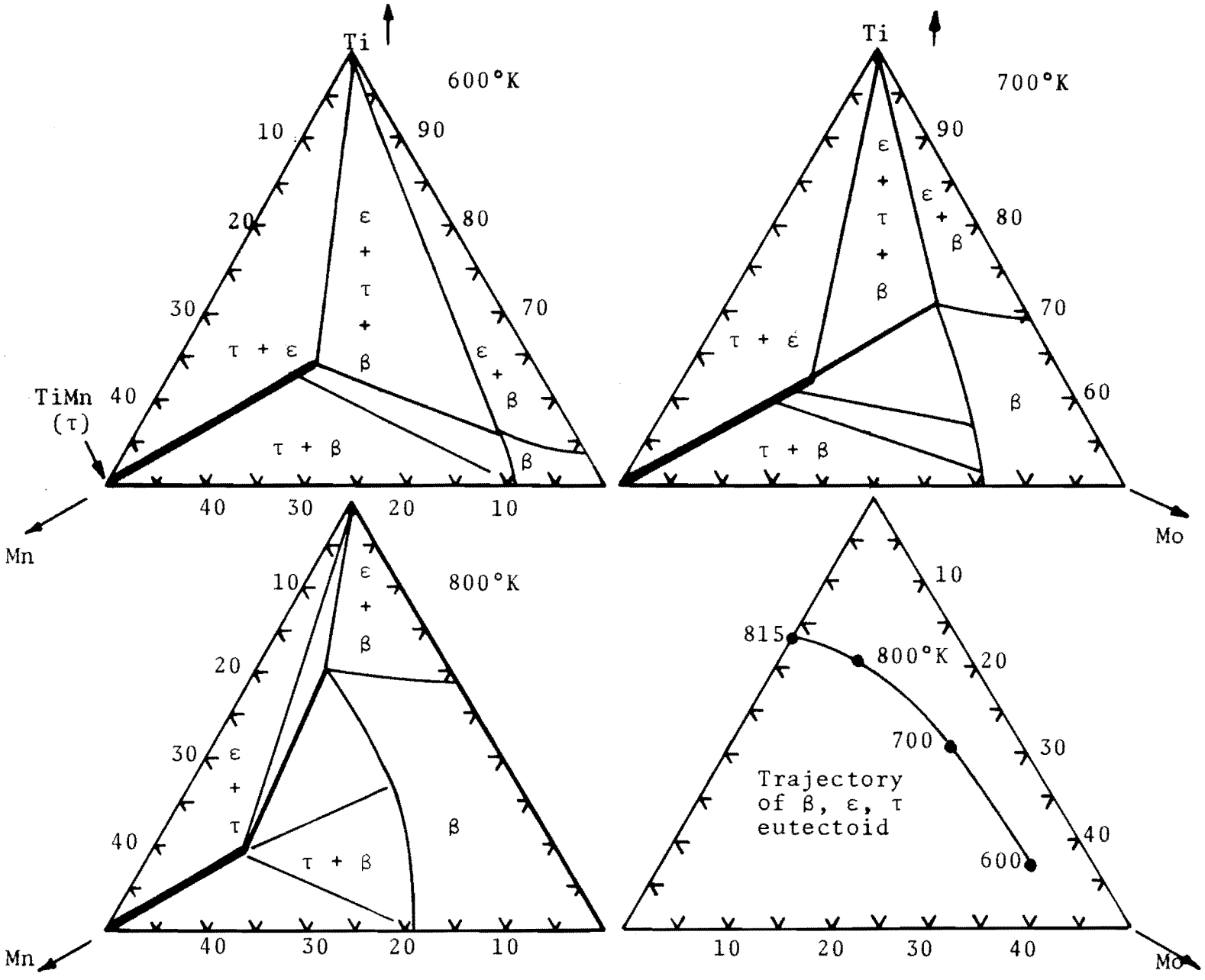

Figure 19. Calculated Phase Boundaries in the Ti-Mo-Mn System.

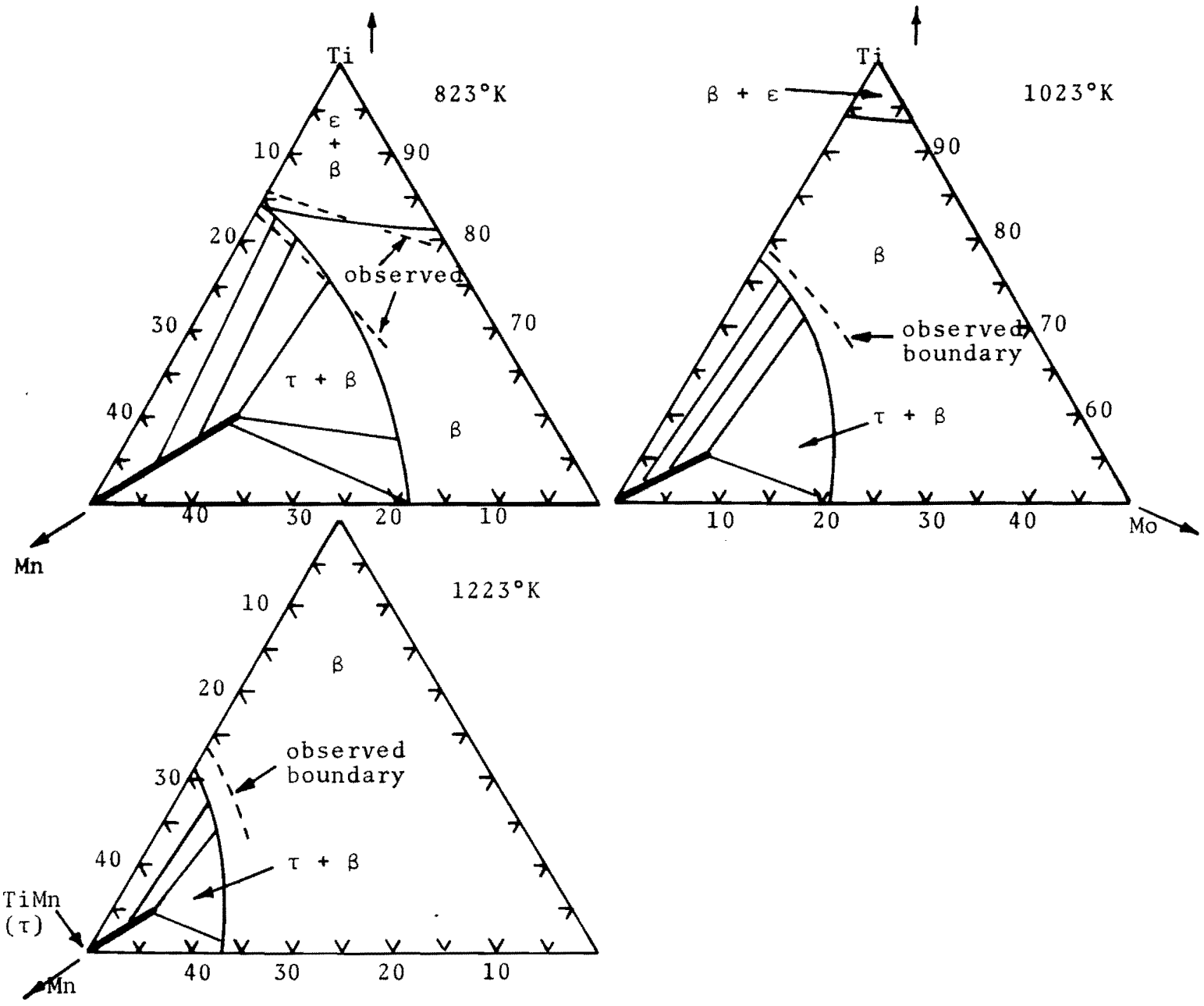

Figure 20 Calculated and Observed Phase Boundaries in the Ti-Mo-Mn System.

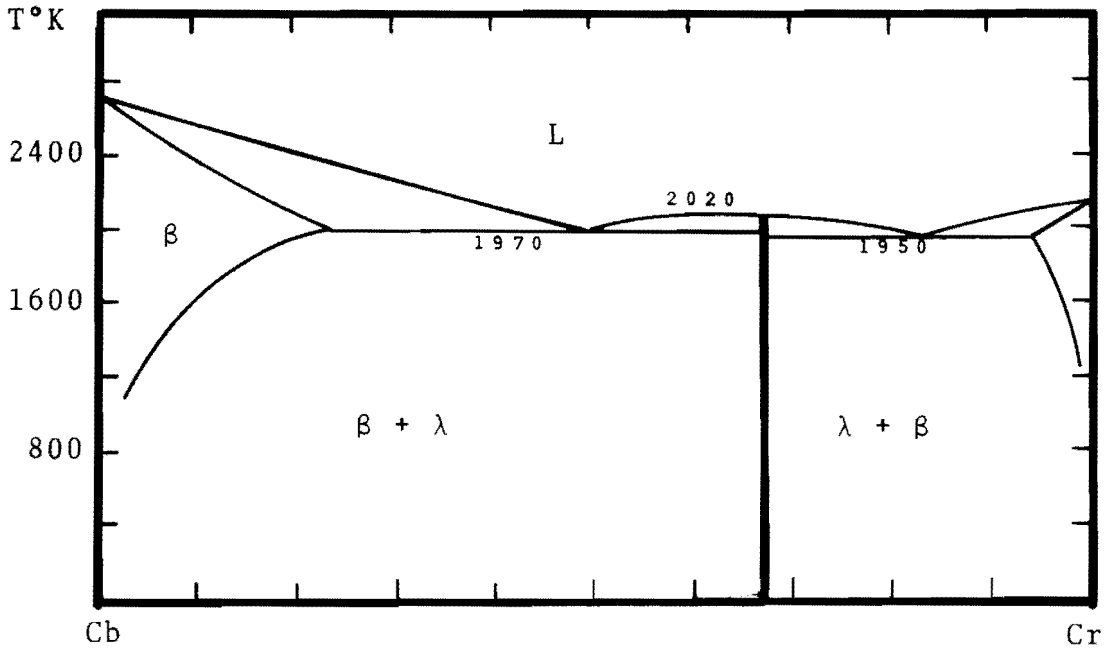

Figure 21. Calculated Phase Diagram for the Cb-Cr System.

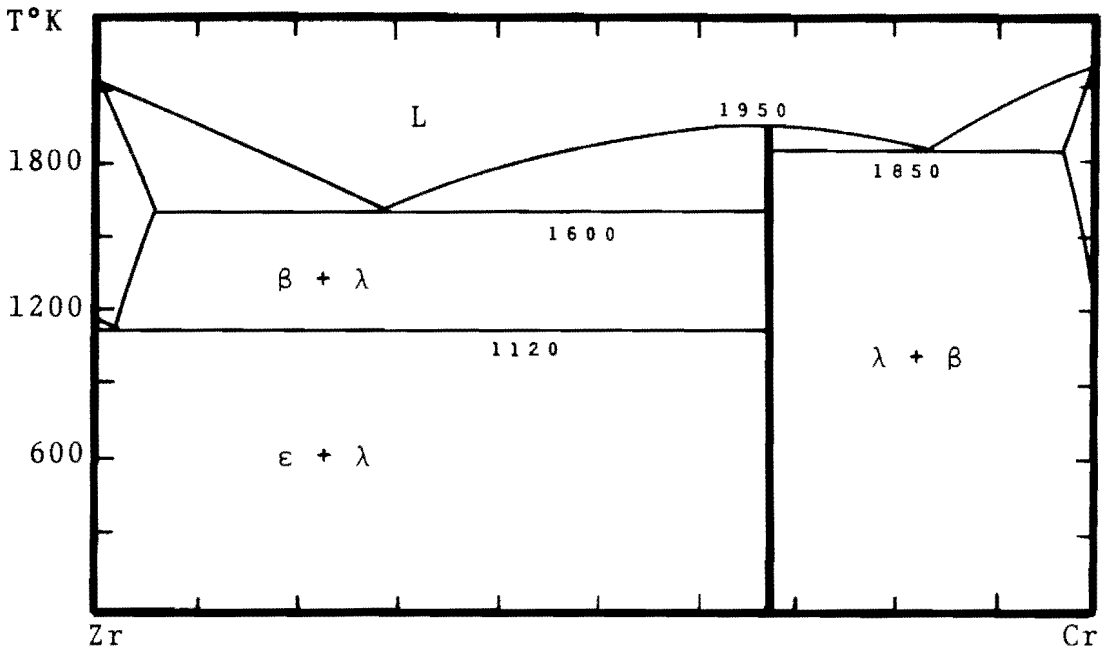

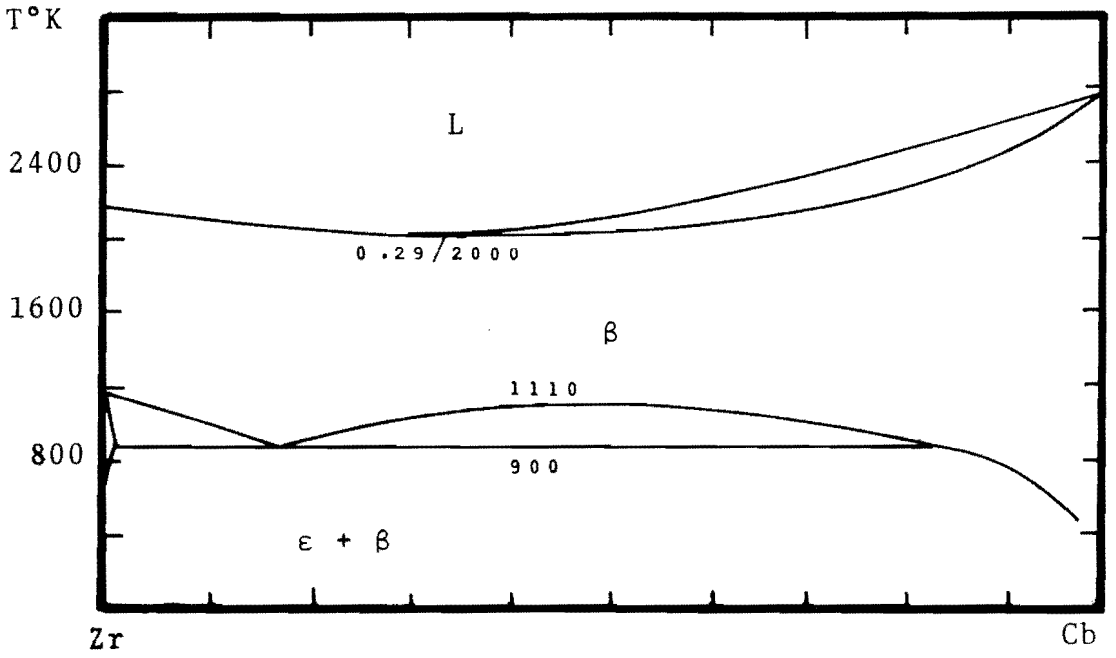

Figure 22 Calculated Zr-Cr and Zr-Cb Phase Diagrams.

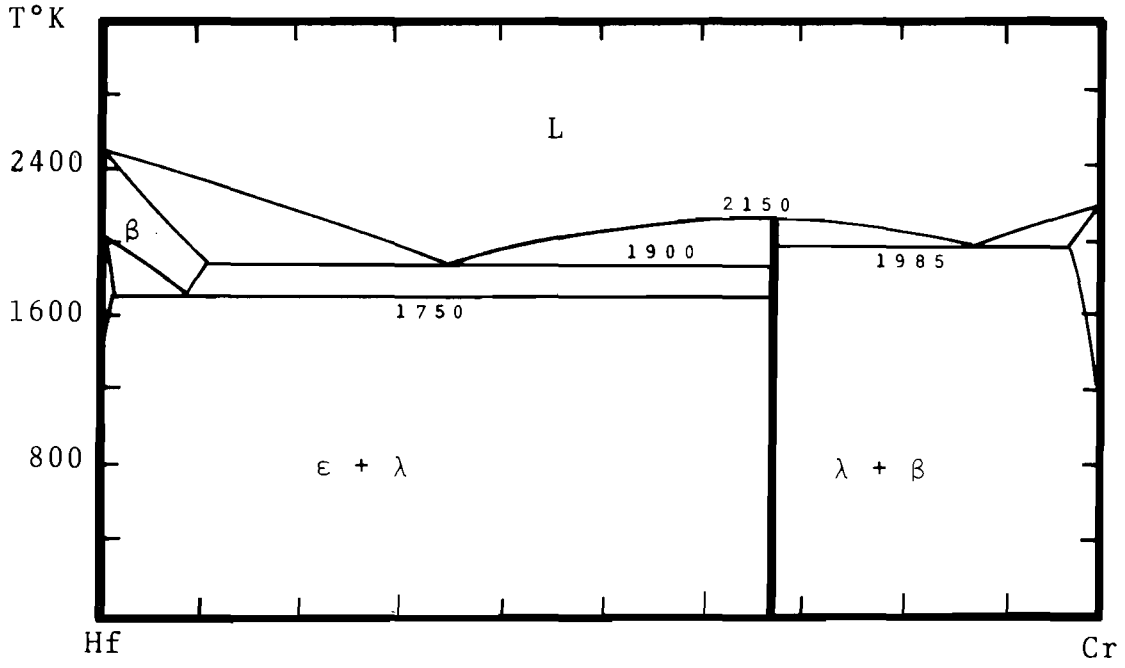

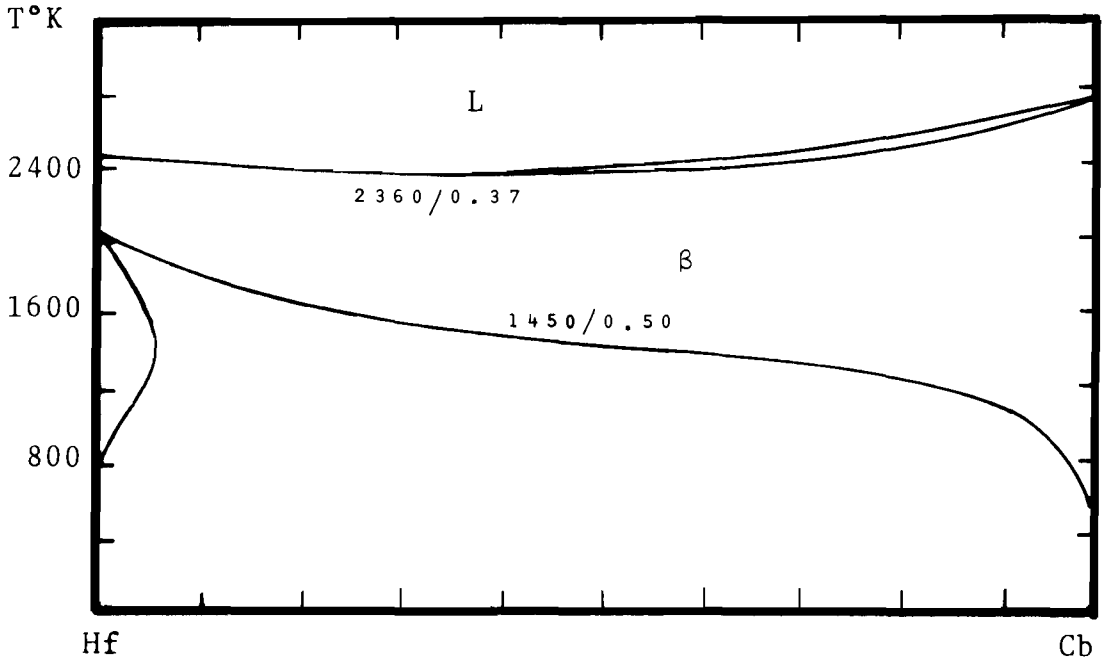

Figure 23 Calculated Hf-Cr and Hf-Cb Phase Diagrams.

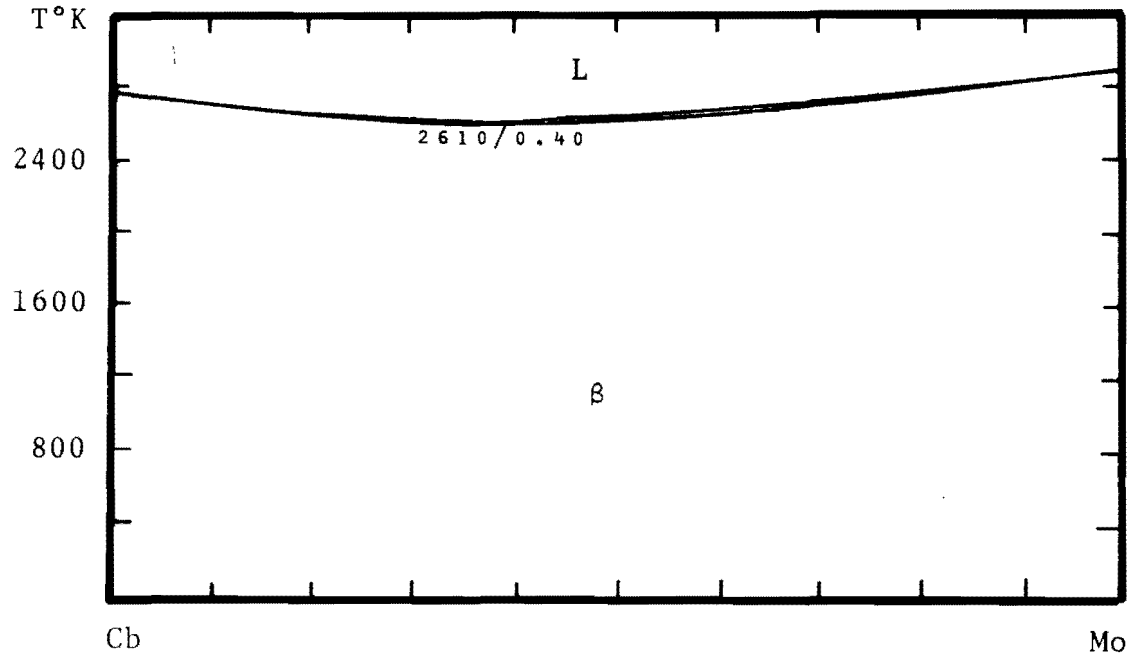

Figure 24 Calculated Cb-Mo Phase Diagram.

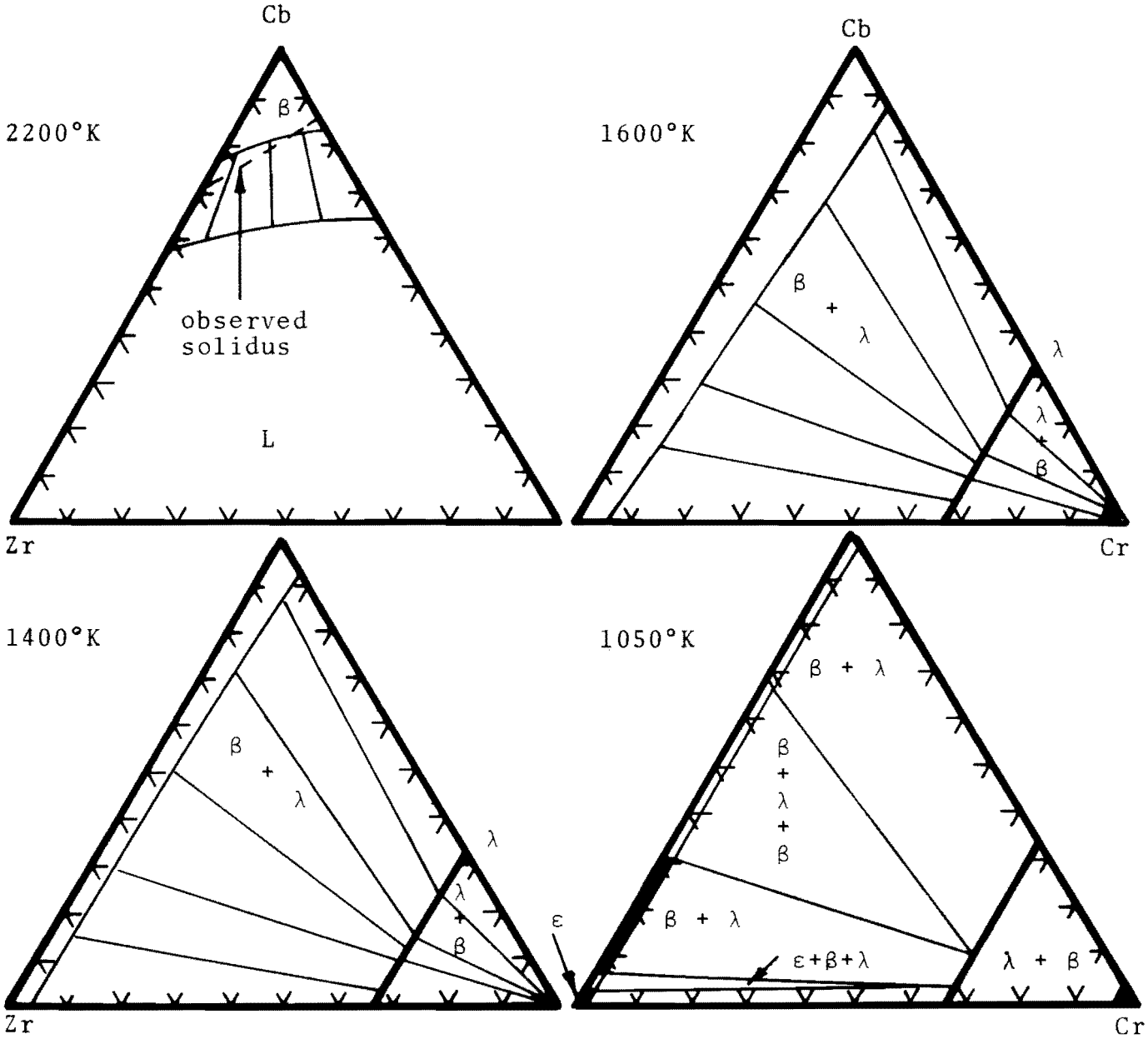

Figure 25 Calculated and Observed Isothermal Sections in the Cb-Cr-Zr System.

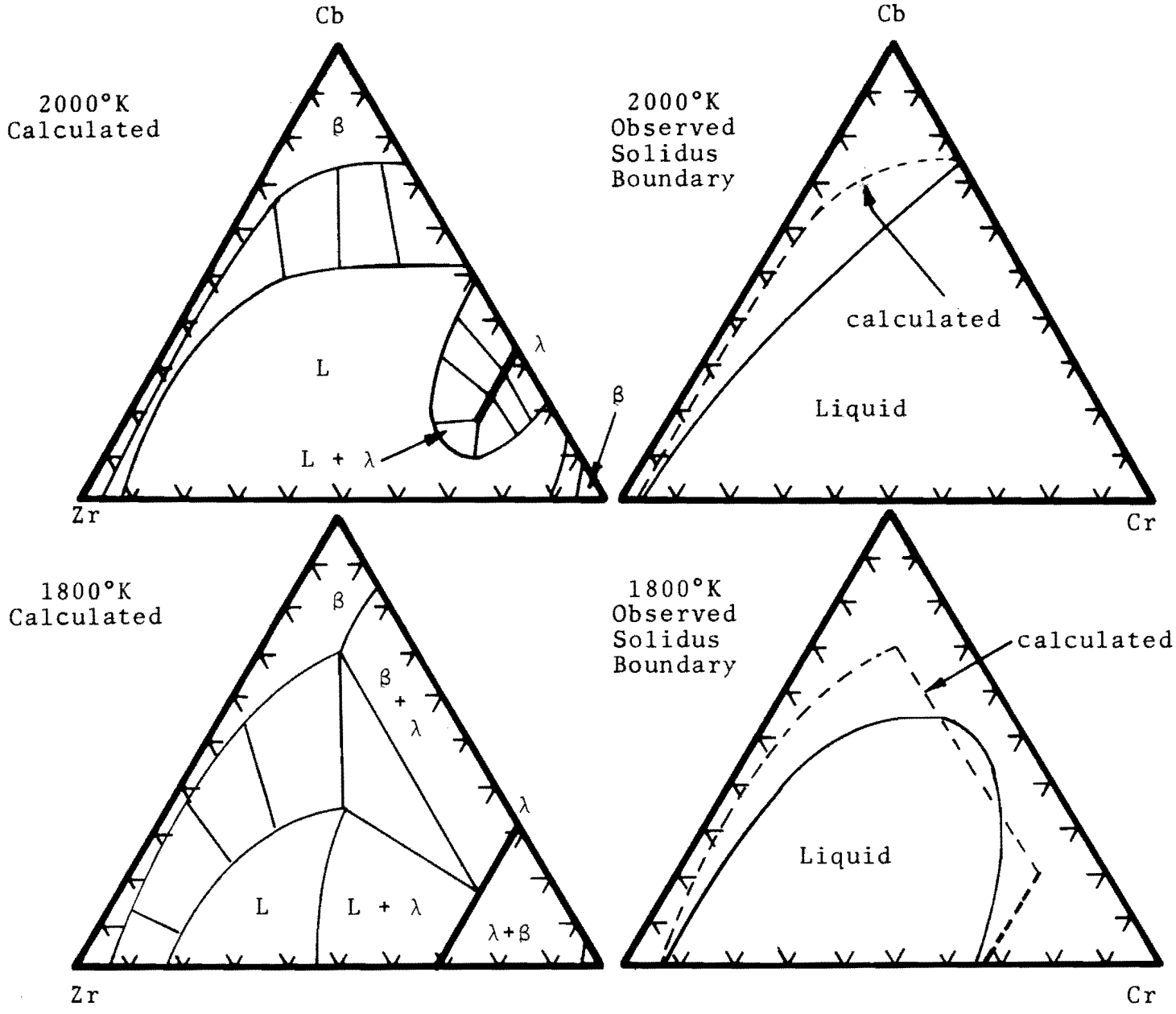

Figure 26 Calculated and Observed Isothermal Sections in the Cb-Cr-Zr System.

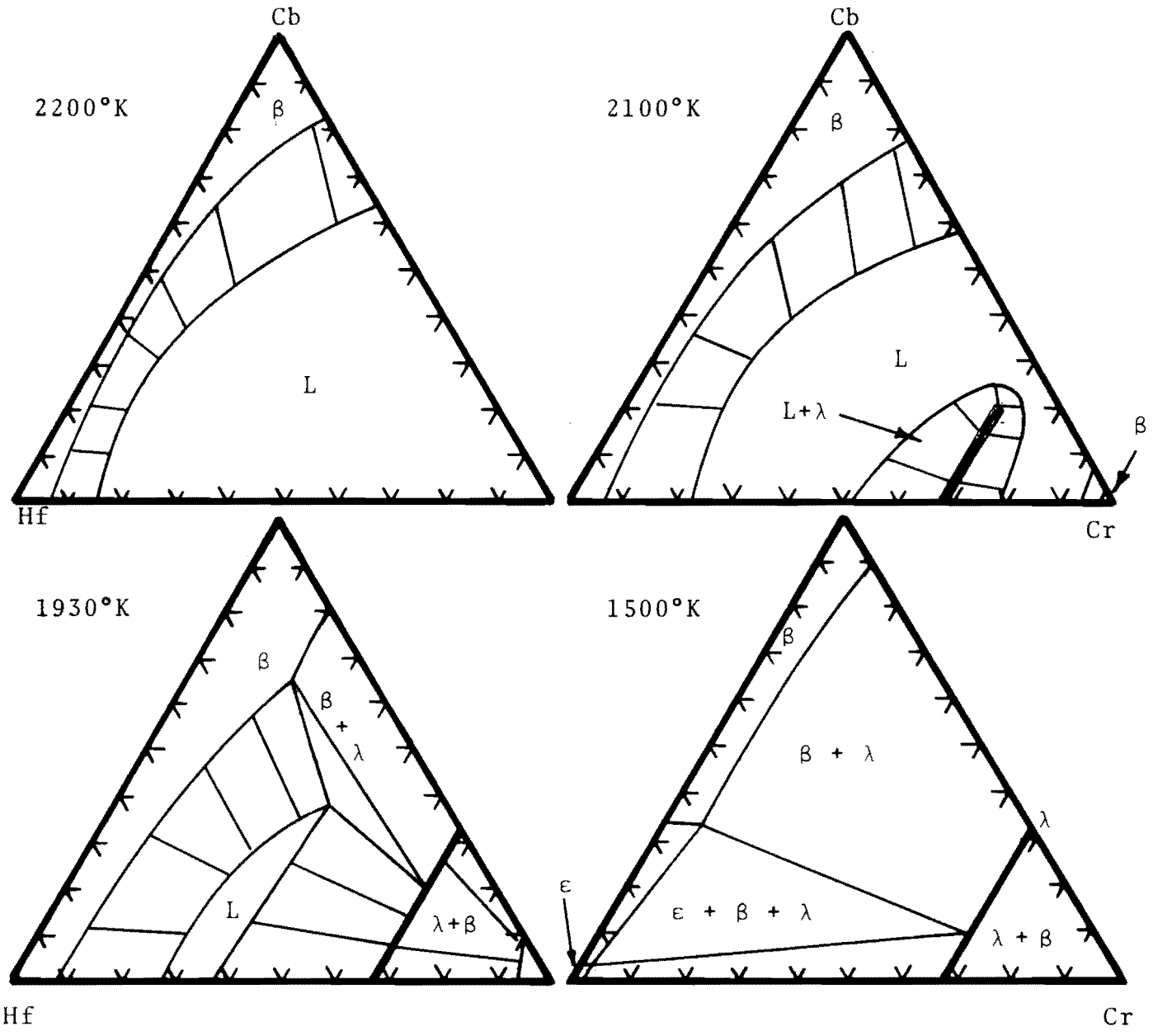

Figure 27 Calculated Isothermal Sections in the Cb-Cr-Hf System.

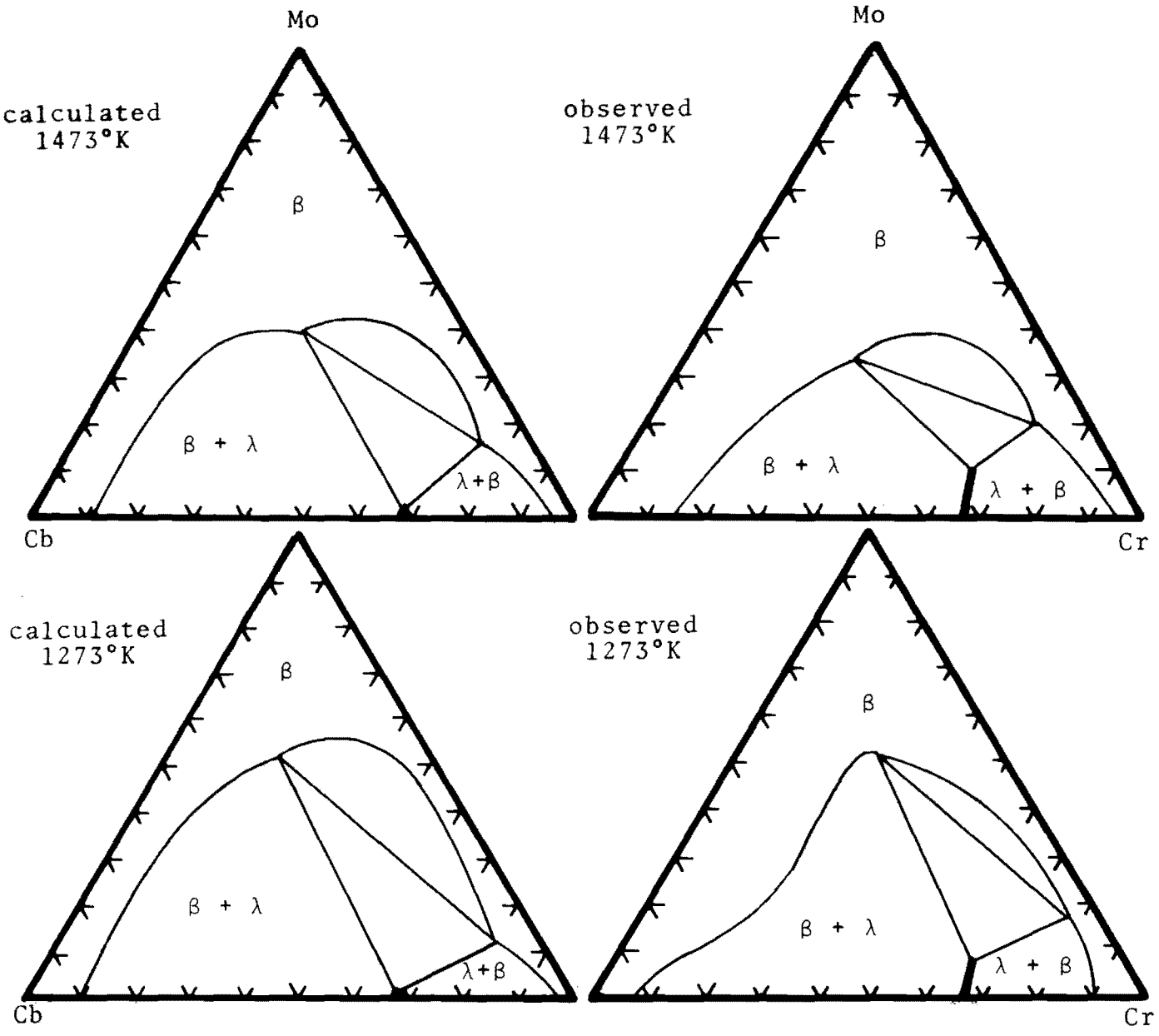

Figure 28 Calculated and Observed Isothermal Sections in the Mo-Cr-Cb System.

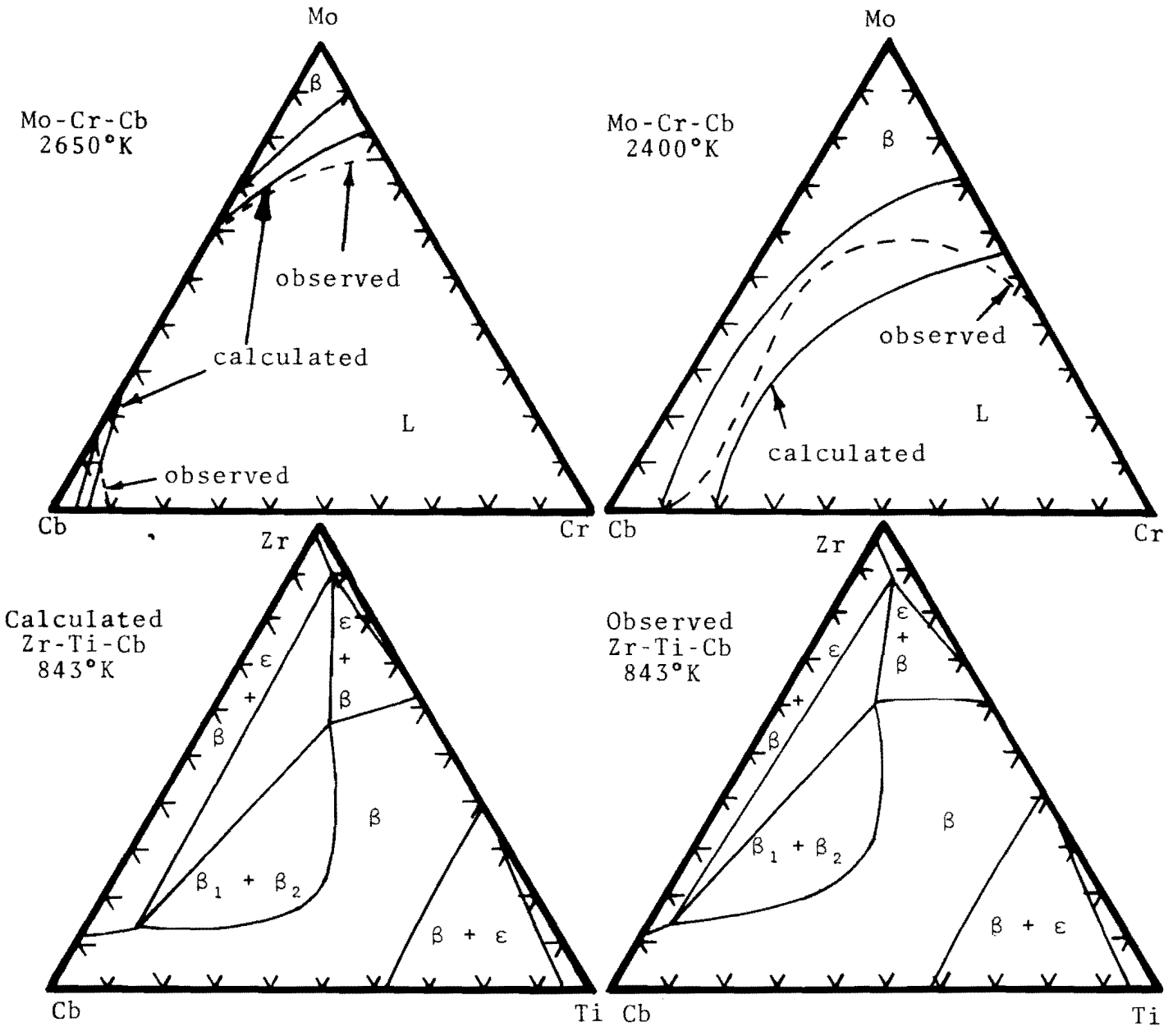

Figure 29 Calculated and Observed Isothermal Sections in Mo-Cr-Cb and Zr-Ti-Cb.

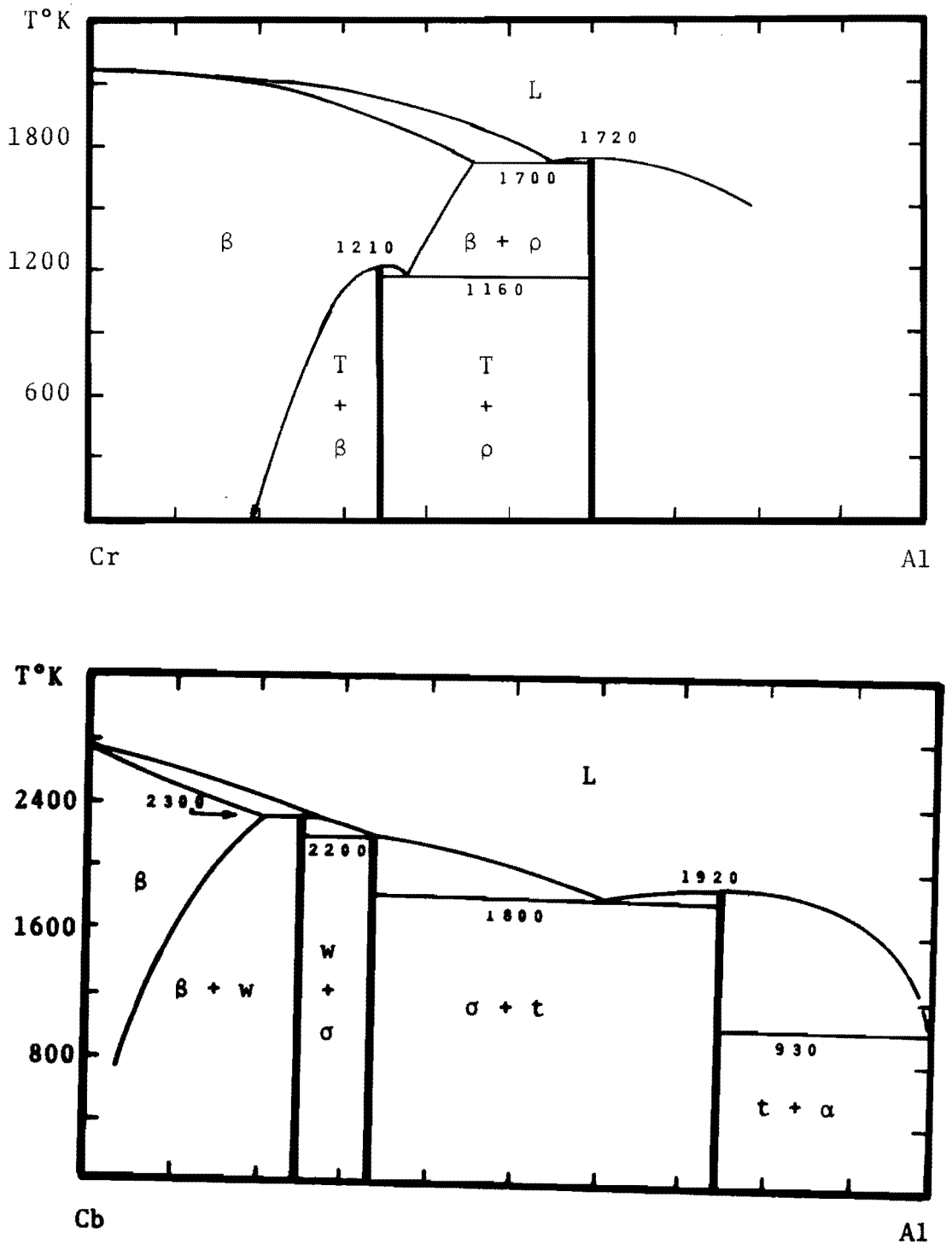

Figure 30 Calculated Phase Diagrams for the Cr-Al and Cb-Al Systems.

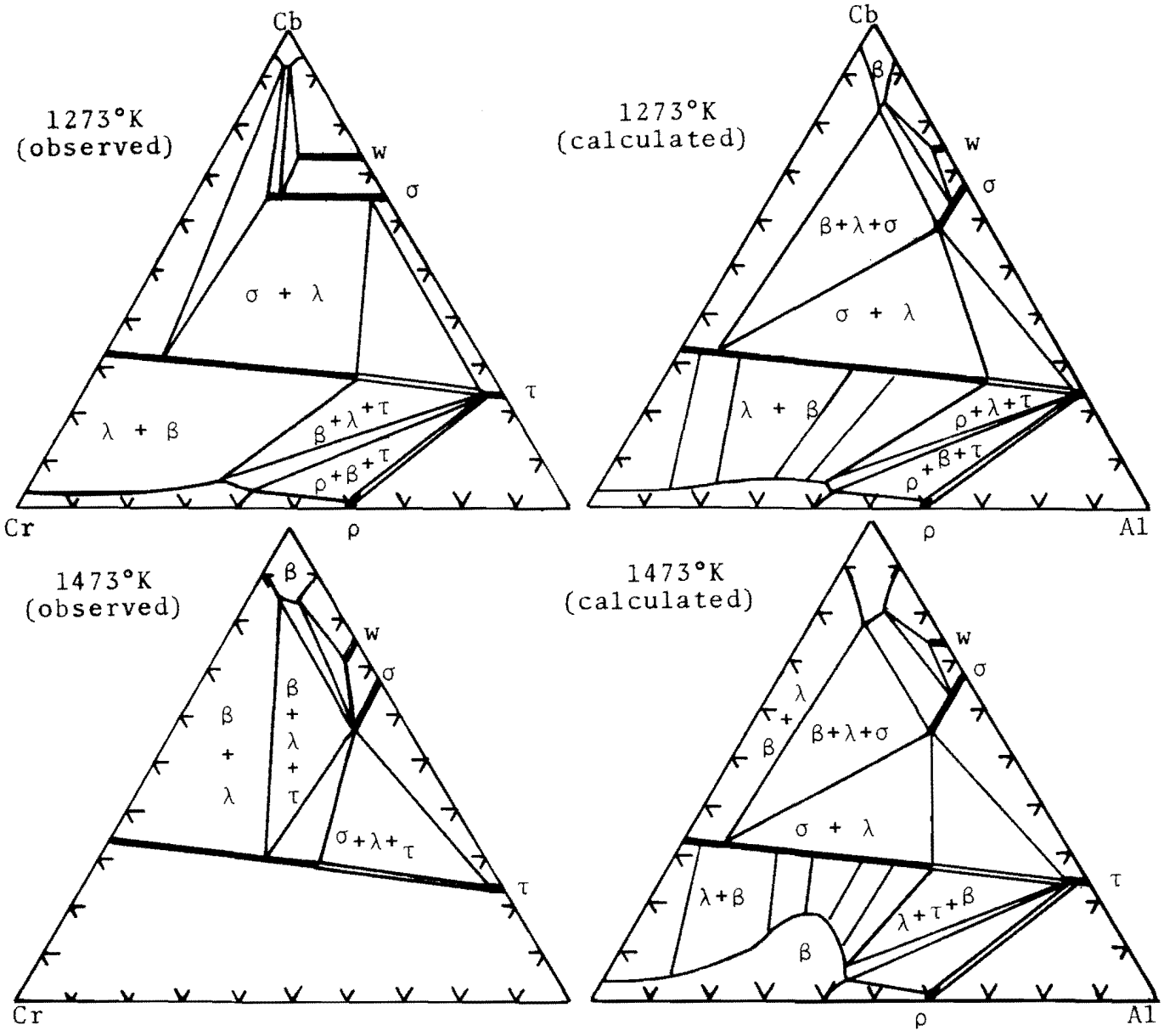

Figure 31 Calculated and Observed Isothermal Sections in Cb-Al-Cr.

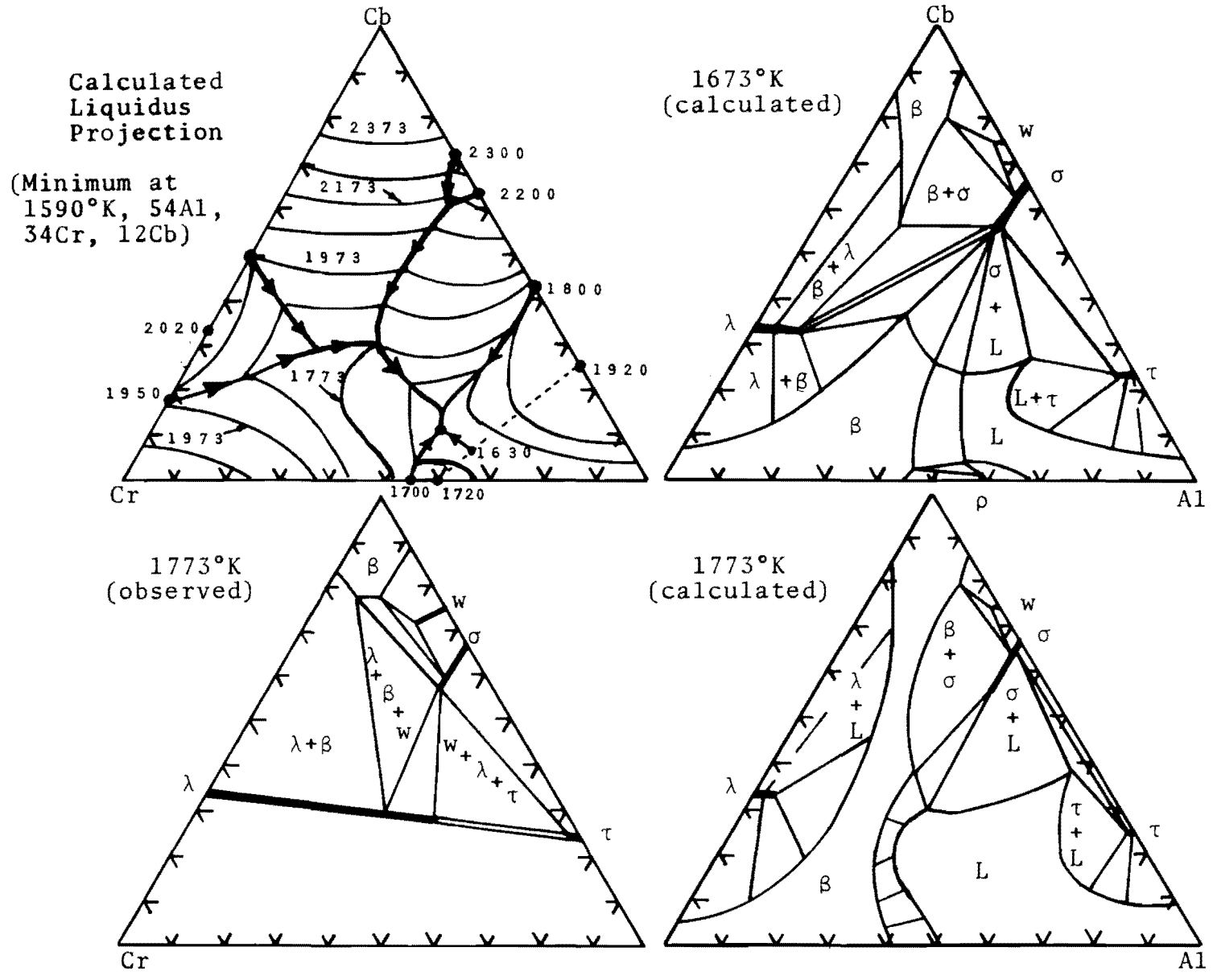

Figure 32 Calculated and Observed Isothermal Sections in Cb-Al-Cr.

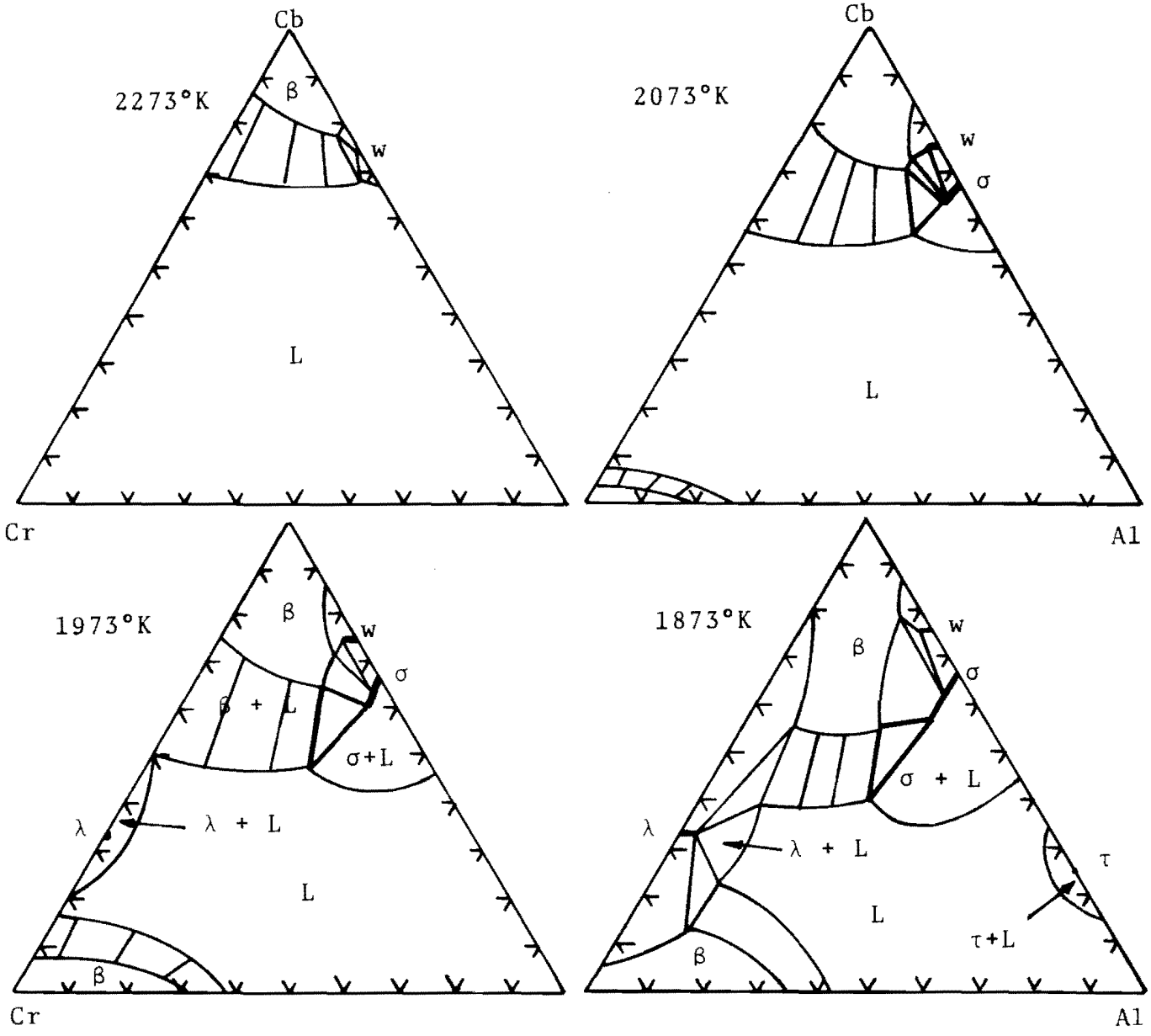

Figure 33 Calculated Isothermal Sections in Cb-Al-Cr.

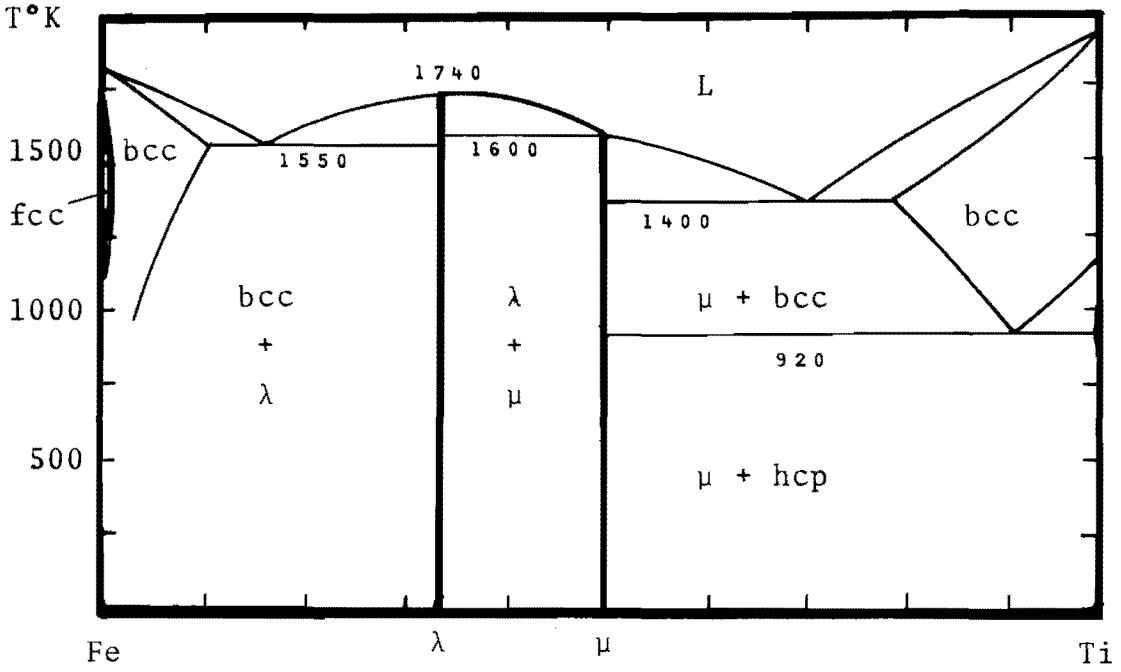

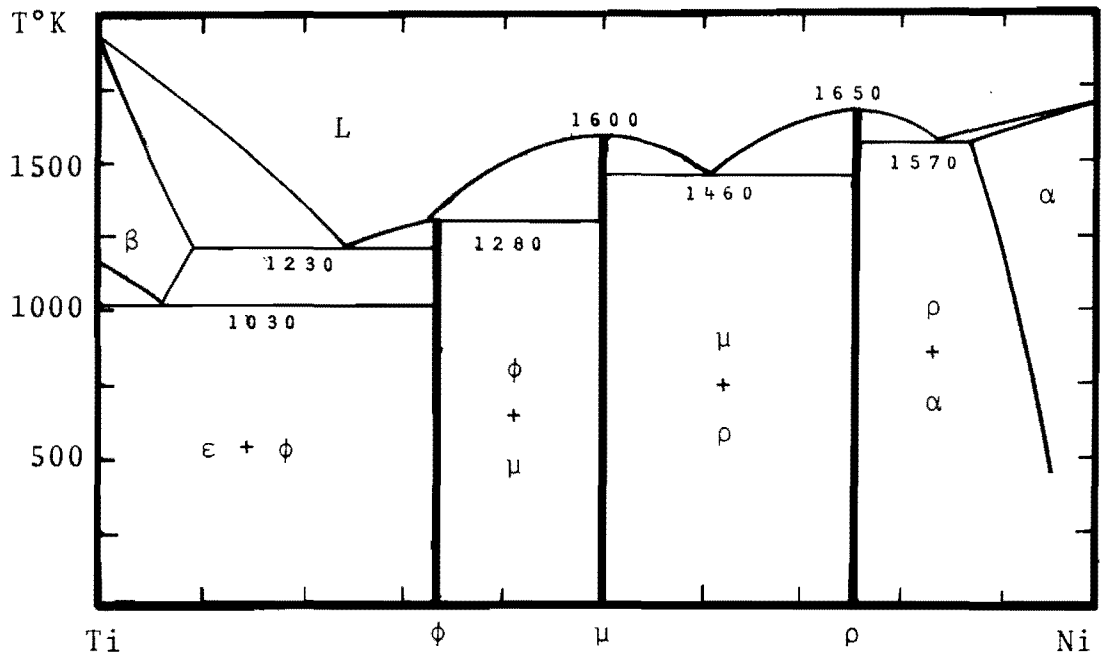

Figure 34 Calculated Phase Diagrams for the Fe-Ti and Ti-Ni Systems.

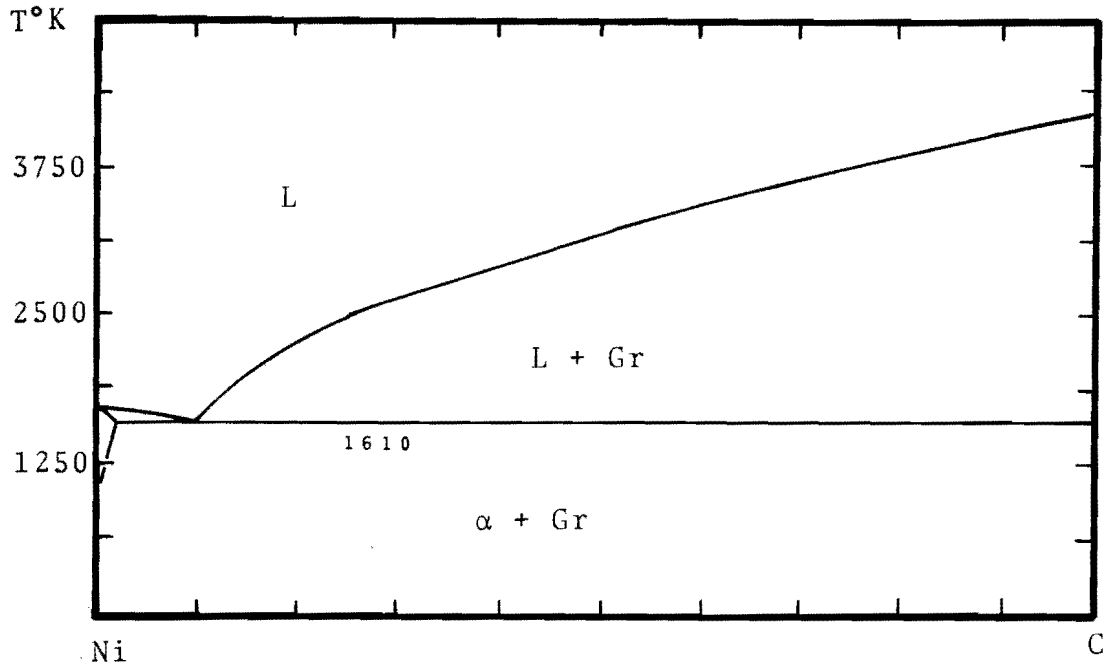

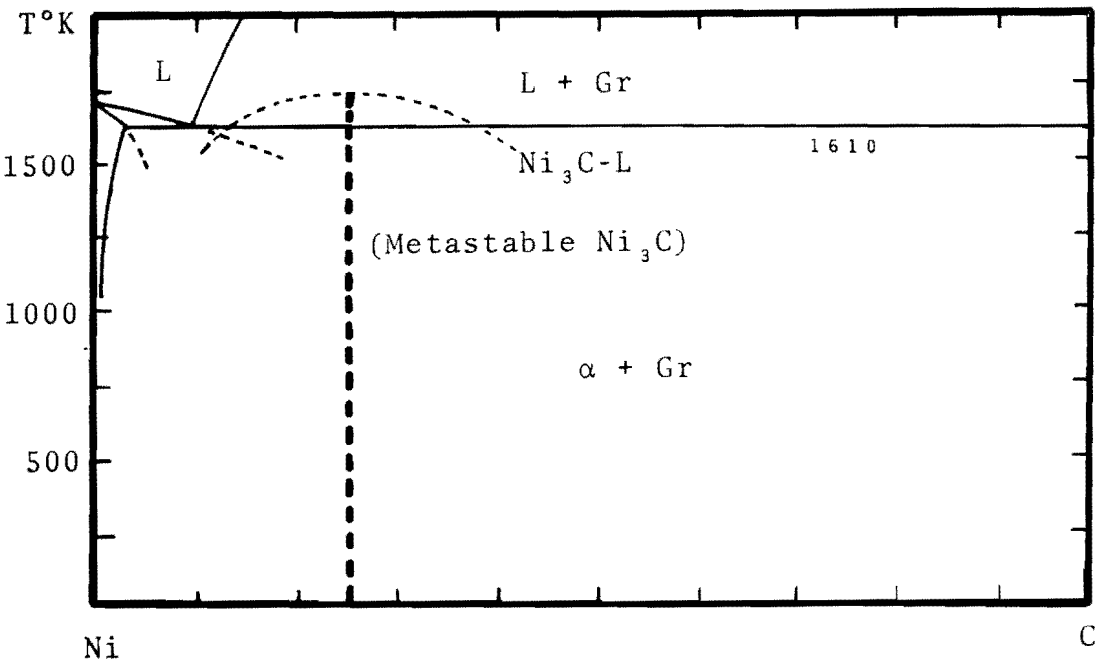

Figure 35 Calculated Phase Diagram for the Ni-C System.

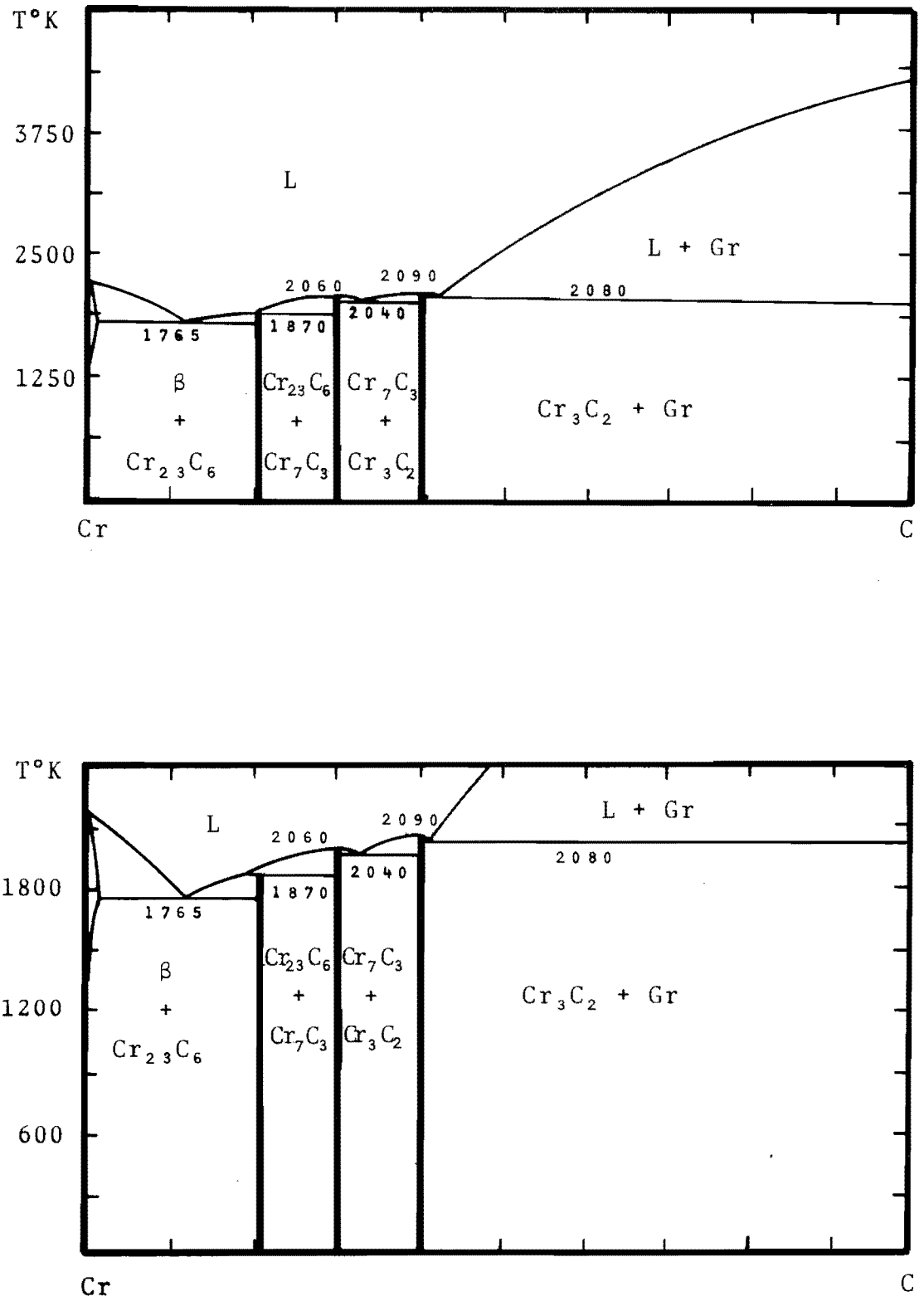

Figure 36 Calculated Phase Diagram for the Cr-C System.

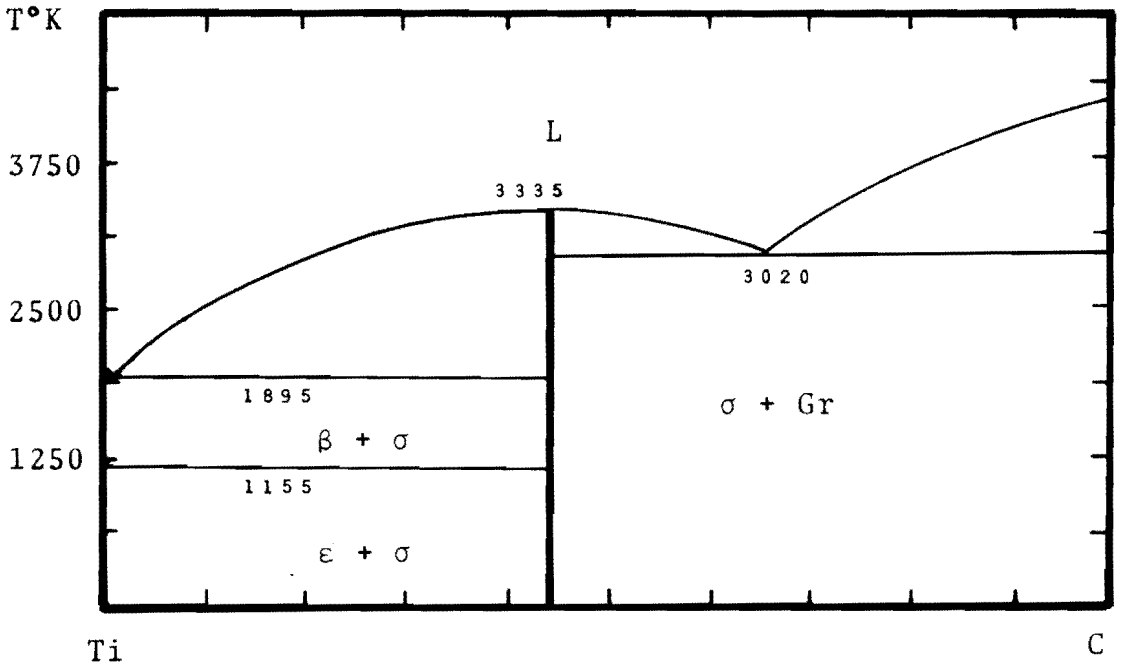

Figure 37. Calculated Phase Diagram for the Ti-C System.

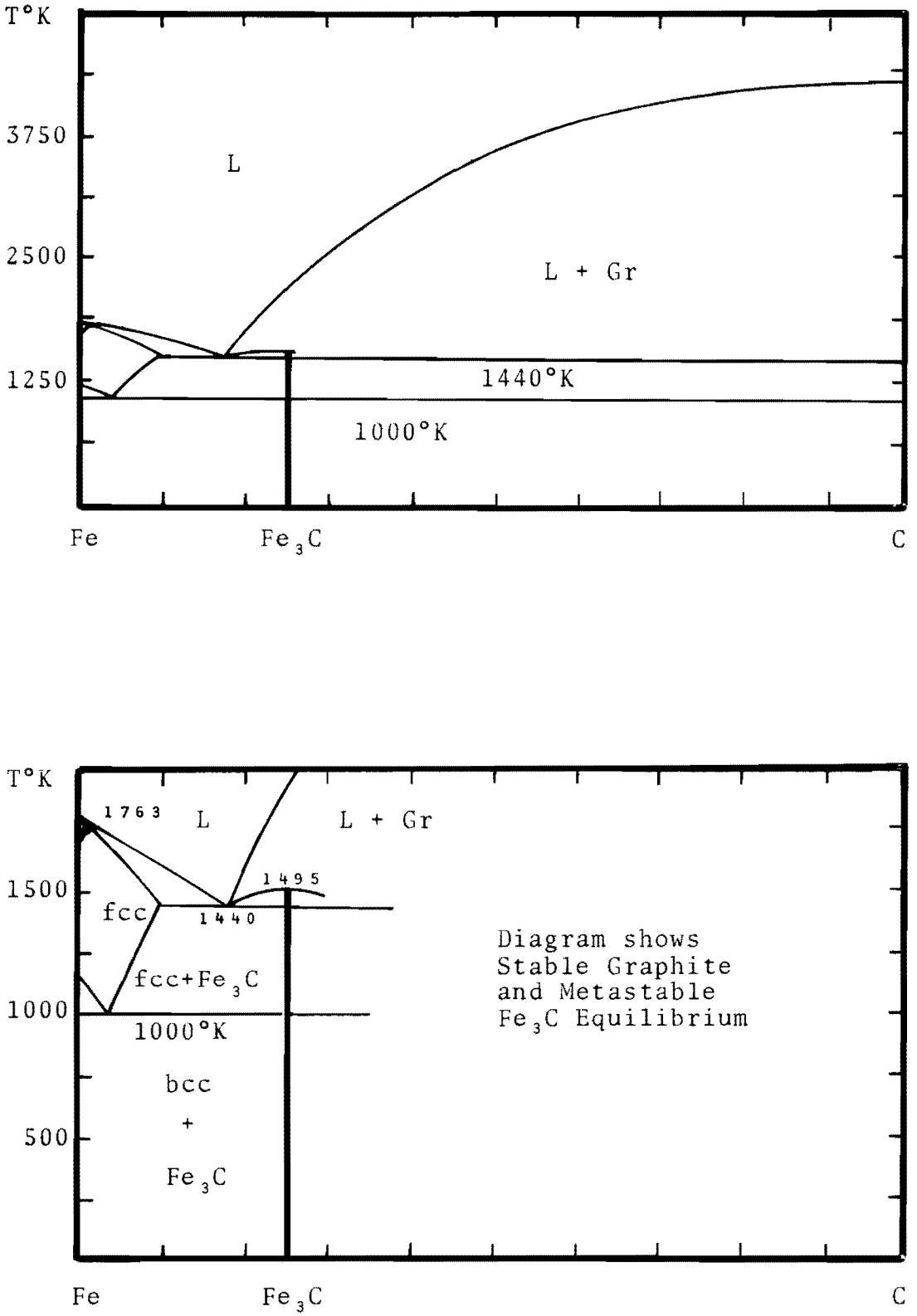

Figure 38 Calculated Phase Diagram for the Fe-C System.

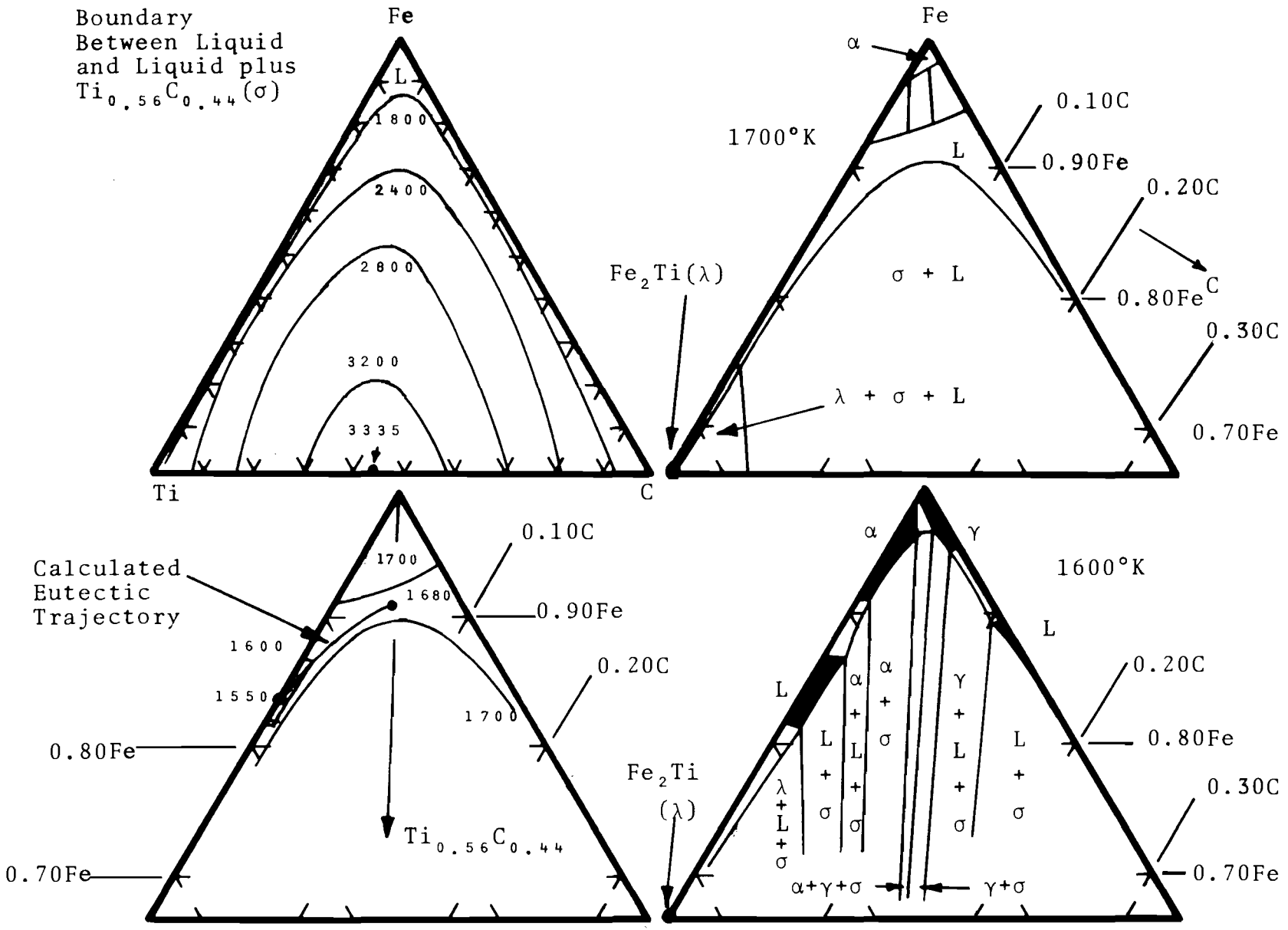

Figure 39 Calculated Liquidus in the Fe-Fe_2Ti-TiC region of the Fe-C-Ti System.

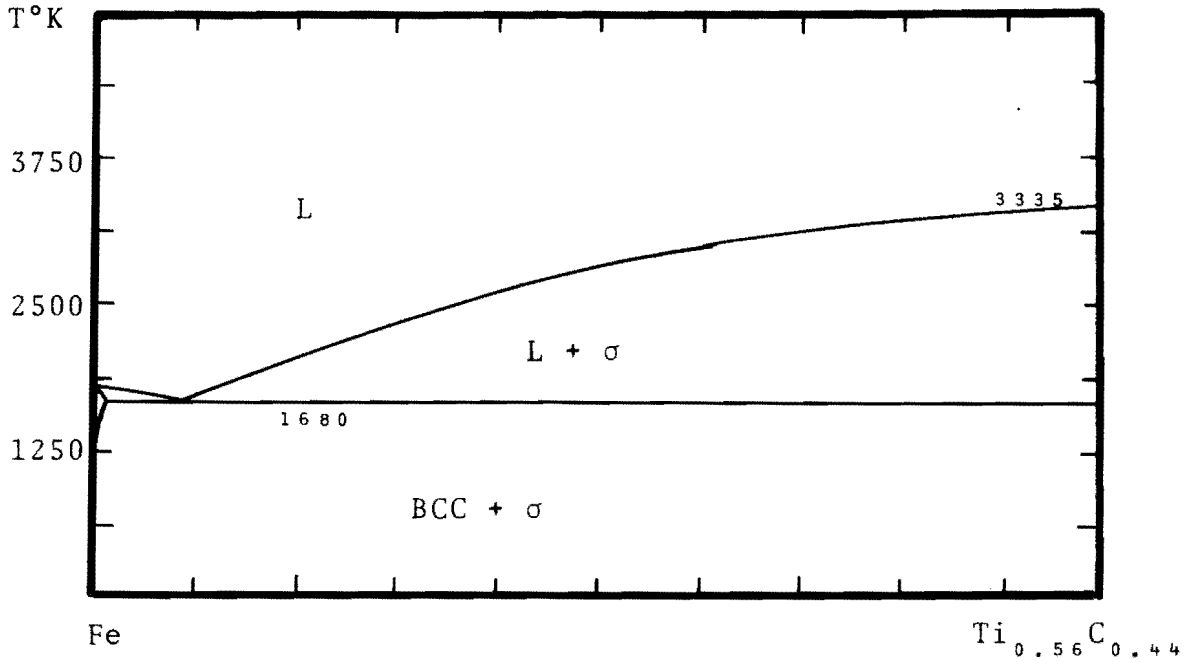

Figure 40 Calculated Quasi-Binary Eutectic in the Fe-C-Ti System.

UNCLASSIFIED
Security Classification

DOCUMENT CONTROL DATA - R & D

(Security classification of title, body of abstract and indexing annotation must be entered when the overall report is classified)

1. ORIGINATING ACTIVITY (Corporate author)	2a. REPORT SECURITY CLASSIFICATION
ManLabs, Inc. 21 Erie Street Cambridge, Massachusetts 02139	Unclassified 2b. GROUP

3. REPORT TITLE

COMPUTER ANALYSIS OF ALLOY SYSTEMS

4. DESCRIPTIVE NOTES (Type of report and inclusive dates)

Final Report - May 1971 to January 1973

5. AUTHOR(S) (First name, middle initial, last name)

Larry Kaufman
Harvey Nesor

6. REPORT DATE	7a. TOTAL NO. OF PAGES	7b. NO. OF REFS
March 1973	331	91

8a. CONTRACT OR GRANT NO.	9a. ORIGINATOR'S REPORT NUMBER(S)
F33615-71-C-1471 b. PROJECT NO. 7353 c. TASK NO. 735302 d.	AFML-TR-73-56 9b. OTHER REPORT NO(S) (Any other numbers that may be assigned this report)

10. DISTRIBUTION STATEMENT

Approved for public release; distribution unlimited.

11. SUPPLEMENTARY NOTES	12. SPONSORING MILITARY ACTIVITY
	Air Force Materials Laboratory (LLM) Air Force Systems Command Wright-Patterson AFB, Ohio 45433

13. ABSTRACT

Computer analysis of twenty-three binary and thirteen ternary titanium and columbium base systems has been performed in order to provide phase stability and thermochemical characterization data which can be used to define fabrication procedures for achieving high temperature stability and improved mechanical properties. M_s temperatures have been calculated for titanium base alloys with simultaneous additions of Mo, V, Al, Mn and Sn. The effect of zirconium on the solubility of Si and Be in hcp titanium was calculated along with the occurrence of miscibility gap formation in bcc titanium base systems. Titanium and columbium base ternary systems were analyzed to predict the temperature-composition trajectories of eutectoid and eutectic troughs and the location of melting point minima. A method was developed for calculation of the eutectic temperature and composition of metal alloy-metal carbide systems and applied to the (Fe,Ni,Cr)-TiC case.

DD FORM 1 NOV 1473 REPLACES DD FORM 1473, 1 JAN 64, WHICH IS OBSOLETE FOR ARMY USE.

UNCLASSIFIED
Security Classification

14. KEY WORDS	LINK A		LINK B		LINK C	
	ROLE	WT	ROLE	WT	ROLE	WT
Computer Analysis						
Binary						
Ternary						
Titanium						
Columbium Base Systems						
Phase Stability						
Thermochemical Characterization						
High Temperature Stability						
M_S Temperatures						
Solubility						
Miscibility Gap						
Eutectoid						
Eutectic Troughs						
Metal Alloy-Metal Carbide Systems						